Optimal Design of Coke Drum Skirt Slots and Analysis of Alternative Skirt Support Structures for Thermal-Mechanical Cyclic Loading

by

Edward Lee Wang

A thesis submitted in partial fulfillment of the requirements for the degree of

Master of Science

Department of Mechanical Engineering
University of Alberta

ABSTRACT

The skirt-to-shell attachment weld on coke drums is susceptible to low-cycle fatigue failure due to severe thermal-mechanical cyclic stresses. Therefore, various skirt attachment designs have been proposed and implemented to reduce stress and thus improve reliability. The most common skirt design is a cylindrical shell attached tangentially by a fillet weld to the coke drum vessel. One inexpensive method to decrease stress in the junction weld is to add vertical slots near the top of the skirt, thereby reducing the local stiffness close to the weld. The conventional skirt slot design is thin relative to its circumferential spacing. An alternative skirt design where the vessel is supported by a number of welded attachment plates and allowed to expand and contract freely through the use of lubricated horizontal sliding plates also exists. In this study, thermal-mechanical elastoplastic 3-D finite element models of coke drums are created to analyze the effect of different skirt designs on the stress/strain field near the shell-to-skirt junction weld, as well as any other critical stress locations in the overall skirt design. The results confirm that the inclusion of the conventional slot design effectively reduces stress in the junction weld. However, it has also been found that the critical stress location migrates from the shell-to-skirt junction weld to the slot ends. The results from an optimization study of the slot dimensions indicate that wider skirt slots improve the stress and strain response and thus increase fatigue life of the weld and slot area compared to the conventional slot design. An optimal slot design is presented. The sliding plate design is found to further improve the stress and strain response at the point of attachment. However, bending of the vessel due to the rising water level during the quench stage is found to cause severe plastic deformation in the sharp corners which are inherent to the design. Thus, a novel design which includes pinned connections at the point of attachment in addition to sliding plates is proposed. The pinned-sliding plate design is found to completely prevent plastic deformation from occurring at the point of attachment and significantly reduce critical stress. Accordingly, the pinned-sliding plate design is the most promising candidate from a reliability standpoint among the designs examined in this study.

ACKNOWLEDGEMENTS

I would like to express my utmost gratitude to my supervisor Dr. Zihui Xia, who has provided endless opportunities, guidance, and support throughout this endeavour.

I would like to thank Dr. Feng Ju, Dr. Jie Chen, Dr. Yejian Jiang, and John Aumuller for their support and advice.

I would also like to acknowledge Suncor Energy Inc. and Mitacs for funding this research.

I am very grateful to my parents, my brother, and my girlfriend for their unwavering support and encouragement.

Table of Contents

List of Tables

List of Figures

CHAPTER 1 INTRODUCTION

1.1 Overview of Delayed Coking Process and Coke Drums

Delayed coking is an important process used by most oil refineries to upgrade heavy crude oil to usable products including but not limited to gasoline, gas oil, and petroleum coke. Vertically-oriented cylindrical pressure vessels wrapped in insulation (referred to as coke drums) are used to facilitate this process. The drums are normally arranged in pairs to enable the batch process to operate without interruption. Depending on the output of the refinery, each process cycle may take between 10-30 hours to complete. A typical cycle of a coke drum involves preheating, filling, quenching, and un-heading stages. During the preheating stage, an empty coke drum is gradually heated from ambient to about 350°C over 4 hours by using injected steam followed by hot vapours. The injected steam and vapours serve a dual purpose: to reduce the severity of thermal shock induced by the hot feed material, and to test the drum for any leaks needing to be repaired before commencing the process. The feed material, at a temperature ranging from 450 to 482°C, is then introduced through nozzles near the bottom of the drum during the 10 hour filling stage. The internal pressure of the coke drum typically reaches 300 to 350 kPa during this stage. Due to the pressure and temperature inside the vessel, thermal cracking of the heavy crude oil proceeds and lighter fractions are sent to a fraction tower where they are separated and stored. At the end of the filling process, a high-density hydrocarbon residue known as petroleum coke is left behind inside the drum. The hot feed material is diverted to the other preheated coke drum and begins the identical process. Cold quench water is then introduced at a high flow rate, rapidly cooling the drum and its contents. After the contents are sufficiently cooled, the un-heading and extraction stage commences. Plates on the top and

bottom of the drum are opened up and a spinning high pressure water drill bit is lowered in through the top opening, cutting the solid coke into loose chunks which eventually fall out the bottom.

As made evident by the description of the process above, the drums are subjected to excessive thermal-mechanical stresses due to severe thermal cycling. The most common failure mechanisms for coke drums are related to cracking, bulging deformation, and low cycle fatigue caused by these excessive stresses [1]. Furthermore, coke drum failures are being reported more frequently as cycle times are reduced to maximize output of the drums in recent times. According to the 1996 API Coke Drum Survey [1], the average number of cycles before first through wall crack is about 4000 cycles, while the maximum number of cycles reported without a through-wall crack is less than 10000 operating cycles. Damage of the drums inevitably leads to unscheduled downtime and costly repair, which result in large economic losses. Therefore, any measure that may potentially extend the life of the coke drums should be explored.

Coke drums typically consist of five main components, which are numbered for convenience and shown in Figure 1-1: (1) top head, (2) cylindrical drum courses, (3) conical bottom head, and (4) skirt support structure. The inner surfaces of components (1) to (3) are directly subjected to varying pressures and temperatures, as well as steam, oil vapours, hot oil, petroleum coke and water. Thus, these components are commonly referred to as pressure components and fabricated with a relatively thin layer of corrosion-resistant clad material. While coke drums have historically been constructed using plates of homogeneous carbon (mild) steel, most modern coke drums have since been made using low alloy steels consisting of varying ratios of Carbon, Molybdenum, and Chromium cladded with stainless steel. The thickness of the coke drum shell is normally based on the specified design pressure. Due to the vertical

orientation of the coke drum and the expected hydrostatic pressure of its contents, the pressure varies linearly from a minimum value at the top of the vessel to a maximum value at the bottom head flange. Thus, the tendency is to design each shell course independently of each other resulting in a step-increase in thickness from one course to another. The pressure components are typically joined together using continuous circumferential weld seams, which are often the site of problematic through-thickness cracks [1] as will be discussed in the subsequent section.

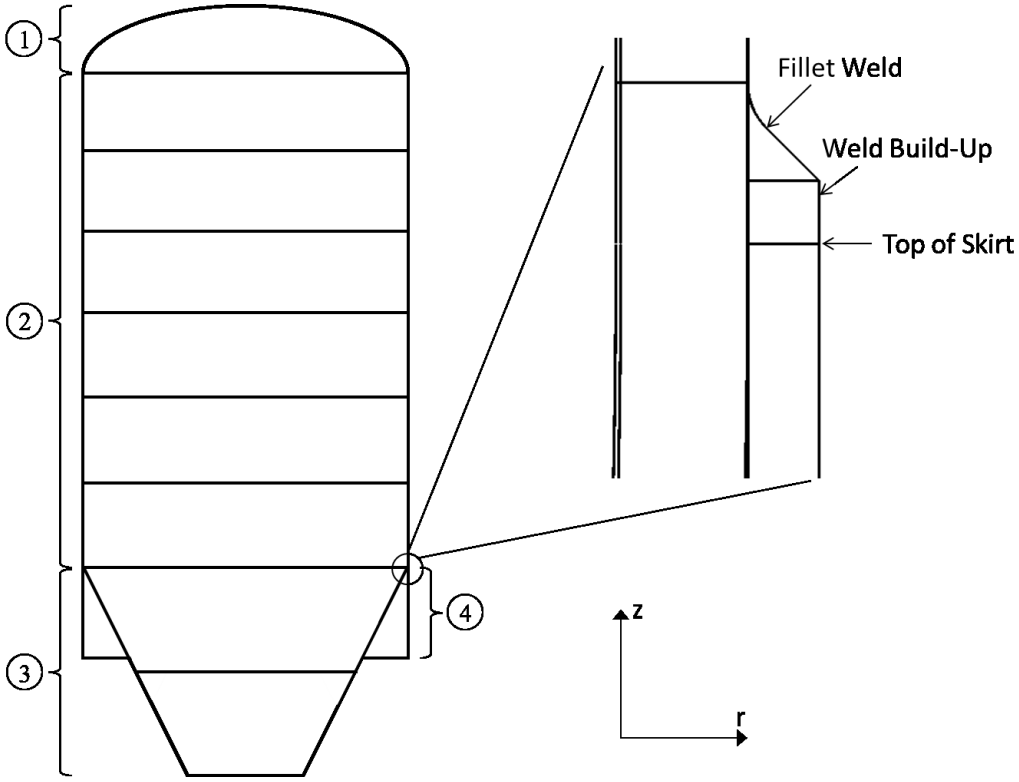

Figure 1-1: Simplified Sketch of Coke Drum with Skirt-to-Shell Attachment Detail

Skirt support structures are used to support the vessel on a raised platform to allow the petroleum coke to exit through the conical bottom head at the end of each process cycle. Presently, the most commonly used type of skirt for coke drums is an insulated cylindrical shell joined tangentially to the vertical portion of the vessel by a continuous fillet weld [2]. Skirt supports and their attachment welds are designed around the loads resulting from the vessel test

and operating weights, wind, and earthquake as required by the ASME Boiler and Pressure Vessel Code [3]. The thickness of the skirt is usually set by the required weld size, unless other minimum thicknesses set by standards or prior experiences apply. The point of attachment to the vessel and insulation detail is generally determined by past practice and company standards, as the Code only provides non-mandatory recommendations for best practice. Much like the circumferential seam welds of the pressure components introduced above, difficulties have also been experienced with welded skirt attachments for vessels in cyclic service as discussed below.

1.2 Literature Review

1.2.1 Common Coke Drum Issues

Several studies on coke drum failure and design optimisation have been conducted by using a combination of material testing, measurement data, and numerical simulation [3-11]. Ramos et al. [3] concluded that fatigue cracks form primarily in the clad material, circumferential shell seam welds, and on the skirt-to-shell attachment welds. A separate study conducted by Ramos et al. [4] gave evidence for the existence of localised hot and cold regions randomly occurring during the quenching stage. It was determined that the temperature difference between these hot/cold regions and the areas immediately adjacent to them can cause stresses and strains severe enough to result in bulging and cracking of the coke drum shell. This finding was confirmed later by thermocouple data published by Oka et al. [5]. More recently, a study carried out by Yan et al. [6] presented a statistical method to estimate the fatigue life of coke drums while taking into consideration the randomness of these hot and cold regions.

Different types of cracks found in coke drums and their likely sources were identified in a metallurgical study done by Penso et al. [7]. The deepest cracks were found in the heat affected

zones of internal welds, while the largest number of cracks was found in the stainless steel clad material. The cracks were attributed to a number of possible sources such as corrosion, stress concentrations caused by weld geometry, cyclic thermal stress, differences in material properties such as CTE and tensile strength, thermal shock, and heat affected zones around welds. Xia et al. [8] conducted a finite element analysis of a coke drum for a complete operating cycle. The results showed that the clad material experiences a biaxial stress cycling with a maximum value higher than that of the yield limit of the material. The critical stress value was attributed to bending caused by thermal cycling and differences in CTE between the clad and base materials. The authors suggest that low cycle fatigue is the main failure mechanism of the simulated coke drum, which aligns both with previous studies and the real case. Several studies have since been conducted [9-11] in an effort to improve the selection of materials for coke drums. Nikic [9] used material properties given in ASME Boiler and Pressure Vessel Code and conducted finite element analyses to explore the effect of different clad/base material combinations. Chen [10] and Rahman [11] carried out extensive material testing to more accurately characterize the thermal-mechanical material properties of common coke drum materials. In addition, the thermal-mechanical properties of weld material and heat-affected base metals were also experimentally determined [10].

As mentioned previously, one of the well-known potential areas of failure is the shell-to-skirt attachment weld. Oka et al. [12] carried out empirical tests on coke drums fitted with measurement gauges to monitor temperature and strain histories at critical points near the skirt-to-shell junction over several process cycles. The results show that the inner side of the upper part of the skirt experiences the most severe thermal strains. During each cycle, two peak strains occur at this point which are compressive at the beginning of the filling stage and tensile at the

beginning of the cooling stage. The measured strains exceed the yield strain of the material used, which indicates plastic deformation and potential fatigue failure.

Weil and Murphy [13] derived a general closed-form numerical solution for the stresses at the junction of a three-cylinder intersection using basic equations for the effect of end shear, moment deflection and rotation. The solution takes into consideration fundamental geometric data, design pressures, and axial thermal gradients at the junction. To demonstrate its general applicability, two numerical examples were solved using parameters from existing coke drums. The vessels were kept identical between the numerical examples, except that the vessel-skirt crotch was filled with insulation on the first example while the second example retained an air gap ("hot box") in the same area. It was concluded that excessive thermal stresses in both examples are caused by the local axial temperature gradient in the immediate vicinity of the three joined shells. Furthermore, these thermal stresses were the main contributor to the total cyclic stress at the junction. The findings suggest that the total stress in the joint of the vessel-skirt crotch filled with insulation exceeds the yield strength of the material. Under cyclic loading conditions as is the case with delayed coking, these stresses may induce plastic strain and, eventually, fatigue failure. The inclusion of the "hot box" was found to cause a reduction of thermal stress by about half, which was attributed to a less severe thermal gradient near the junction. It was suggested that the addition of vertical slots to the upper portion of the skirt would further reduce the thermal stresses. The authors also suggest that the choice of attachment weld and its location along the vessel contribute greatly to the stresses experienced by the weld area. In a later study, Cheng and Weil [14] adapted the equation developed in the aforementioned study to include the effect of conventional skirt slots (which are thin relative to their circumferential spacing and terminate in drilled keyholes). The slot design examined in the study

is still commonly used on slotted skirts as of the writing of the current paper. The authors concluded that slotting the skirt caused a significant reduction in junction stress. The reduction of stress was attributed to the decrease of local stiffness near the junction due to the presence of the slot.

The studies [13,14] above were conducted using temperature-independent material properties, steady state thermal conditions, and elastic theory. However, it is well known that the vessels are subjected to varying temperatures and stresses exceeding the yield strength of the materials being used, the results and conclusions drawn from these studies may not be accurate. Furthermore, the authors [14] neglected to comment on the degree of stress concentration near the skirt slots. According to the 1996 API Coke Drum Survey [1], 89% of the skirts with slots experienced cracking. Thus, it is apparent that further research into the design of skirt support structures and skirt slots may contribute to the improvement of the reliability of coke drums.

1.2.2 Skirt Support Structure Designs and Improvements

According to the ASME Boiler and Pressure Vessel Code, design of skirt supports for vertical vessels must consider: loading transferred to the skirt due to the weight of the vessel and contents above and below the point of attachment; externally applied moments and forces such as wind, earthquake and piping loads; localized stresses at the skirt attachment location; and thermal gradients. As such, rules governing the geometry or type of skirt do not exist. In other words, as long as any skirt support structure has been evaluated to meet the specified acceptance criterion, it may be deemed as a satisfactory design. Some examples outlined in the Code include lug and leg supports, as well as the conventional cylindrical shell support. Simplified sketches of these skirt types are shown in Figure 1-2. Several attempts at optimizing skirt design have recently been made by minimizing thermal gradients and localized stresses at the skirt

attachment weld in various ways. In this section, some established alternative skirt designs will be discussed.

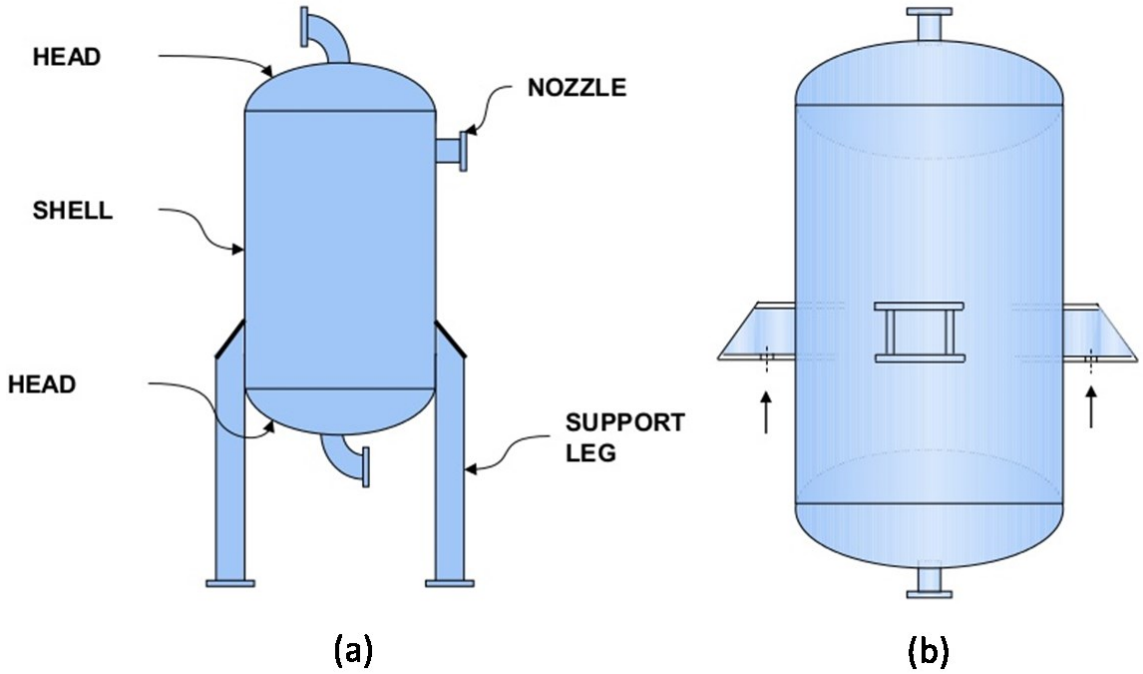

Figure 1-2: Diagrams of different support structure designs. (a) Leg supports; (b) lug supports

Stewart et al. [15] reported that Chicago Bridge and Iron (CB&I), a large multinational conglomerate engineering and construction company based out of Texas, owns patents to two skirt support structure designs named "T-Rex" and "Wrapper". The T-Rex skirt is joined tangentially to the vertical portion of the vessel using discontinuous attachment welds separated by slots which penetrate to the top of the skirt. Additionally, the design includes a hot box which, as mentioned in an earlier section, results in a more gradual thermal gradient. The main advantage of the T-Rex skirt is a less stiff point of attachment compared to a conventionally slotted skirt due to the discontinuous welds and slots which are considerably wider than the conventional slots. However, stress concentrations will inevitably occur near the slot ends and points of attachment. The effectiveness of this design would be determined by the magnitude of

these elevated stresses compared to the conventional slot. The Wrapper skirt is designed to support the coke drum primarily by bearing and frictional forces rather than load bearing weld attachments. To accomplish this, the skirt conforms to the geometry of the cone at the knuckle bend. Therefore, as the authors note, the skirt provides a flexible connection absent of the large pre-stresses associated with weld-induced heat-affected zones. Furthermore, the extended contact between the shell and the skirt theoretically improves the heat transfer between the two components, which may cause a reduction in thermally induced stresses compared to a conventional skirt. In the opinion of the author of the current study, the functionality of the Wrapper skirt is heavily dependent on how similarly the constructed skirt behaves to the theoretical skirt. For example, the constructed skirt will likely not conform perfectly to the vessel, which would severely compromise its effectiveness.

Recently, a patent for a coke drum skirt filed by Lah [16] demonstrates a shift of tendency away from continuous circumferential fillet attachment welds. The basic principle of the design is to eliminate the restriction normally imposed by a conventional cylindrical shell skirt and to allow the drum to freely expand and contract instead. As shown in Figure 1-3, the weight of the vessel is transferred through welded attachment plates and support ribs to circumferential horizontal plates which are free to slide in the radial direction relative to the vessel. The number of attachment plates and thickness of support ribs are dependent on the loading conditions as outlined by the Code. The horizontal slide plates are sandwiched between a lower supporting plate and upper retaining plates which prevent the coke drum from tipping or falling over. The lower plate is anchored to a concrete support similarly to the conventional skirt design. In order for the design to be effective, the surfaces of the plates are coated with a low friction material or machined to reduce friction. Theoretically, the added degree of freedom

should reduce the stress level near the points of attachment. However, the design is inherently more complex than the conventional skirt in its geometry. The attachment plates, support ribs, and sliding plates all form re-entrant corners between one another, which may be the source of excessive stress concentration effects. The effectiveness of this design will be examined in more detail in a later chapter.

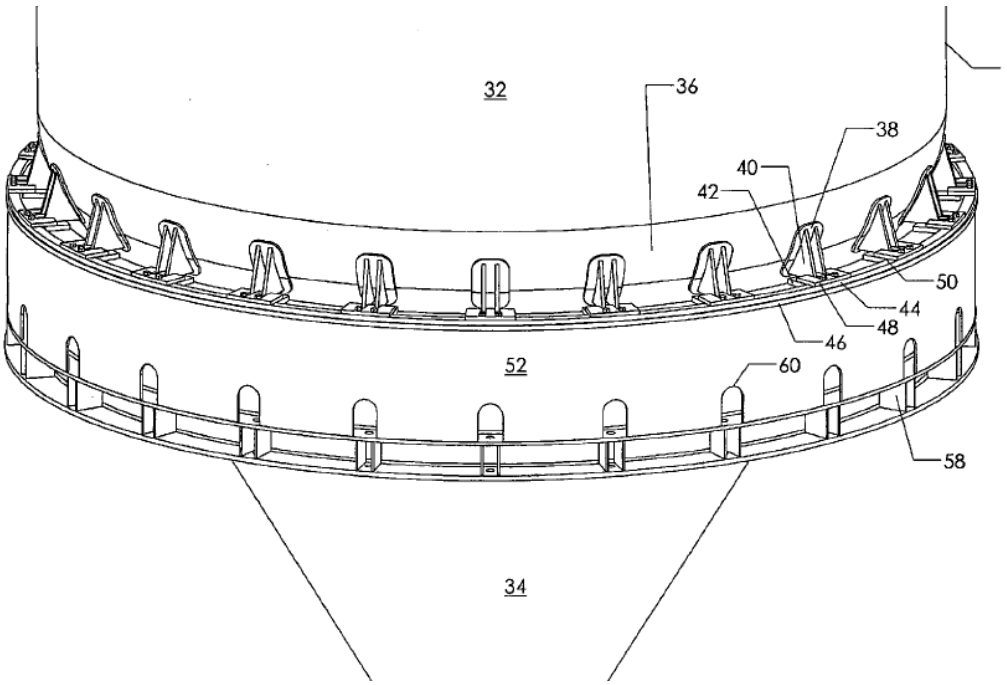

Figure 1-3: Circumferential sandwiched plate skirt support structure [16]

Sasaki and Niimoto [17] conducted a study in which an integral machined plate or forging, instead of the conventional weld build-up, was proposed as an alternative shell-to-skirt attachment. The authors cite high stress near the weld and heat affected zones and lower fatigue strength of the weld metal (compared to the base metal) as the principal cause of fatigue failure in the conventional skirt attachment. The fatigue life can be improved simply by having the high stress area occur in base metal as opposed to the weld metal since the integral design, shown in Figure 1-4, effectively replaces the weld build-up with base metal. The welds joining the drum body and skirt to the integral plate are aligned vertically, such that any forces associated with the

weight of the coke drum and its contents are directed downwards and there is no bending moment on the support structure. Furthermore, the authors note that the machining process allows for a larger inner radius, more accurate dimensions, and complex shapes such as ellipses in order to further mitigate stress concentration effects. The results of a finite element analysis conducted by the authors provide conclusive evidence that the integral skirt attachment has a longer fatigue life than the conventional attachment method. However, a major drawback of this design is its manufacturing cost.

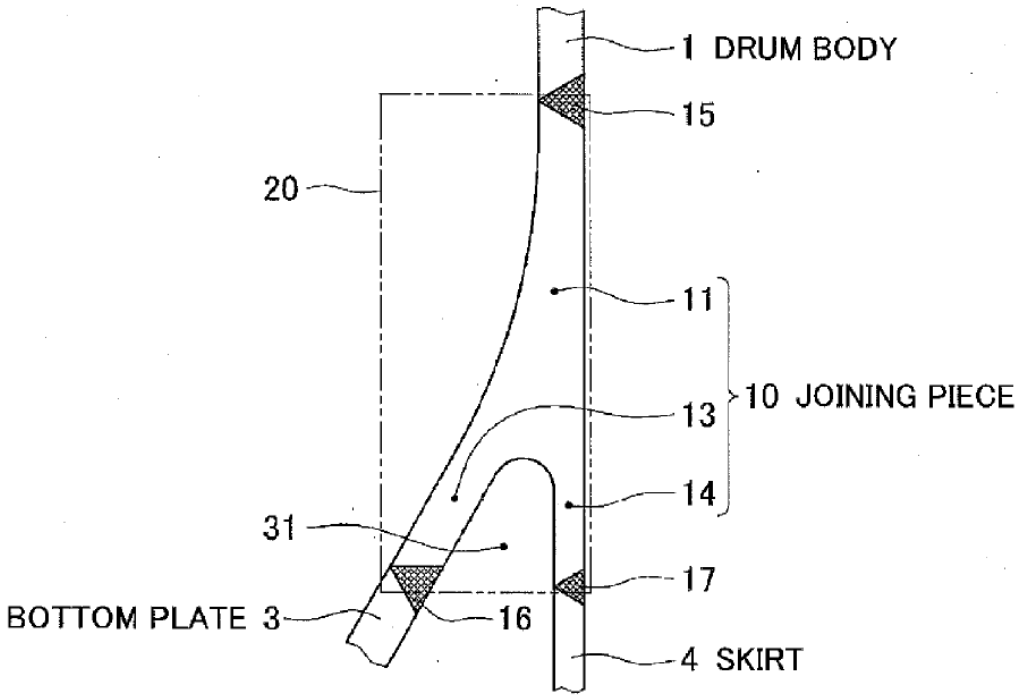

Figure 1-4: Integral skirt attachment design [18]

A study conducted by Oka et al. [12] examined the effect of hot feed injection time on the fatigue life of the shell-to-skirt junction area. In the study, four coke drums identical in geometry and cycle time were fitted with strain and temperature gauges to provide empirical data over each cycle. The hot feed injection time for each drum was averaged over 35-40 cycles and maximum axial strain data was used in conjunction with fatigue failure theory to determine

operational life of each coke drum. The injection time was found to significantly affect the operational life, as an increase in injection time corresponded with a decrease in maximum axial strain. A similar study by Oka et al. [19] explored the effect of switching temperature on the fatigue life of the junction area. The switching temperature is defined as the temperature of the drum just before the hot feed material is injected. The same coke drums fitted with strain and temperature gauges from the previous study [12] were used. The results show that an increase in switching temperature improved operational life. The authors attribute the improvement of operational life to a decrease in thermal shock as a result of the difference between the coke drum and feed material temperatures. The results from these studies [12,19] suggest that the fatigue life of the skirt-to-shell junction is heavily influenced by the process cycle parameters.

It is evident from the studies presented in the literature review above that researchers have identified the main cause of failure of skirt support structures as cyclic periods of high stress found in the welded attachment point. One of the most inexpensive methods of decreasing stress in the junction weld is to slot the skirt, thereby decreasing the local stiffness. However, experience has shown that the stress concentration effect of skirt slots is shown to cause cracking in most slotted skirts. To the knowledge of the author of the current study, research into the effectiveness of skirt slots and their associated stress concentration effects has not yet been conducted. Thus, research into these topics may contribute to the improvement of the reliability of coke drum skirts.

1.3 Thesis Objectives

The work presented in this thesis focuses on optimisation of coke drum skirt support structures. The primary objective of the current study is to explore skirt slot designs and find an optimal design which minimizes cyclic stresses and plastic strain in the junction weld. Next, an

alternative skirt design is to be examined in more detail and compared to the conventional slotted skirt design. Finally, a novel design based on the cumulative research conducted in this study will be presented.

To achieve these objectives, the following is required:

- To develop a thermal-mechanical elastoplastic finite element model of a slotted coke drum skirt to analyze the stress/strain field near the shell-to-skirt junction weld, as well as the stress concentration effect near the slots
- To determine the effect of conventional slots on the stress and strain response in the junction weld and slotted section
- To determine the change in stress and strain response due to incrementally altering slot dimensions from the conventional design
- To analyze the stress/strain field of an alternative skirt design using the same method as the previous analyses
- To develop a novel design based on observations from analysis results from the conventional and alternative skirt designs

As discussed previously, a skirt design which minimizes the cyclic stress and strain experienced by the point of attachment to the vessel while simultaneously minimizing the concentration of stress elsewhere on the skirt would result in a more reliable coke drum. Ideally, experimental models of several coke drum skirt designs would provide the most accurate data for this study. However, the process of designing, fabricating, and carrying out each test would not only be costly but also exceedingly time-consuming. Therefore, finite element analysis (FEA) will be used extensively in this study as it provides a method to quickly and effectively explore

many skirt designs. The finite element analyses conducted in this study will be developed using the ANSYS software package [20]. As will be shown in subsequent chapters, special care is taken when applying boundary conditions to simulate the thermal-mechanical loads experienced by the actual coke drum. Also, justifiable assumptions are made to simplify the model and reduce computational expense. Process parameters such as internal and hydrostatic pressures, quench water and hot feed material temperatures, quench rate, and switching temperature, as well as vessel geometry are kept constant through each analysis. In this way, the focus of this study is kept on the geometrical effect of each skirt design.

While the author of the current study fully acknowledges the limitations of finite element analysis and its application to practical situations, the results from these analyses will provide some insight into the general stress-strain and temperature distributions in the junction weld and around the slots. Furthermore, an assumption can be made that as long as the underlying foundation (ie. boundary conditions, dimensions, mesh, analysis settings, and simplifications) stays consistent, the comparison of results between analyses can lend some conclusive evidence of the efficacy of each skirt design.

CHAPTER 2 PRELIMINARY STUDY ON SKIRT SLOT EFFECTS USING THERMAL-ELASTOPLASTIC FINITE ELEMENT ANALYSIS

2.1 Introduction

The objective of the current chapter is to conduct a preliminary study of the effect of skirt slots on the stress and strain response of the skirt-to-shell junction and slotted section. To accomplish this, 3-D cyclicly symmetrical finite element models are created and solved based on dimensions and process parameters from an existing coke drum with a slotted skirt. The simulation software suite ANSYS® Workbench, Release 15.0 is used because it enables the user to quickly make changes to solid models and to conduct coupled thermal-elastoplastic analyses. These features allow for a convenient and efficient method to analyse and compare skirt designs.

The slot design used for this study follows the conventional design and is henceforth referred to as the "original slot design." In addition to the slotted skirt model, a theoretical coke drum model identical to the example coke drum except with a solid (un-slotted) skirt is also created and analyzed. Thus, the two models solved in this section are named No Slot (NS) and Original Slot (OS). The slot designs are compared to each other using nodal stress and strain results from two main areas of interest: (1) the interface between the top of the skirt and junction weld ('Junction Face'), and (2) the material immediately surrounding the slot ('Slot Area'). The Slot Area is further divided into three specific areas of interest: (2a) the top keyhole, (2b) bottom keyhole, and (2c) mid-point between two slots. The results show that the original skirt slot design causes a significant reduction in equivalent stress and strain when compared to the un-

slotted skirt. However, the slot ends experience severe stress ranges resulting in high levels of plastic deformation.

2.2 Coke Drum Geometry and Materials

2.2.1 Vessel and Skirt Geometry

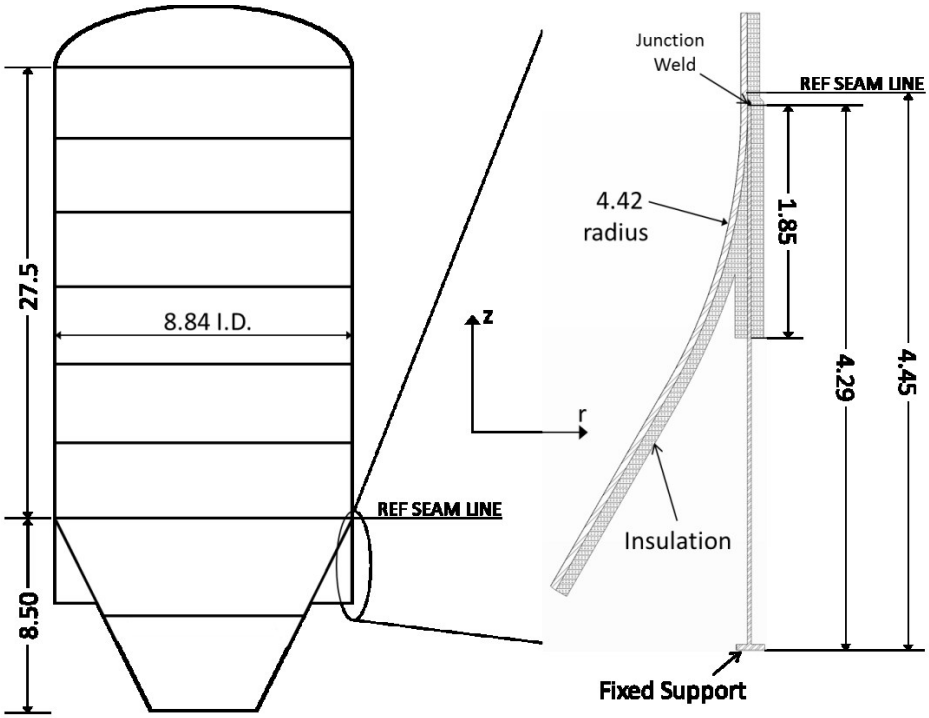

Figure 2-1: Coke drum vessel and skirt dimensions. Values in m.

The vessels are roughly 36 m (120 ft) tall and 9 m (29 ft) inner diameter. The skirt support structure is about 4.5 m in height and 2.86 cm (1.125 in) thick. The important dimensions for the vessel and skirt of the considered coke drum are summarized in Figure 2-1. Detailed dimensions of the junction weld are shown in Figure 2-2.

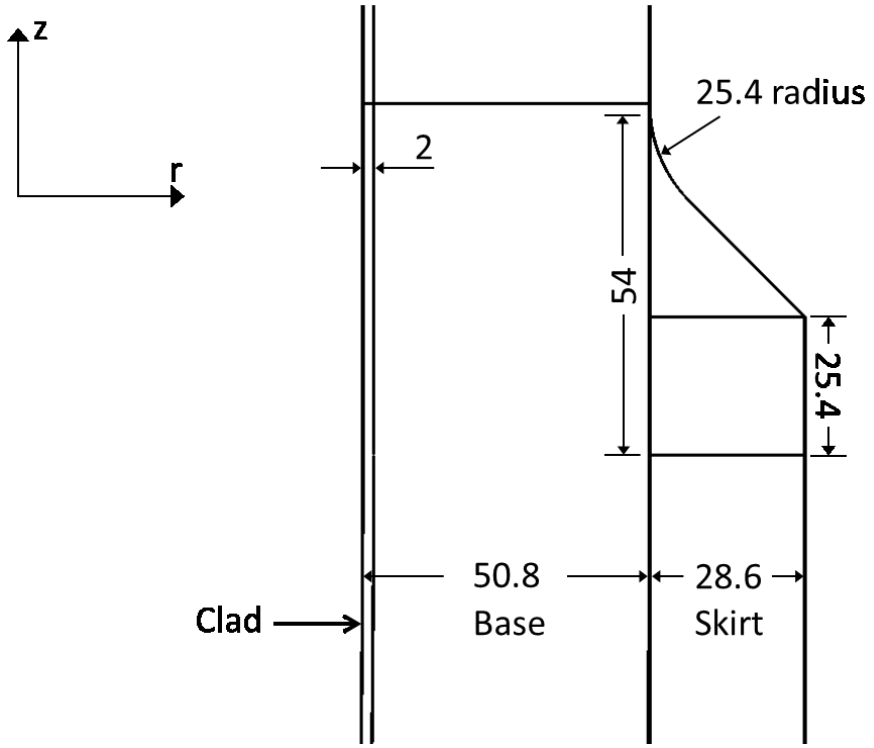

Figure 2-2: Detailed dimensions of junction weld. Values in mm.

2.2.2 Skirt Slot Geometry

The original skirt slots, shown in Figure 2-3, are 7.62 cm (3 in) from the top of the skirt, span 30.48 cm (12 in) in the axial direction, and evenly spaced every 10.16 cm (4 in) in the circumferential direction for a total of 277 slots. The slots terminate in drilled and chamfered 1.905 cm (3/4 in) diameter circular holes. The skirt slot dimensions are summarized in Table 2-1.

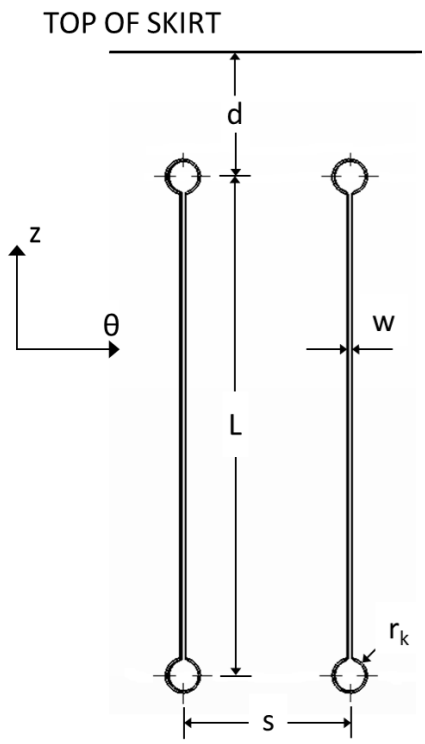

Figure 2-3: Important dimensions of original skirt slot design

Table 2-1: Dimensions for Original Slot Design

Parameter	Original Slot Value	
	(mm)	(in)
d	76.2	3
L	304.8	12
w	3.175	1/8
r_k	9.525	3/8
s	101.6	4

2.2.3 Materials

The shell courses of the coke drums are made of SA387 Grade 12 Class 2 steel of varying thickness from 28.575 mm (1-1/8 in) in the top course to 50.8 mm (2 in) in the conical bottom head. Each course is cladded with a 2 mm (5/64 in) thick layer of SA240-TP410S stainless steel.

The skirt support structure is also made of SA387-12-2 steel. Effects of weld and clad material are not included in this analysis as previously explained. In a previous study conducted by Yan et al. [REF], temperature-dependent material properties such as elastic modulus E, coefficient of thermal expansion CTE, tangent modulus E_t and yield strength S_y of SA387 Gr.12 Cl.2 and SA240-TP410S steels were determined through material testing and analytical modelling. The important thermal and mechanical properties for both materials are summarized in Table 2-2 and Table 2-3. The thermal conductivity, specific heat capacity, and density of each material can be found from the ASME Boiler and Pressure Vessel Code (BPVC) Section II [21]. All material properties are temperature dependent.

Table 2-2: Material Properties of SA387-12-2 Base Metal

Temp., T (°C)	Young's Modulus, E (GPa)	Yield Strength, S_y (MPa)	Tangent Modulus, E_t (MPa)	CTE ($\times 10^{-6}$ °C^{-1})
20	202.4	435	10714	12.3
100	192.9	393	10333	12.8
250	185.0	362	10000	13.6
480	170.7	330	8441	14.7

Table 2-3: Material Properties of SA240-TP410S Clad Metal

Temp., T (°C)	Young's Modulus, E (GPa)	Yield Strength, S_y (MPa)	Tangent Modulus, E_t (MPa)	CTE ($\times 10^{-6}$ °C^{-1})
20	178.0	272	13333	11.0
100	175.8	270	9705	11.2
250	161.1	220	11111	11.6
480	161.5	188	6878	12.1

The method of attachment of the skirt onto the shell is a continuous circumferential fillet weld. The attachment is accomplished through submerged arc welding (SAW) and adheres to American Welding Society (AWS) F8P2-EB2-B2 classification. In practice, the weld and base material properties near the attachment point are difficult to predict due to the complexity of the weld-induced heat-affected zone and therefore may differ significantly. Therefore, experimental evaluation of weld metal material properties would have to be conducted on a case-by-case basis to improve the accuracy of the calculated stress response. However, in the context of this study, the skirt-to-shell junction weld material properties are assumed to be identical to the base metal (SA387-12-2).

2.3 Model Set-Up

2.3.1 Solid Modeling and Meshing

Solid models of each of the considered skirt designs are meshed using 3-D elements. The element type is dependent on the analysis being solved. Within the thermal analysis, the SOLID90 20-node thermal element is used. The elements are replaced by SOLID186 20-node structural elements for the structural analysis. The SOLID186 element was chosen because it supports plasticity, stress stiffening, and large deflection and strain capabilities. The element sizes in the critical junction area and around the slot are set to 2 mm and 5 mm, respectively. The mesh is set to become increasingly coarse further away from the critical areas.

In areas where excessive penetration between elements is found, such as in the crotch formed by the shell and skirt, contact and target elements are specified. The convex outer surface of the toroidal vessel section is specified as the contact surface and meshed using 8-node CONTA174 surface elements, which is intended for general flexible-flexible contact analysis.

The cylindrical inner surface of the skirt is specified as the target surface and meshed using the corresponding TARGE170 target segments. Suggestions for best practice provided by the ANSYS Help Guide [22] were taken into account when selecting the contact and target surfaces. The contact type is set to 'Frictionless' and the formulation method is set to 'Augmented Lagrange' with a normal stiffness of 0.1. These settings allow for some penetration to occur for a significant decrease in computational expense. The maximum penetration found in any analysis solution in this chapter is about 0.02 mm.

Each of the solid models is given a similar mesh to ensure the differences in stress values come from changes in the geometry, rather than changes in the mesh itself. To accomplish this, mesh controls are used in various areas of the models to enforce element size and shape. These mesh controls are kept consistent between models. Sweep meshing is specified on all regular surfaces, such as rectangular and circular surfaces, to ensure a regular mesh that is easily duplicated. An unstructured mesh is used anywhere that a swept mesh will fail due to complex geometry, such as the area around the slot. One particular advantage of using an unstructured mesh around the slot area is the ability of the mesh to adapt to constantly changing geometries between models, as is the case in this optimization study. Due to the large circumferential deformation normally experienced by coke drums, bending stresses and contact near the junction corner are of particular concern. Thus, an adequate number of elements are specified through thickness in order to accurately capture the bending stress profile.

Due to the large computational expense of solving 3-D analyses, some steps are taken to simplify the geometry of the coke drum models while still maintaining validity. The entire coke drum may be treated as a body having cyclic symmetry about its vertical axis since the skirt slots are spaced evenly in the circumferential direction. Thus, a cyclic symmetric 'slice' of the entire

coke drum is used as the model domain as shown in Figure 2-4. In other words, the model domain extends circumferentially between the midpoints of a slot and its adjacent column. Also, the vessel model is cut radially at an axial distance equal to $2.5\sqrt{rt}$ above the junction weld, where *r* and *t* are the radius and thickness of the vessel, respectively. This distance represents the minimum distance for the calculation of surface temperature differences for the purposes of fatigue analysis screening as detailed in ASME Sec. VIII Div. 2 [23] As shown in Figure 2-4, the vessel section above the cut is discarded since it is not the focus of the current study. Appropriate boundary conditions are applied to the cut surfaces to simulate the presence of material, as will be explored in more detail in the next section.

Bilinear kinematic hardening plasticity model is used because of cyclic thermal and mechanical loading. In this way, low cycle fatigue and ratcheting behavior of the materials can be analyzed. For each analysis, two complete process cycles are solved in real time.

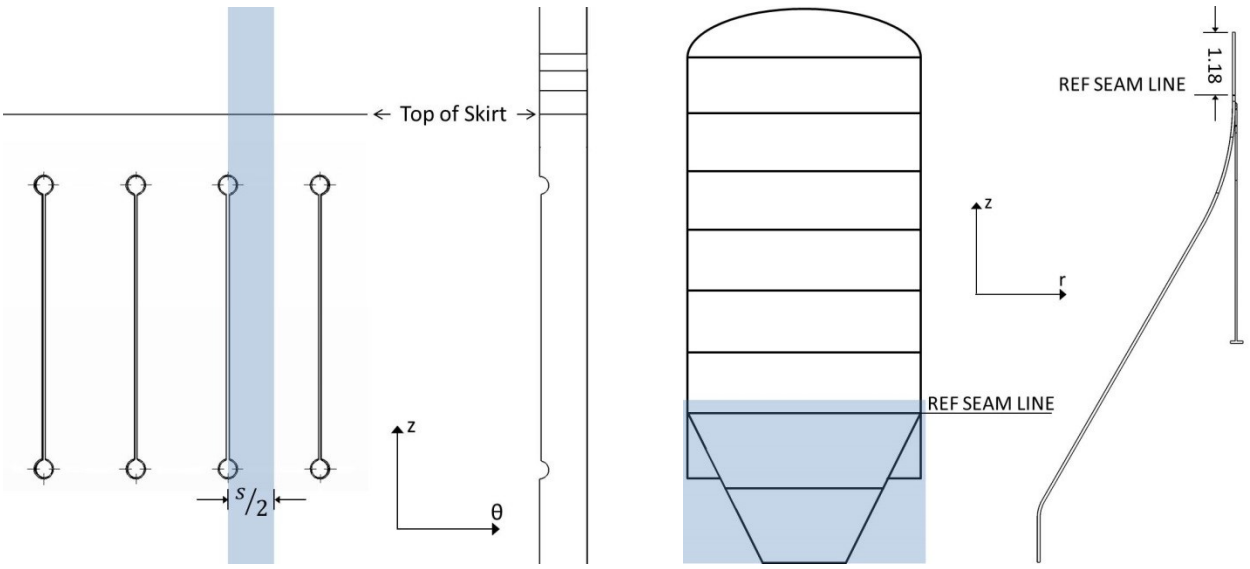

Figure 2-4: Simplification of model domain by cut boundaries

2.3.2 Boundary Conditions

The coupled analyses conducted in this study require a number of thermal and structural boundary conditions to simulate the temperature variation of the operating cycle. These boundary conditions are applied separately in ANSYS Workbench, as the thermal analysis is solved first and then its solution is transferred into the structural analysis as an imported load. The boundary conditions are described in detail below:

- Convective and pressure loads applied to the inner surfaces of the vessel. The corresponding pressures P, heat transfer coefficients h, and bulk temperatures T_b are summarized in Table 2-4 [8].
- Adiabatic boundary conditions specified on insulated surfaces and all cut surfaces.
    - Xia et al. [8] previously concluded that the layer of insulation can be simulated by a simple adiabatic boundary condition with minimal effect on the solution.
- Fixed support boundary condition is applied to the skirt base.
    - Simulates the skirt being bolted to a concrete support structure. It is assumed to have simple geometry and perfect contact with the concrete since the method of attachment will not be discussed in the current study.
- Circumferential displacement is set to zero at all cyclic symmetry cut boundaries.
    - This condition is critical to maintain the validity of the cyclic symmetry of the structural model.
- Pressure loads equivalent to the forces applied by the weight of the drum, as well as internal and hydrostatic pressures are applied to the top and bottom cut surfaces

- 'Plane-remains-plane' condition are applied to the top and bottom cut surfaces to simulate the discarded sections of the vessel
    - 'Plane-remains-plane' condition is achieved by coupling the nodal vertical displacements such that all nodes on the cut surfaces move equally in the vertical direction.

Table 2-4: Prescribed Boundary Conditions for Each Process Stage [8]

Process Stage	Time (s)	h (W/m^{2o}C)	T_b (°C)	P (kPa)
Steam Testing **(ST)**	7200	113.4	142	300
Vapor Heating **(VH)**	7200	54.9	316	300
Oil Filling **(OF)**	36000	141	482	300 + P_s*
Water Quenching **(WQ)**	7200	345	93	300 + P_s*
Unheading **(UH)**	5400	63.7	38	120

* P_s is the hydrostatic pressure due to the coke, oil and water slurry at 80% drum capacity

2.3.3 Model Simplifications

For the purposes of reducing computational expense further in order to complete many analyses in a short timeframe, some simplifications were made which may directly affect the results. Firstly, the transient thermal loads used to simulate the oil filling and water quenching stages of each cycle are applied to the all inner surface nodes simultaneously to reduce the number of load steps required. In reality, the oil and water fill the drum at a finite rise speed. Furthermore, features such as fillets around the slot edges are omitted from the models.

The above simplifications are justifiable since the results from each of the models will be compared in the next chapter to obtain an optimized slot design. It can be said that as long as the

same simplifications are applied to each model, the differences in stress and strain response will still provide a valid understanding of the effect of each slot design. The designs which are deemed most effective at protecting the junction weld and slot area based on results obtained in Chapters 2 and 3 will be re-analyzed in more detail in Chapter 4. In those analyses, the effect of rising quench water level is included, the models are given more refined meshes, and fillets are added around the slots for a more accurate solution.

2.4 Thermal-Elastoplastic Finite Element Analysis Results

2.4.1 Thermal Analysis

The calculated temperature history at the inner junction face of both designs is shown in Figure 2-5 for a single cycle. It is obvious from the figure that the coke drum experiences several instances of thermal shock corresponding to the start of each cycle phase which result in thermal gradients. Each of these instances is labeled with a letter for future reference. It is found that the calculated results from the thermal analysis are in good agreement with measured results of an identical coke drum from previous literature [8].

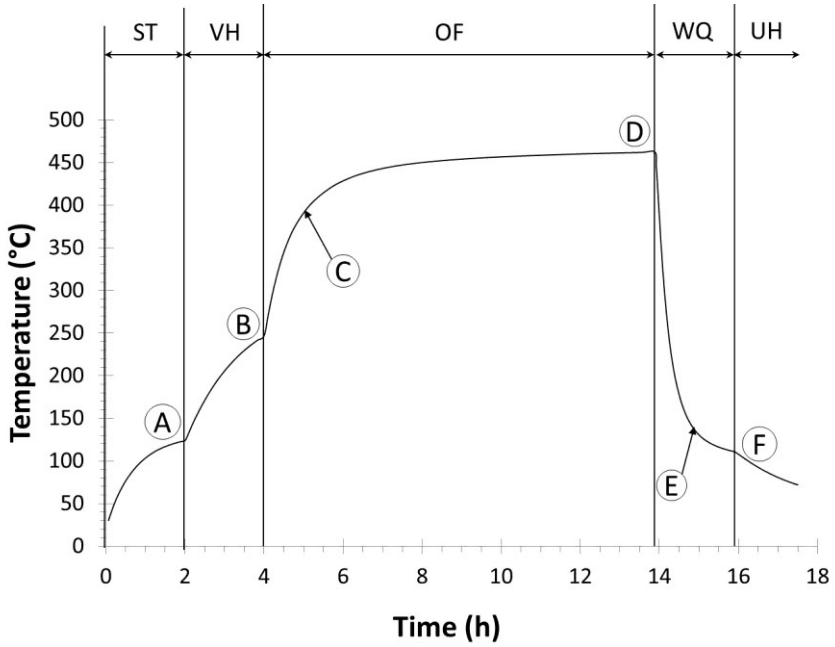

Figure 2-5: Temperature history of a point on inner junction face surface over a complete operation cycle

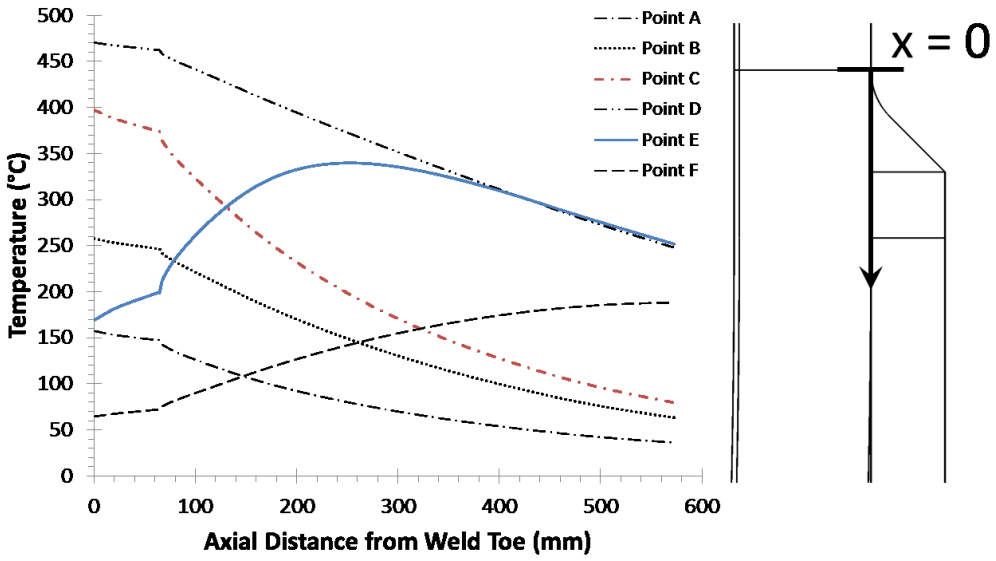

Figure 2-6: Axial (z-direction) thermal gradients of inner skirt surface at each time point

The vertical temperature distribution along the inner surface of the skirt starting at the weld toe is plotted in Figure 2-6 for each time point. Evidently, the most severe temperature gradient along the skirt vertical (z-) direction occurs during the quenching phase as the temperature of the vessel drops quickly while the skirt maintains a relatively elevated

temperature. This effect is clearly shown from the curve corresponding to the start of the quench phase (Point E). The temperature profile starts from a minimum of about 170°C at the weld toe and gradually increases through the weld build-up to about 200°C. At the point where the skirt begins, the temperature increases to about 340°C in the span of about 19 cm before gradually decreasing. The temperature profile during the quench stage described above is due to the rapid cooling of the inner surface of the drum while heat is retained in the skirt further away from the point of attachment. Another large thermal gradient occurs at the start of the oil filling stage. In this case, the temperature profile starts from a maximum of about 370°C and decreases to about 230°C over the same span.

The through-thickness radial (r-) thermal gradient is shown in Figure 2-6 for the oil filling and water quenching phases. The x-axis from this figure represents the distance from the inner surface of the drum (x = 0 mm) to the outer surface of the skirt (x = 79.4 mm) along the junction face. It is obvious that the quench phase of the coking cycle induces a more severe radial thermal gradient than the oil filling phase. The quench phase represents a temperature difference of about 100°C between the inner and outer surfaces, whereas the oil filling phase causes a temperature difference of about 50°C. As will be shown in the next section, the peak stress/strain in the junction weld and slot area will occur during one of these stages, or both.

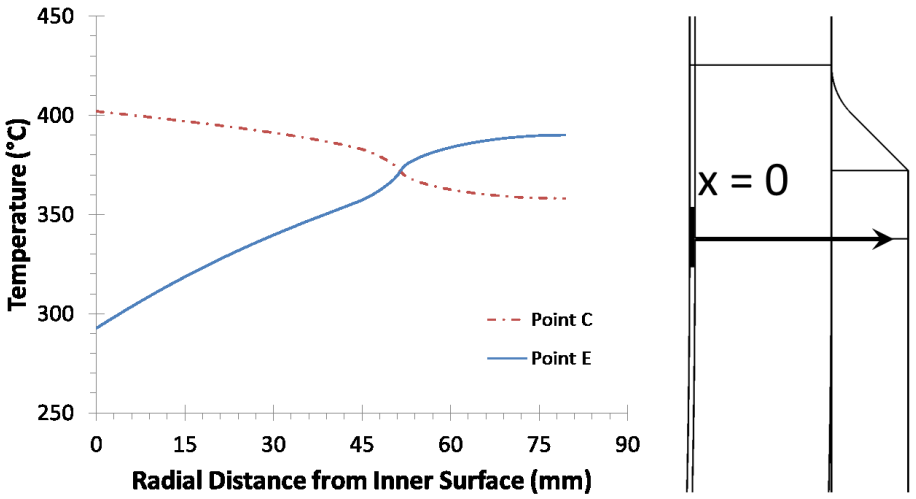

Figure 2-7: Through-thickness temperature distribution at junction face during Oil Filling and Water Quenching stages

2.4.2 Skirt Deformation

The effects of the aforementioned thermal gradients on skirt deformation during each of the oil filling and water quenching phases are shown in Figure 2-8. The deformation is scaled by a factor of 8 for ease of viewing. During the oil filling stage, the hot vessel encounters the cold skirt and forces it outward causing high compressive and tensile axial stresses on the inner and outer junction surfaces, respectively. As the quench water rises in the vessel, the rapidly cooling vessel contracts and pulls the hot skirt inward causing the opposite to occur. This deformation response is typical for each of the coke drum analyses conducted in this study.

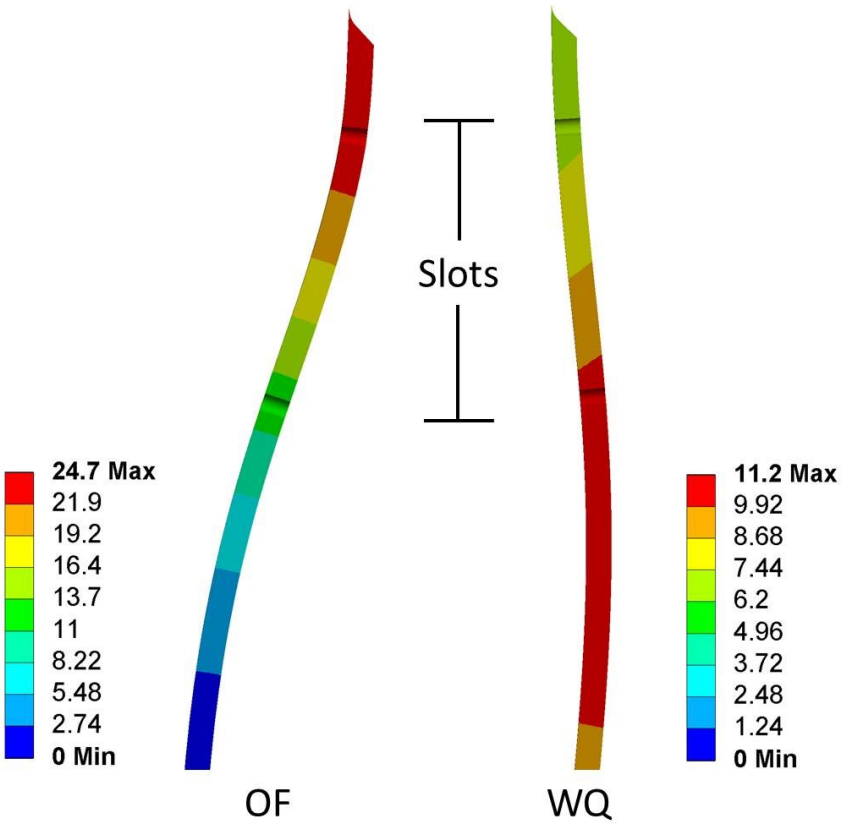

Figure 2-8: Skirt deformation response during oil filling (left) and water quenching (right) stages scaled by a factor of 8. Values in mm.

2.4.3 Comparison of Un-Slotted and Slotted Skirt Junction Stress/Strain Responses

The stress and strain responses at the inner junction location of each model are shown in Figure 2-9 to Figure 2-12 and summarized in Table 2-5 and Table 2-6. As expected from the deformation profile, the axial strain component is the major contributor to the overall strain response. Also, a multi-axial cyclic stress state is found to occur at the junction inner junction location due to cyclic compressive and tensile stresses during the heating and cooling stages, respectively. However, it can be seen that the combination of rapid contraction due to cooling and the geometry of the shell-to-skirt crotch area causes the stresses to be larger in tension than in compression at the inner junction location. Thus, the maximum junction stress and strain in both designs are found to occur during the quench stage. For the same reason, the maximum

stresses/strains and stress amplitudes are much higher at the inner junction location than at the outer surface.

The maximum equivalent stress at the inner junction of the NS design is found to exceed the yield strength of the material at the mean cycle temperature of 250°C. Hence, it can be seen that plastic deformation occurs as shown by the existence of plastic strain in Table 2-5. However, at the inner junction location of the OS design, a small amount of plastic strain occurs despite the maximum equivalent stress being lower than the yield strength as can be seen in Table 2-6. Thus, it is determined that the maximum equivalent stress results are not fully representative of the junction stress state and that the individual stress amplitudes a more reliable tool for comparison due to the multi-axial stress state.

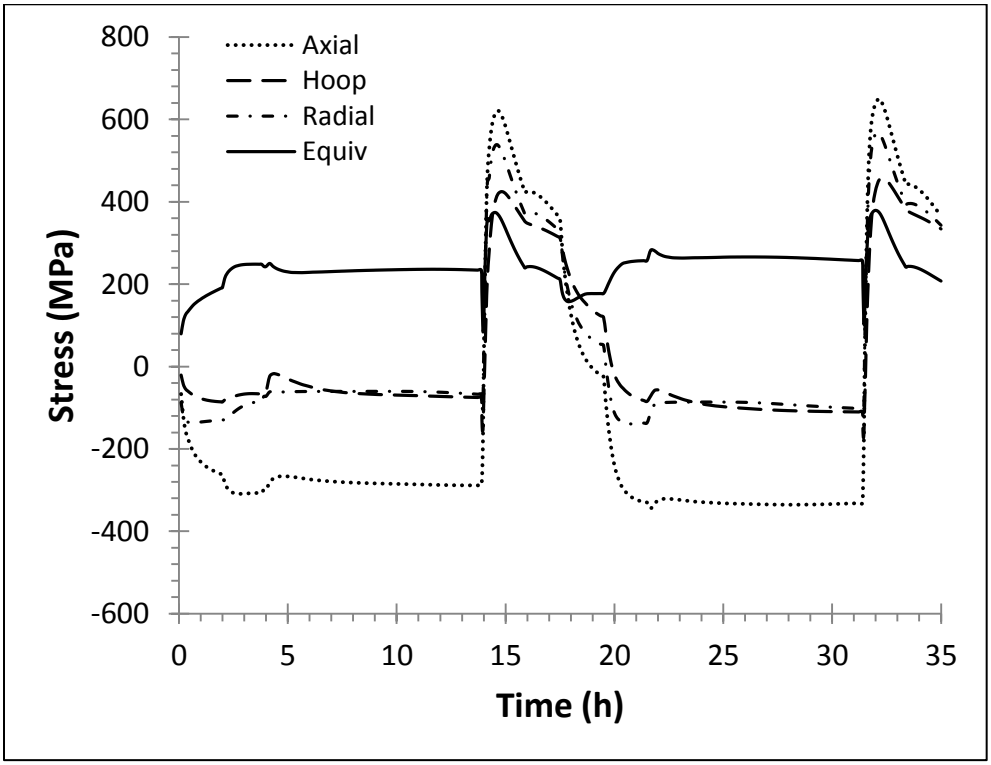

Figure 2-9: Stress components at the inner junction face of the No Slot (NS) model over two complete operation cycles

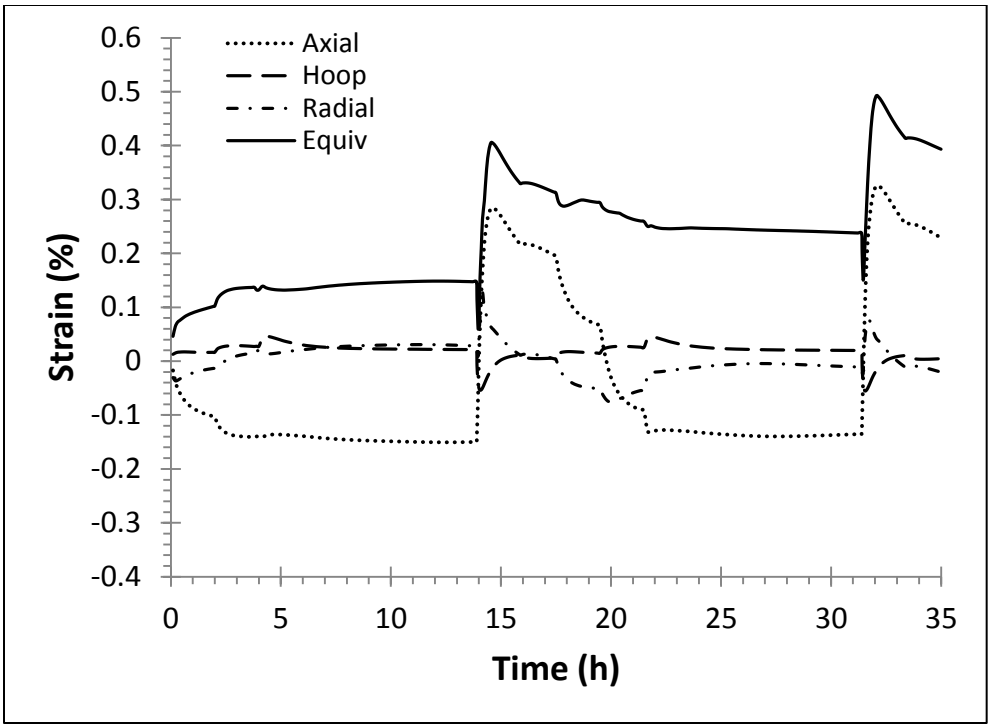

Figure 2-10: Mechanical strain components at the inner junction face of the No Slot (NS) model over two complete operation cycles

Table 2-5: Summary of stress and strain results at the inner junction face of the No Slot (NS) model

	Cycle 1				Cycle 2			
Stress (MPa)	Min	Max	Amp.	Mean	Min	Max	Amp.	Mean
Axial	-309.0	621.4	465.2	156.2	-344.1	650.1	497.1	153.0
Hoop	-157.1	424.4	290.8	133.7	-173.2	457.5	315.3	142.2
Radial	-136.6	537.7	337.2	200.6	-139.3	568.3	353.8	214.5
Mises	-	373.8	-	-	-	378.8	-	-
Strain (%)	Min	Max	Amp.	Mean	Min	Max	Amp.	Mean
Axial	-0.151	0.284	0.218	0.067	-0.140	0.326	0.233	0.093
Hoop	-0.054	0.046	0.050	-0.004	-0.055	0.045	0.050	-0.005
Radial	-0.036	0.128	0.082	0.046	-0.076	0.074	0.075	-0.001
Mises	-	0.405	-	-	-	0.493	-	-
Eqv. Plastic	-	0.200	-	-	-	0.282	-	-

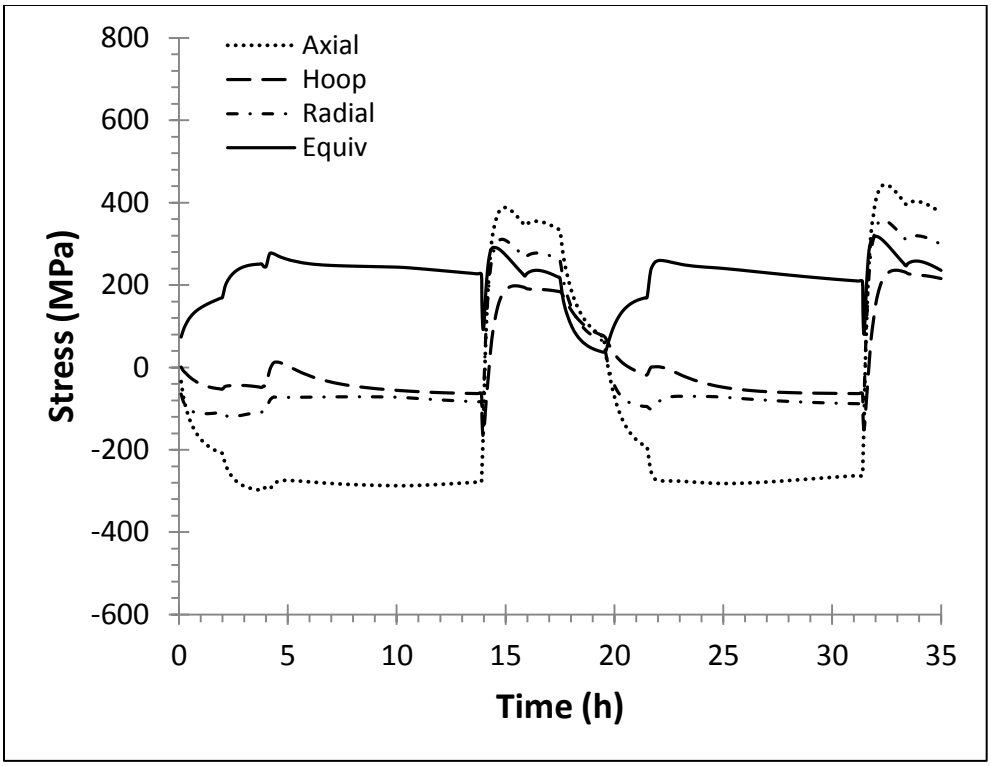

Figure 2-11: Stress components at the inner junction face of the Original Slot (OS) model over two complete operation cycles

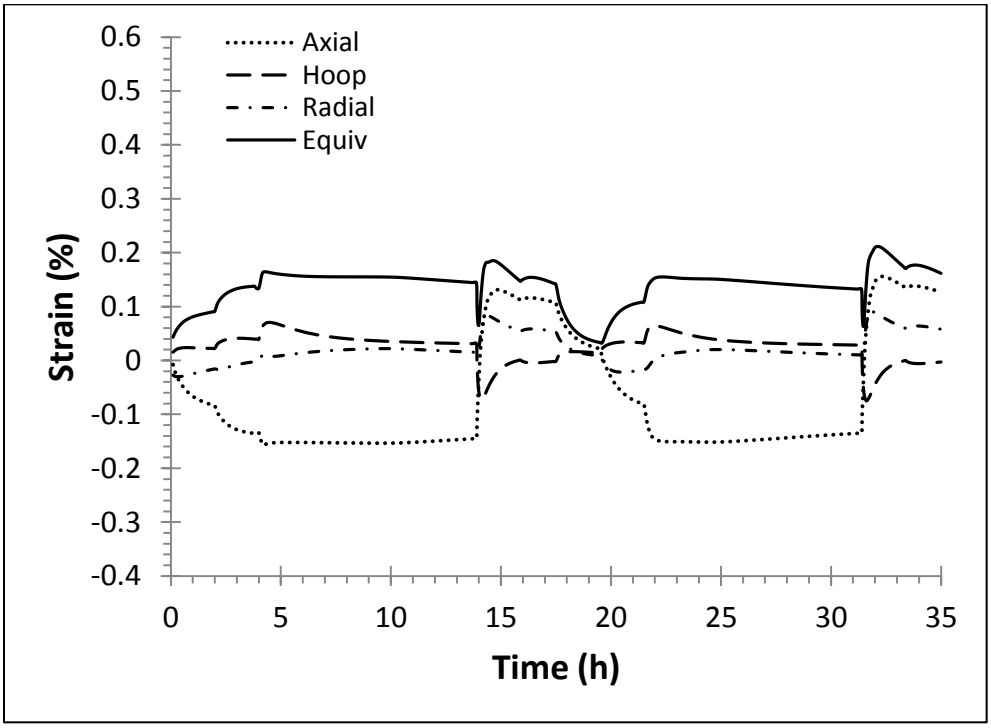

Figure 2-12: Mechanical strain components at the inner junction face of the Original Slot (OS) model over two complete operation cycles

Table 2-6: Summary of stress and strain results at the inner junction face of the Original Slot (OS) model

	Cycle 1				Cycle 2			
Stress (MPa)	Min	Max	Amp.	Mean	Min	Max	Amp.	Mean
Axial	-298.3	388.2	343.2	44.9	-281.9	443.2	362.5	80.7
Hoop	-165.8	198.1	181.9	16.1	-150.6	235.9	193.3	42.6
Radial	-119.8	311.0	215.4	95.6	-101.0	358.2	229.6	128.6
Equiv.	-	291.0	-	-	-	318.3	-	-
Strain (%)	Min	Max	Amp.	Mean	Min	Max	Amp.	Mean
Axial	-0.156	0.131	0.144	-0.012	-0.152	0.156	0.154	0.002
Hoop	-0.072	0.071	0.071	-0.001	-0.075	0.064	0.070	-0.005
Radial	-0.030	0.083	0.056	0.026	-0.022	0.090	0.056	0.034
Equiv.	0.043	0.185	-	-	0.032	0.211	-	-
Eqv. Plastic	-	0.010	-	-	-	0.026	-	-

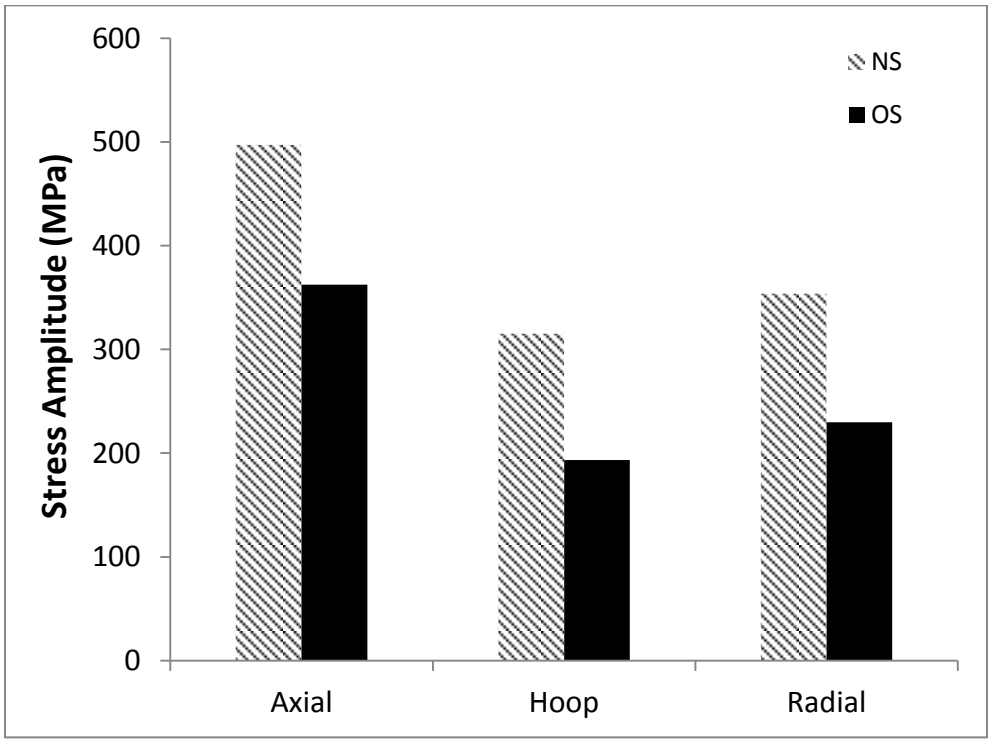

Figure 2-13: Comparison of second-cycle stress component amplitudes at the inner junction face location

The comparison of second-cycle stress amplitudes at the inner junction surface of the NS and OS designs are shown graphically in Figure 2-13. It can be seen that the inclusion of skirt slots causes a significant decrease in each of the examined stress amplitudes. As a result, a significant reduction in plastic strain occurs at the critical inner junction face. The percent changes of these values are summarized in Table 2-7. Thus, it can be concluded from the standpoint of stress and strain reduction that the original skirt slot examined in this section provides substantial protection of the junction weld.

Table 2-7: Percent difference due to inclusion of skirt slots on maximum equivalent stress and plastic strain at the inner junction face location

Value	Cycle 1	Cycle 2
Equivalent Stress	-22.1%	-16.0%
Plastic Strain	-94.9%	-90.9%

2.4.4 Stress and Strain Response in Slot Area of Original Slot (OS) Model

The slotted section of the skirt is analyzed using results from three critical areas of interest as shown in Figure 2-14. These areas were chosen due to the existence of stress concentration effects around the top and bottom keyholes. The stress and strain histories at the critical areas of the slotted area are shown in Figure 2-15 to Figure 2-20. The slot area stress and strain results are summarized in Table 2-8 to Table 2-10.

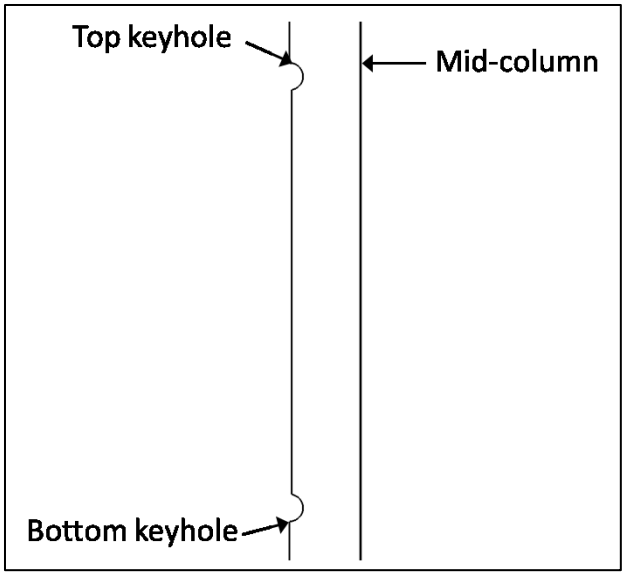

Figure 2-14: Locations of the critical areas of interest around the slot

It is found that tensile and compressive hoop stresses are the main contributor to the overall stress level at the slot ends during the oil filling and water quenching stages, respectively. It can be seen that the maximum stress magnitude during the oil filling stage is either close to or exceeds the stress magnitude during the quench stage. Furthermore, the maximum equivalent stress at both slot ends exceeds the yield strength of the material, and more severely, nearly fully reversed hoop stress histories occur. Also, the stress amplitudes experienced by the top and bottom keyholes do not differ significantly, whereas the strain level in the top keyhole is found to be much higher. The difference in strain response can be explained by the difference in maximum temperature at each keyhole as previously shown by the thermal gradient in Figure 2-6. It should also be noted that the peak stress at the top keyhole location is greater than that of the bottom keyhole during each quench stage. At the mid-column location, the axial stress component (compressive during oil fill, tensile during water quench) is shown to be the main contributor to the equivalent stress, which also exceeds the base metal yield strength. However, the maximum strain experienced by the mid-column location is still much lower than near the top keyhole.

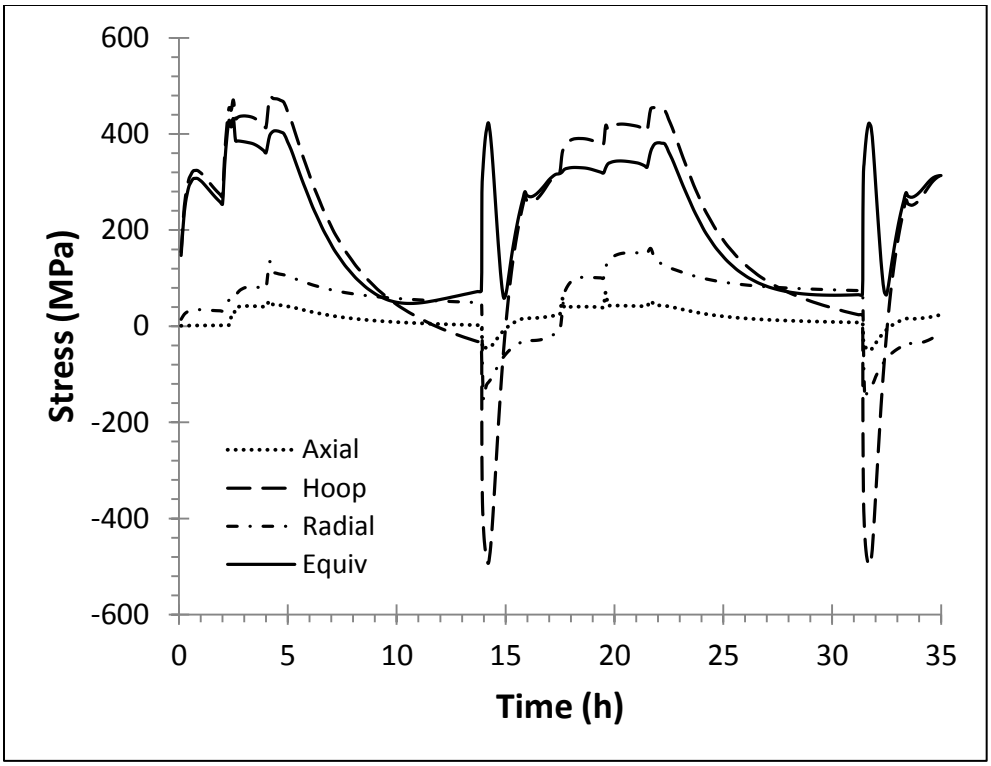

Figure 2-15: Stress components at the top keyhole of the Original Slot (OS) model over two complete operation cycles

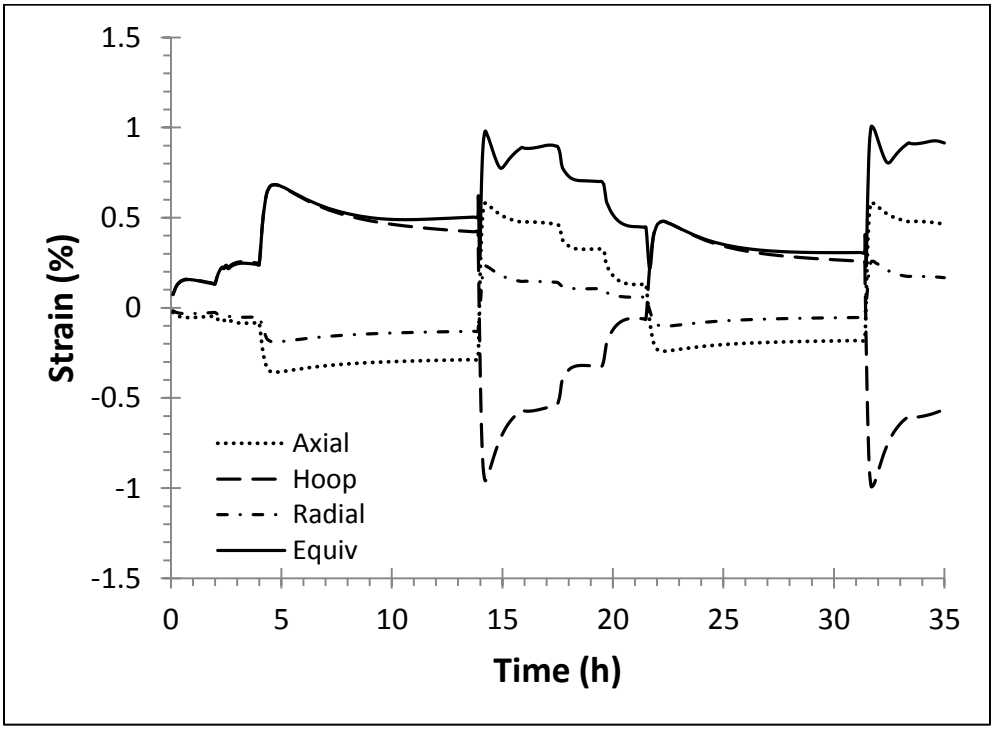

Figure 2-16: Mechanical strain components at the top keyhole of the Original Slot (OS) model over two complete operation cycles

Table 2-8: Summary of stress and strain results at the top keyhole of the Original Slot (OS) model

	Cycle 1				Cycle 2			
Stress (MPa)	Min	Max	Amp.	Mean	Min	Max	Amp.	Mean
Axial	-45.3	53.3	49.3	4.0	-49.1	70.3	59.7	10.6
Hoop	-492.7	477.2	484.9	-7.7	-497.3	455.5	476.4	-20.9
Radial	-152.6	133.7	143.2	-9.5	-150.6	161.9	156.3	5.6
Equiv.	-	431.6	-	-	-	422.7	-	-
Strain (%)	Min	Max	Amp.	Mean	Min	Max	Amp.	Mean
Axial	-0.357	0.580	0.469	0.112	-0.241	0.585	0.413	0.172
Hoop	-0.957	0.682	0.820	-0.138	-0.991	0.480	0.736	-0.255
Radial	-0.189	0.231	0.210	0.021	-0.103	0.258	0.180	0.078
Equiv.	-	0.979	-	-	-	1.006	-	-
Eqv. Plastic	-	0.743	-	-	-	0.769	-	-

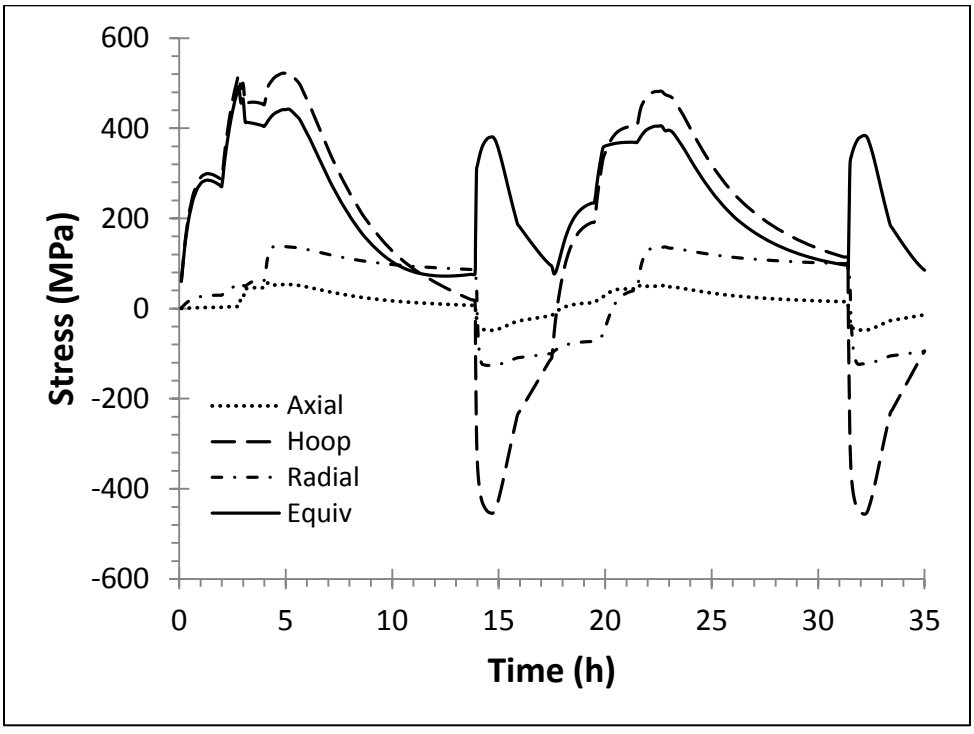

Figure 2-17: Stress components at the bottom keyhole of the Original Slot (OS) model over two complete operation cycles

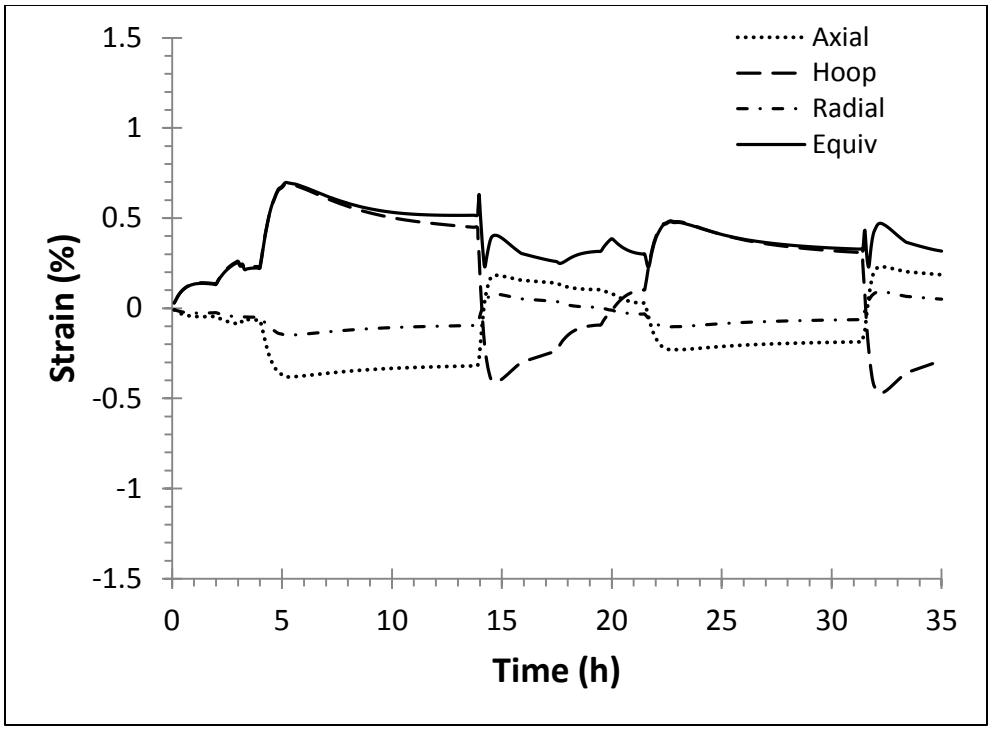

Figure 2-18: Mechanical strain components at the bottom keyhole of the Original Slot (OS) model over two complete operation cycles

Table 2-9: Summary of stress and strain results at the bottom keyhole of the Original Slot (OS) model

	Cycle 1				Cycle 2			
Stress (MPa)	Min	Max	Amp.	Mean	Min	Max	Amp.	Mean
Axial	-48.3	57.0	52.7	4.3	-48.1	53.3	50.7	2.6
Hoop	-454.1	522.9	488.5	34.4	-456.3	482.1	469.2	12.9
Radial	-126.5	138.6	132.5	6.0	-123.8	136.9	130.4	6.6
Equiv.	-	492.0	-	-	-	405.0	-	-
Strain (%)	Min	Max	Amp.	Mean	Min	Max	Amp.	Mean
Axial	-0.381	0.183	0.282	-0.099	-0.231	0.231	0.231	0.000
Hoop	-0.410	0.689	0.549	0.140	-0.473	0.485	0.479	0.006
Radial	-0.150	0.079	0.114	-0.035	-0.103	0.093	0.098	-0.005
Equiv.	-	0.724	-	-	-	0.505	-	-
Eqv. Plastic	-	0.494	-	-	-	0.294	-	-

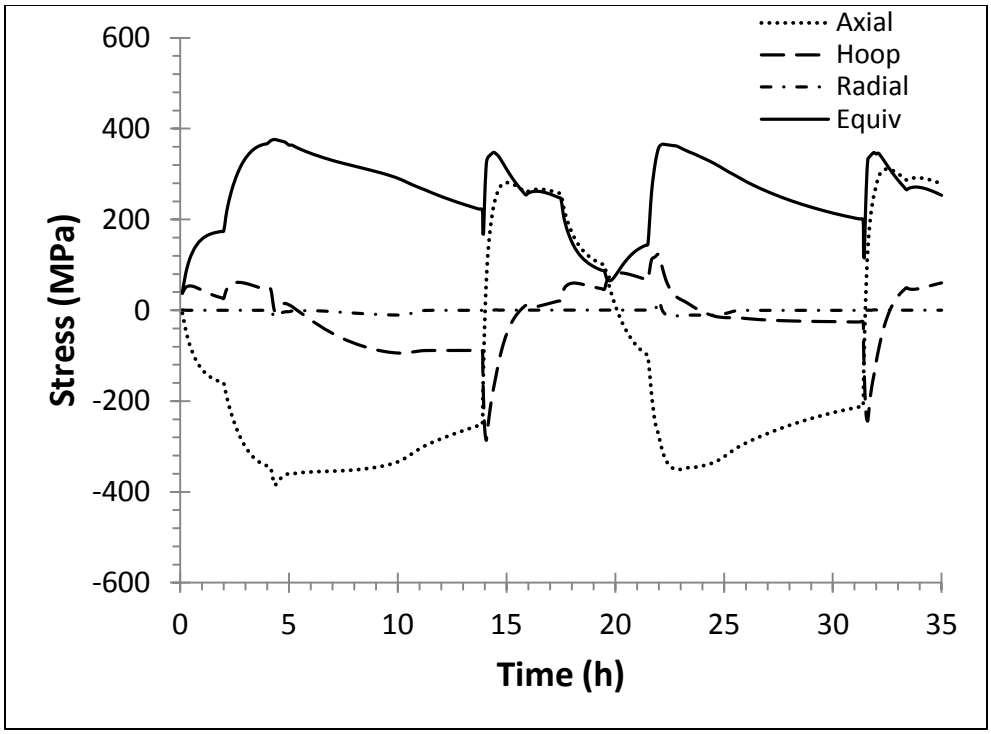

Figure 2-19: Stress components at the mid-column location of the Original Slot (OS) model over two complete operation cycles

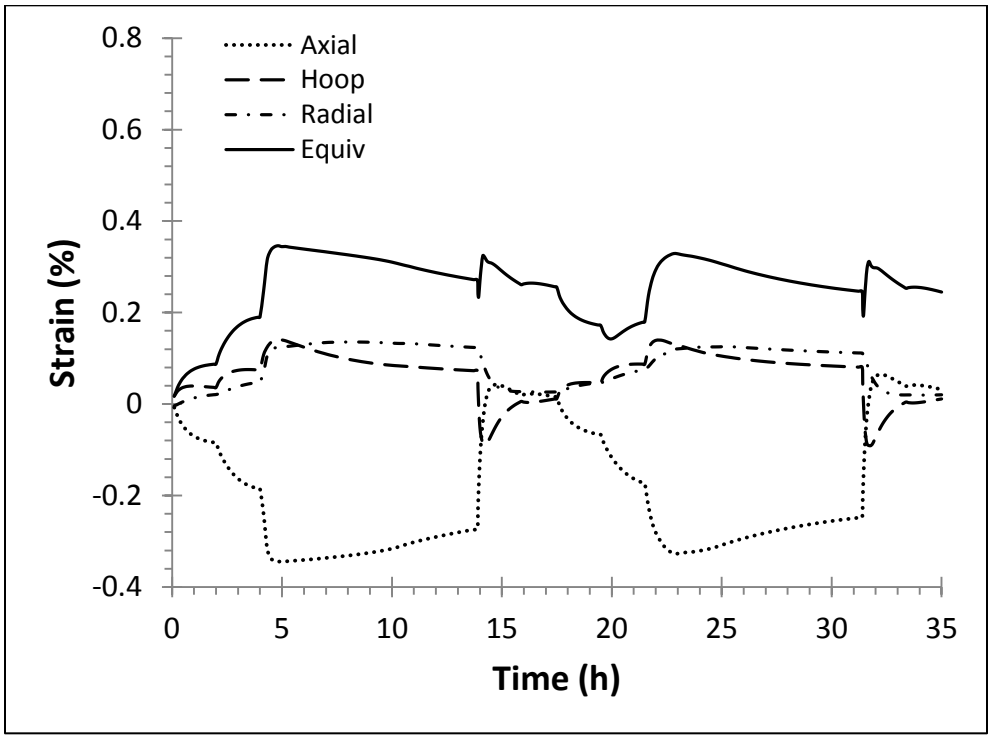

Figure 2-20: Mechanical strain components at the mid-column location of the Original Slot (OS) model over two complete operation cycles

Table 2-10: Summary of stress and strain results at the mid-column location of the Original Slot (OS) model

	Cycle 1				Cycle 2			
Stress (MPa)	Min	Max	Amp.	Mean	Min	Max	Amp.	Mean
Axial	-383.5	281.2	332.3	-51.2	-351.2	311.2	331.2	-20.0
Hoop	-285.7	61.5	173.6	-112.1	-243.5	122.4	182.9	-60.5
Radial	-15.2	1.2	8.2	-7.0	-13.1	21.4	17.2	4.1
Equiv.	-	376.1	-	-	-	365.5	-	-
Strain (%)	Min	Max	Amp.	Mean	Min	Max	Amp.	Mean
Axial	-0.345	0.042	0.194	-0.151	-0.327	0.065	0.196	-0.131
Hoop	-0.089	0.142	0.116	0.026	-0.091	0.140	0.115	0.025
Radial	-0.004	0.136	0.070	0.066	0.020	0.126	0.053	0.073
Equiv.	-	0.354	-	-	-	0.347	-	-
Eqv. Plastic	-	0.150	-	-	-	0.144	-	-

2.4.5 Comparison of Stress/Strain Response at Critical Locations of NS and OS Designs

It can be seen from the previous sections that the point on the skirt which experiences the maximum equivalent stress and plastic strain migrates from the inner junction surface to the top keyhole area after the inclusion of skirt slots. The equivalent stress and plastic strain profiles of the critical points are compared in Figure 2-21 and Figure 2-22.

As Figure 2-21 shows, the equivalent stress profiles differ significantly. Both critical points experience stress peaks exceeding the yield strength of the material during the quench stage. However, the top keyhole of the original slot (OS) model experiences an additional plasticity-inducing stress peak during the oil filling stage. Furthermore, the magnitude of the peak stress during the quench stage is significantly greater in the top keyhole of the skirt slot. Hence, the top keyhole of the OS model is subject to more severe plastic deformation compared to the inner junction surface of the NS model, as shown in Figure 2-22.

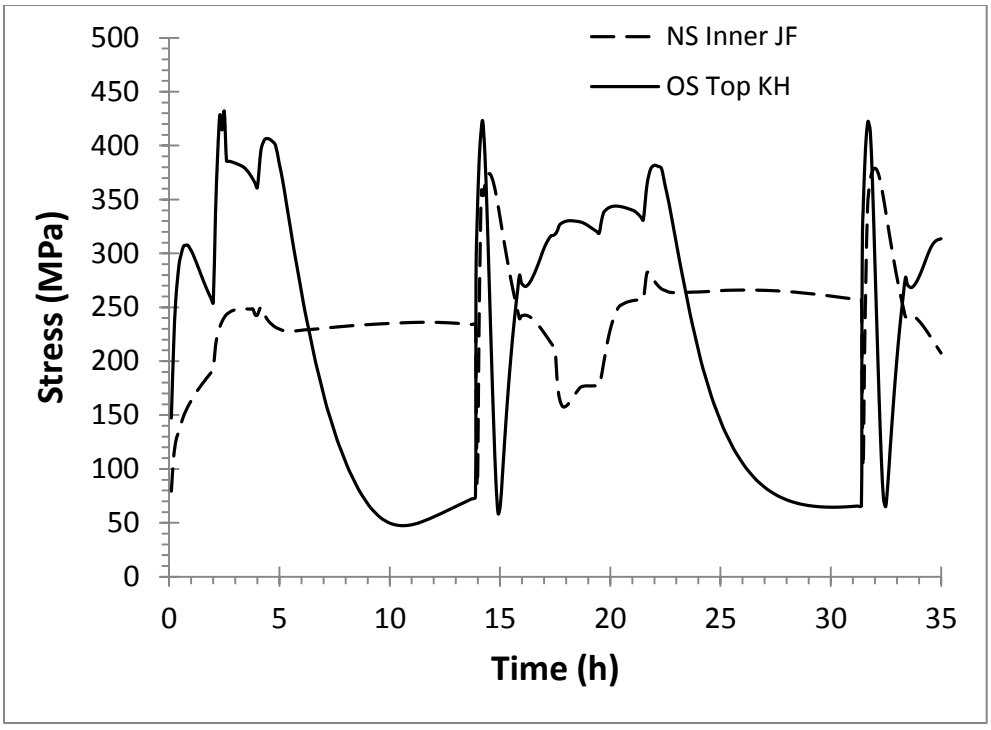

Figure 2-21: Comparison of equivalent stress profiles at critical points in NS and OS models

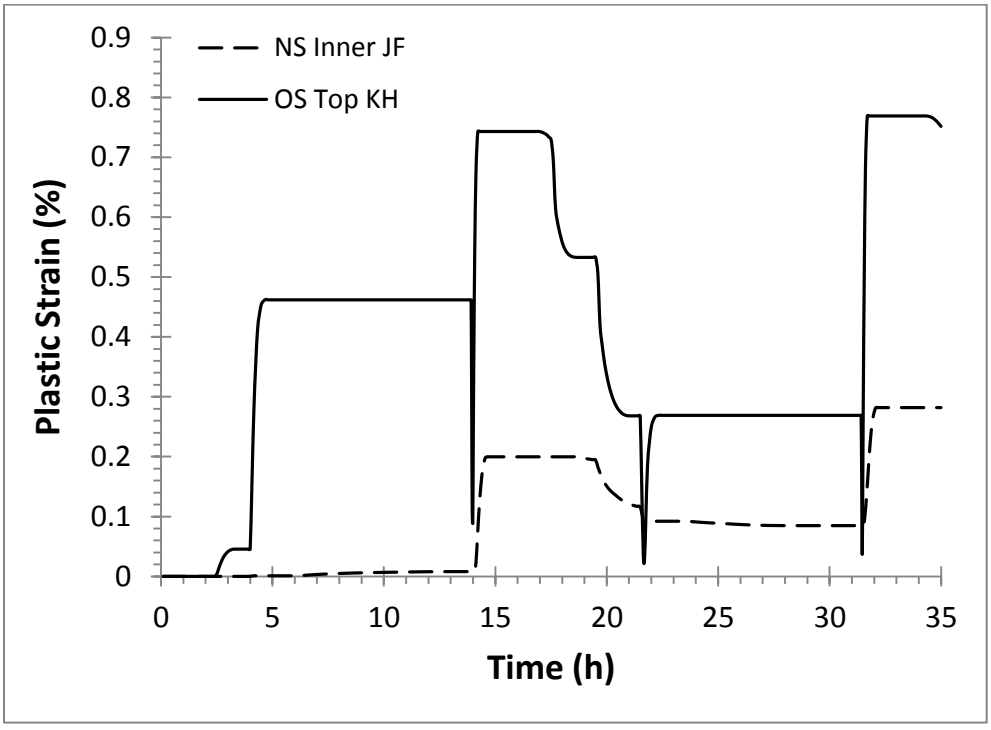

Figure 2-22: Comparison of equivalent plastic strain profiles at critical points in NS and OS models

2.5 Summary

Two finite element models of identical coke drum vessels with different skirt designs are solved and compared using stress and strain results at critical areas of interest. It is found for both designs that the peak stress and strain occurs on the inner side of the top of the skirt during each water quenching stage. Bending stress about the circumference of the weld is found to be the major contributor to the overall stress and strain state at the point of peak equivalent stress. Severe stress cycling in the No Slot (NS) model is found to cause high levels of plastic strain at the critical skirt-to-shell junction location. Stress and strain results from the junction of the Original Slot (OS) model show that the inclusion of a conventional slot design causes significant reduction cyclic stress amplitudes of each of the main contributory stress components (axial, hoop, and radial) compared to the NS model. As a result, the peak equivalent stresses and plastic strains are significantly lower in the junction.

The areas near the ends of the slots (keyholes) are found to be adversely affected by stress concentration effects. Both keyholes experience similar magnitudes of cyclic stress amplitude and significant plastic strain. The peak strain near the top keyhole is found to be more than double than that of the bottom keyhole by the second cycle. Furthermore, the maximum plastic strain near the top keyhole is found to be about 30 times greater than that of the inner junction surface. Cyclic stresses causing plastic deformation are also found at the mid-column location between two slots. However, the level of plastic strain at the mid-column location is not critical since it does not exceed the peak plastic strain at the inner junction surface.

CHAPTER 3 PARAMETRIC STUDY OF SKIRT SLOT DIMENSIONS USING THERMAL-ELASTOPLASTIC FINITE ELEMENT ANALYSIS

3.1 Introduction

In this chapter, slot dimensions are optimized to minimize stress and strain ranges in the junction and slot area of the coke drum presented in the previous chapter. To accomplish this, 3-D cyclic-symmetrical finite element models identical to the ones introduced in the previous chapter will be used to analyze and compare each slot design. Slot width, length, and vertical distance from weld are independently altered from the original slot design. Each incremental change in any slot dimension is treated as a separate slot design model and solved separately. The process parameters, boundary conditions, analysis settings, and mesh density are kept constant throughout each analysis to ensure differences in stress and strain response are solely due to changes in slot geometry.

Stress and strain results from four areas of interest (inner junction, top and bottom keyholes, and mid-column) are used to compare the effectiveness of each design. Each of the slot designs will be compared to the stress and strain response of the Original Slot (OS) model as presented in the previous chapter. The primary goal is to minimize the magnitude of stress amplitude and plastic strain in the junction area to reduce the likelihood of cracks forming near the attachment weld. The same approach is applied to the slot area to reduce premature cracking at the slot ends and ensure that the columns between the slots are able to endure cyclic expansion and contraction of the drum.

3.2 Skirt Slot Design Methodology

A total of 10 skirt slot designs are examined in this section. Each design is created by incrementally changing one skirt slot dimension while keeping all of the other dimensions constant. Thus, each design is assigned a name referencing the dimension being altered (L, D, or W) followed by the numerical value of the dimension in inches. For example, a slot design with a length of 8 inches (203 mm) would be named L8. Examples of the examined slot designs are shown annotated with dimensions in Figure 3-1. The slot design shown to the left in Figure 3-1 mimics the Original Slot design examined in the previous chapter, while the "wide slot" design shown to the right is used to determine the effect of changing slot width on the stress and strain profiles. The values of the dimensions characterizing each design are shown in Table 3-1.

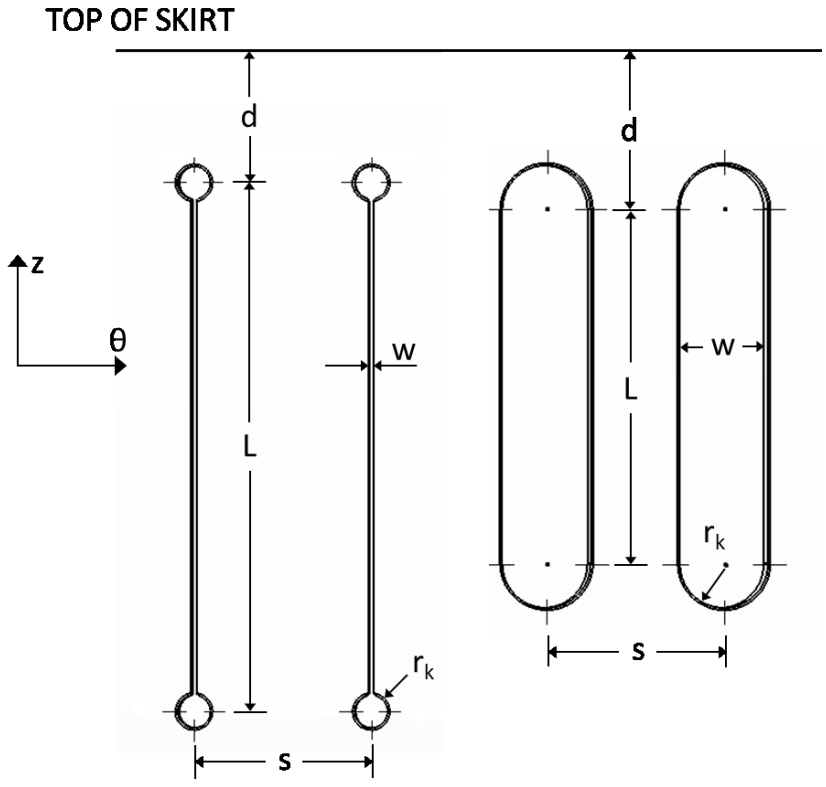

Figure 3-1: Schematic of examined skirt slot designs annotated with dimensions (Left: Original slot width; Right: Increased slot width)

Table 3-1: Characteristic dimension values for each of the examined skirt slot designs

L		*d*		*w*	
(mm)	(in)	(mm)	(in)	(mm)	(in)
254	10	25.4	1	25.4	1
203	8	50.8	2	50.8	2
152	6	102	4	76.2	3
		127	5		

When altering the slot dimensions, an important issue which arises is the ability of the slotted section of the skirt to withstand buckling failure due to the weight of the drum. Hence, by approximating the slotted section of the skirt by a series of columns separated by slots and applying basic column buckling theory, some dimensional constraints can be set. The main dimensions which influence buckling strength are slot length, width, and circumferential spacing. The slot spacing is kept constant throughout each of designs in order to keep similarity between cyclic symmetric finite element models of the coke drum. Furthermore, the effect of altering the circumferential spacing between slots can also be achieved by altering the slot width. Based on the buckling calculations, the load experienced by the slotted section of the Original Slot (OS) model is within 10% of the critical buckling load with a safety factor of 3 applied. It is determined based on these findings that a longer version of the original slot design would result in a skirt design which does not meet the buckling failure criteria. However, wider slots can be made to meet the criteria if the slot length is decreased accordingly. The results from the buckling failure analysis are summarized in Table 3-2.

Table 3-2: Effect of altering slot width and length on critical buckling load of slotted section

Dimensions (mm)		W_T/F_{crit}	Description
w	L		
3.175	304.8	1.07	Original Slot
3.175	406.4	**1.46**	Length increased by 101.6 mm (4")
25.4	304.8	**1.38**	Width increased by 22.2 mm (0.875")
25.4	254	0.96	Width increased by 22.2 mm and length decreased by 50.8 mm (2")

*W_T = weight of coke drum and its contents at maximum capacity

3.3 Model Set-Up

The cyclic-symmetric finite element models used in this chapter are almost identical to the models described in CHAPTER 2, with changes only occurring in the slot geometry. For a detailed description of the model set-up, refer to Section 2.3. The important dimensions and constraints are summarized below:

- The vessels are roughly 36 m (120 ft) tall and 9 m (29 ft) inner diameter. The skirt support structure is about 4.5 m in height and 2.86 cm (1.125 in) thick. Detailed schematics of the vessel and junction weld dimensions can be found in Figure 2-1 and Figure 2-2.
- The original skirt slots are 7.62 cm (3 in) from the top of the skirt, span 30.48 cm (12 in) in the axial direction, and evenly spaced every 10.16 cm (4 in) in the circumferential direction for a total of 277 slots. The slots terminate in drilled and chamfered 1.905 cm (3/4 in) diameter circular holes. A detailed schematic of the skirt slot dimensions is shown in Figure 3-1.

- The model is given material properties of SA387 Grade 12 Class 2 base metal and TP410S clad metal, as summarized in Table 2-2 and Table 2-3, respectively.
- Convective and pressure loads, summarized in Table 2-4, are applied to the inner surfaces of the vessel to simulate the process cycle.
- Adiabatic boundary conditions specified on insulated surfaces and all cut surfaces.
- Fixed support boundary condition is applied to the skirt base.
- Circumferential displacement is set to zero at all cyclic symmetry cut boundaries.
- Pressure loads equivalent to the forces applied by the weight of the drum, as well as internal and hydrostatic pressures are applied to the top and bottom cut surfaces.
- 'Plane-remains-plane' condition is applied to the cut surfaces to simulate the discarded sections of the vessel.

3.4 Thermal Analysis Results

The effect of altering slot dimensions on the thermal solution is determined by comparing the axial thermal gradient of each skirt design during the water quenching stage. The results from the thermal analysis of the Original Slot (OS) model are used as a basis of comparison. Figure 3-2 to Figure 3-4 show the axial temperature distribution starting from the weld toe (point of attachment) and moving down along the inner side of each skirt. The temperature distributions shown occur at a point in time roughly 0.8 hours after the beginning of the quench stage.

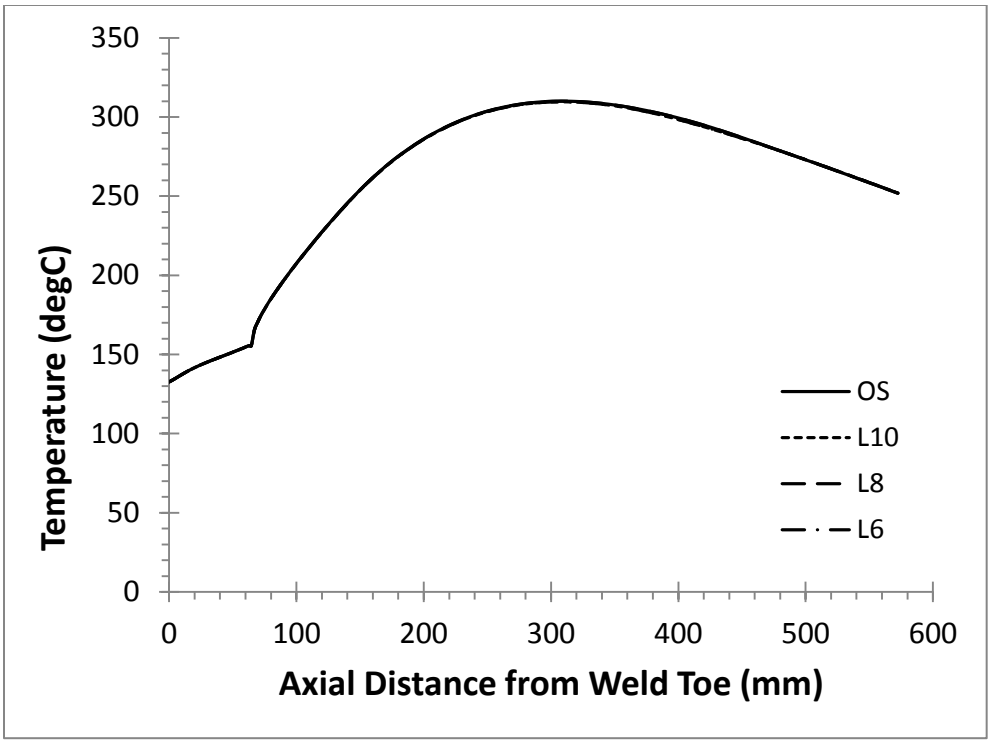

Figure 3-2: Effect of slot length on axial thermal gradient during quench stage

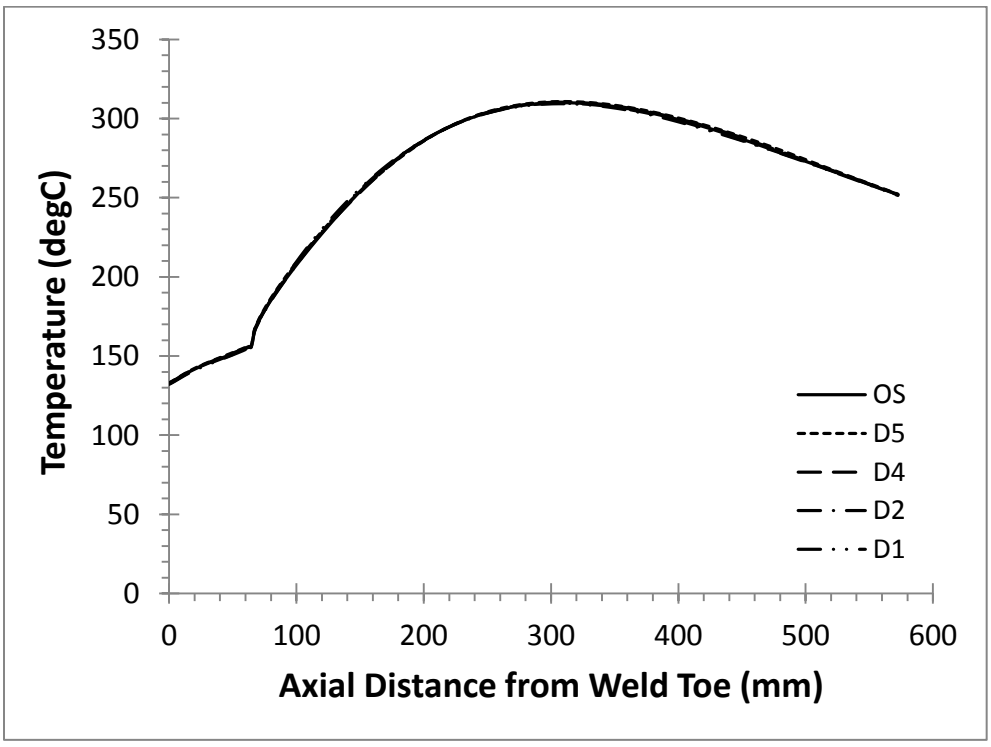

Figure 3-3: Effect of junction-to-slot distance on axial thermal gradient during quench stage

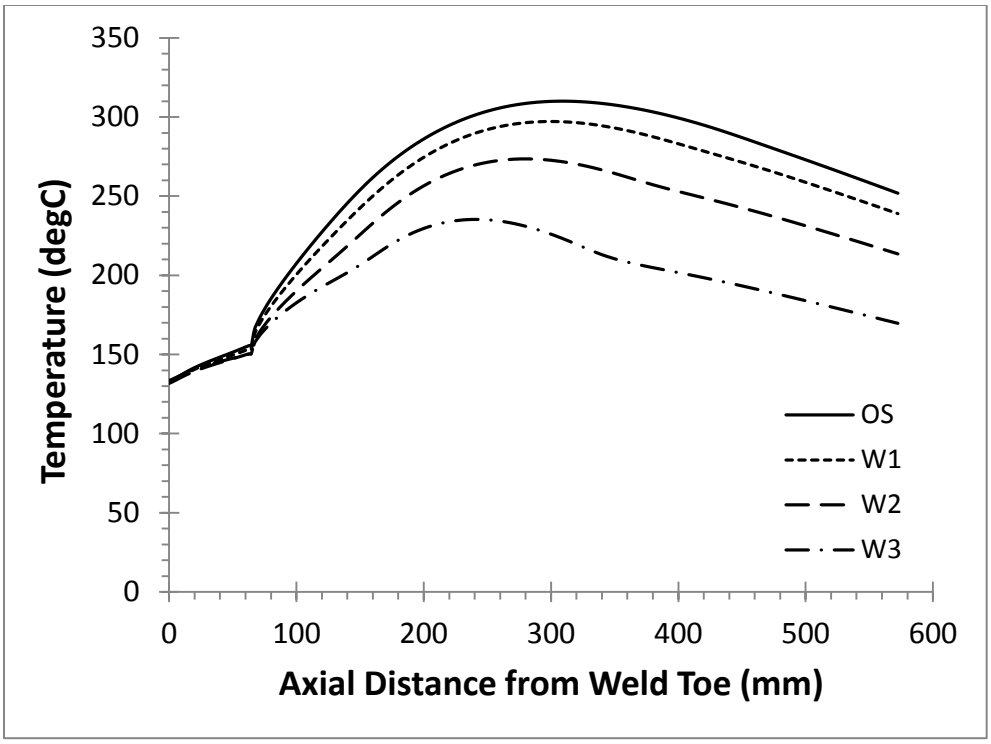

Figure 3-4: Effect of slot width on axial thermal gradient during quench stage

It can be seen that changes in length and skirt-to-slot distance are not found to significantly affect the thermal solution since each of the curves collapse onto one another, whereas changes in slot width cause a significant change in the axial thermal gradient. As shown in Figure 3-4, increasing slot width from 3.175 mm to 76.2 mm causes the thermal gradient during the quench stage to increase from 177°C to 101°C over identical distances. The decrease in axial thermal gradient can be attributed to a decrease of mass in the slotted section allowing the thinner columns to more quickly reach the equilibrium temperature.

3.5 Stress Analysis Results

In this section, the stress component amplitudes and maximum equivalent stress and plastic strains from the inner side of the Junction Face and three Slot Area points of interest are compared to determine the effects of altering each individual dimension. Stress and strain results

from the first cycle are omitted from comparison since it cannot be considered as stable due to material plasticity. Therefore, only the second cycle results are used for comparison since they are found to be more stable.

3.5.1 Effect of Skirt Slot Length *L* on Junction Stress/Strain Response

The comparison of stress amplitudes at the inner junction surface during the second cycle is shown in Figure 3-5 and summarized in Table 3-3. It can be seen that decreasing slot length causes each of the stress component amplitudes to increase. Similarly, the maximum equivalent stress value increases as the slot shortens. These changes are reflected in the maximum value of equivalent plastic strain, which experiences a significant increase as the slot shortens. Based on the findings, a decrease in slot length can be attributed to an undesirable increase of plastic deformation in the junction weld.

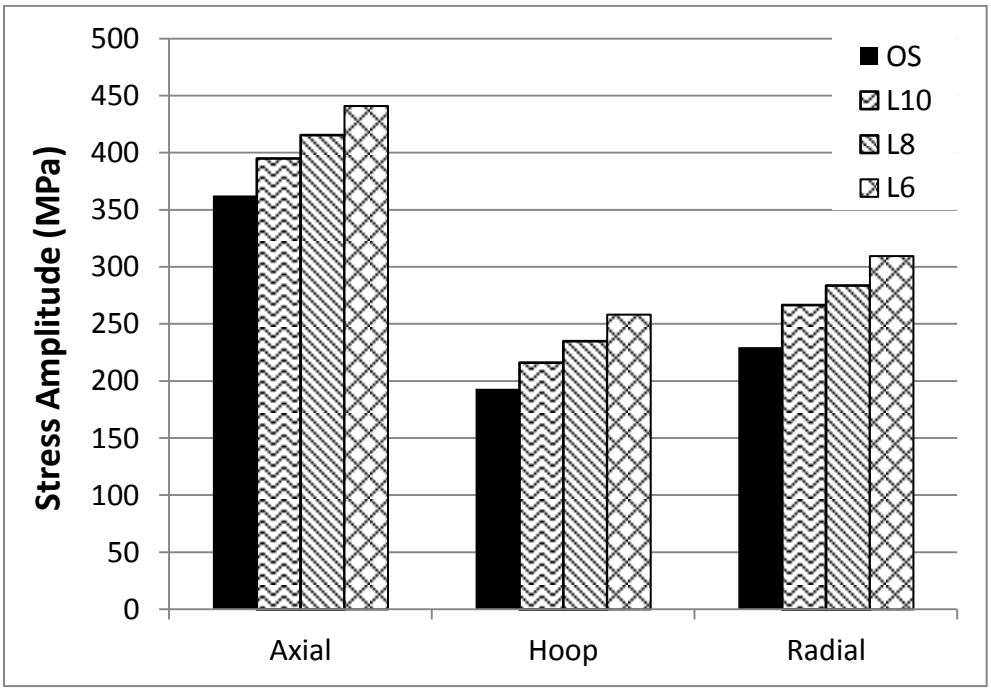

Figure 3-5: Effect of slot length on inner junction stress amplitudes during second cycle

Table 3-3: Inner junction stress amplitude results and percent change due to slot length

Model	Axial Stress Amp.		Hoop Stress Amp.		Radial Stress Amp.	
	Value (MPa)	% Change	Value (MPa)	% Change	Value (MPa)	% Change
OS	362.5	-	193.3	-	229.6	-
L10	395.0	8.9	216.2	11.9	266.5	16.1
L8	415.6	14.6	234.9	21.6	283.9	23.6
L6	441.0	21.6	258.3	33.6	309.6	34.8

Table 3-4: Maximum equivalent stress and plastic strain results at inner junction and percent change due to slot length

Model	Max Equivalent Stress		Max Plastic Strain	
	Value (MPa)	% Change	Value (%)	% Change
OS	318.3	-	0.026	-
L10	343.6	7.9	0.041	59.8
L8	366.7	15.2	0.067	159.6
L6	392.5	23.3	0.111	332.5

3.5.2 Effect of Skirt Slot Length *L* on Slot Area Stress/Strain Response

Top Keyhole Location

Figure 3-6 shows the comparison of second-cycle stress amplitudes at the top keyhole. As the results summarized in Table 3-5 shows, the stress amplitudes decrease slightly as the slot is made shorter. The maximum equivalent stress and plastic strain also experience a slight decrease, as shown in Table 3-6. The changes in stress and strain response are deemed insignificant when compared to the magnitudes of stress and strain found near the top keyhole.

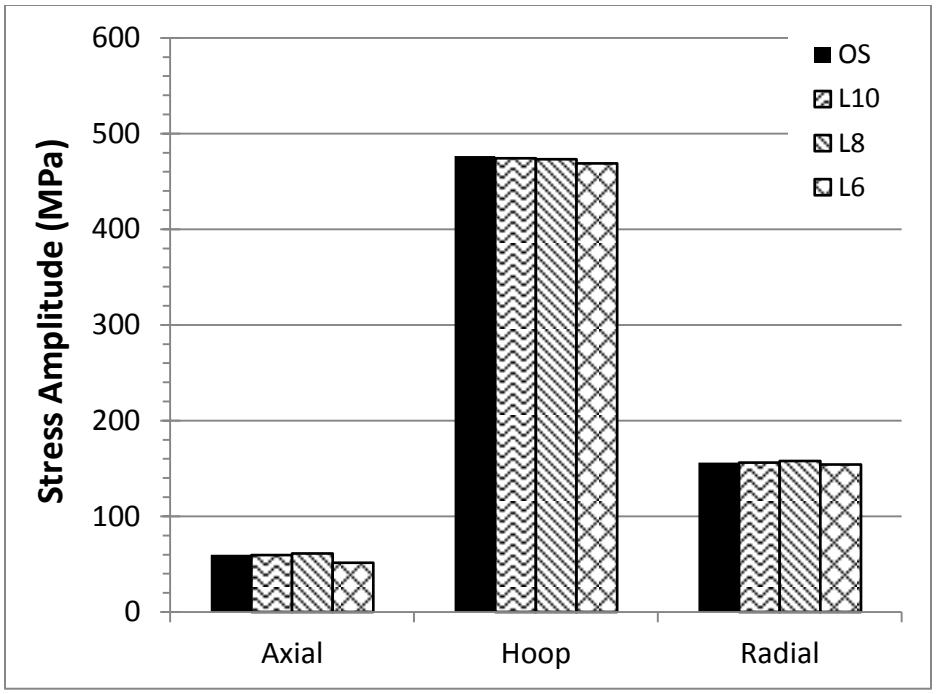

Figure 3-6: Effect of slot length on stress amplitudes at the top keyhole location during second cycle

Table 3-5: Top keyhole location stress amplitude results and percent change due to slot length during second cycle

Model	Axial Stress Amp.		Hoop Stress Amp.		Radial Stress Amp.	
	Value (MPa)	% Change	Value (MPa)	% Change	Value (MPa)	% Change
OS	59.7	-	476.4	-	156.3	-
L10	59.4	-0.6	474.3	-0.4	156.2	0.0
L8	61.3	2.7	473.1	-0.7	157.9	1.1
L6	51.5	-13.8	468.7	-1.6	154.0	-1.4

Table 3-6: Maximum equivalent stress and plastic strain results at top keyhole location and percent change due to slot length during second cycle

Model	Max Equivalent Stress		Max Plastic Strain	
	Value (MPa)	% Change	Value (%)	% Change
OS	422.7	-	0.769	-
L10	420.7	-0.5	0.749	-2.6
L8	416.9	-1.4	0.710	-7.6
L6	412.8	-2.3	0.668	-13.2

Bottom Keyhole Location

The comparison of second-cycle stress amplitudes at the bottom keyhole location is shown in Figure 3-7. The results are summarized in Table 3-7. It can be seen that the amplitudes for each of the stress components increase slightly as the slot length decreases, with the largest change occurring in the radial direction. As Table 3-8 shows, the maximum plastic strain increases significantly as the slot becomes shorter while the maximum equivalent stress does not experience any significant change. The main contributing factor for the considerable rise in maximum plastic strain is the position of the bottom keyhole location relative to the axial thermal gradient. As the slot gets shorter, the bottom keyhole location moves upward into an area on the skirt which experiences a higher mean temperature. Hence, the bottom keyhole location consists of material which becomes increasingly susceptible to plastic deformation as reflected in the results.

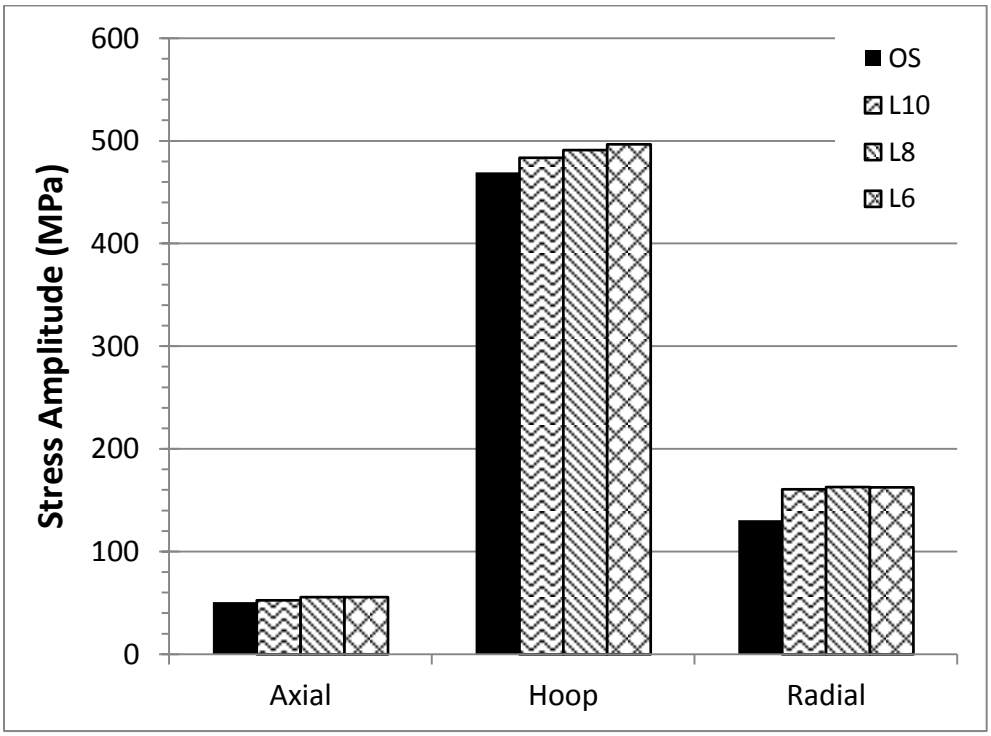

Figure 3-7: Effect of slot length on stress amplitudes at the bottom keyhole location during second cycle

Table 3-7: Bottom keyhole location stress amplitude results and percent change due to slot length during second cycle

Model	Axial Stress Amp.		Hoop Stress Amp.		Radial Stress Amp.	
	Value (MPa)	% Change	Value (MPa)	% Change	Value (MPa)	% Change
OS	50.7	-	469.2	-	130.4	-
L10	52.5	3.5	483.6	3.1	160.8	23.3
L8	55.6	9.7	491.2	4.7	162.9	24.9
L6	55.8	10.0	496.8	5.9	162.8	24.8

Table 3-8: Maximum equivalent stress and plastic strain results at bottom keyhole location and percent change due to slot length during second cycle

Model	Max Equivalent Stress		Max Plastic Strain	
	Value (MPa)	% Change	Value (%)	% Change
OS	405.0	-	0.294	-
L10	408.5	0.9	0.369	25.7
L8	413.2	2.0	0.476	62.0
L6	414.9	2.5	0.604	105.6

Mid-Column Location

Figure 3-8 shows the comparison of second-cycle stress component amplitudes at the mid-column location. The values from each of the examined designs are summarized in Table 3-9. It can be seen that the stress amplitudes are varied in their response to the decrease in slot length. However, the changes are deemed to be insignificant when considering the absolute differences between the OS and examined designs. The insignificance of the changes in stress amplitudes is further proven when considering the change in maximum equivalent stress and plastic strain values, which can be seen in Table 3-10.

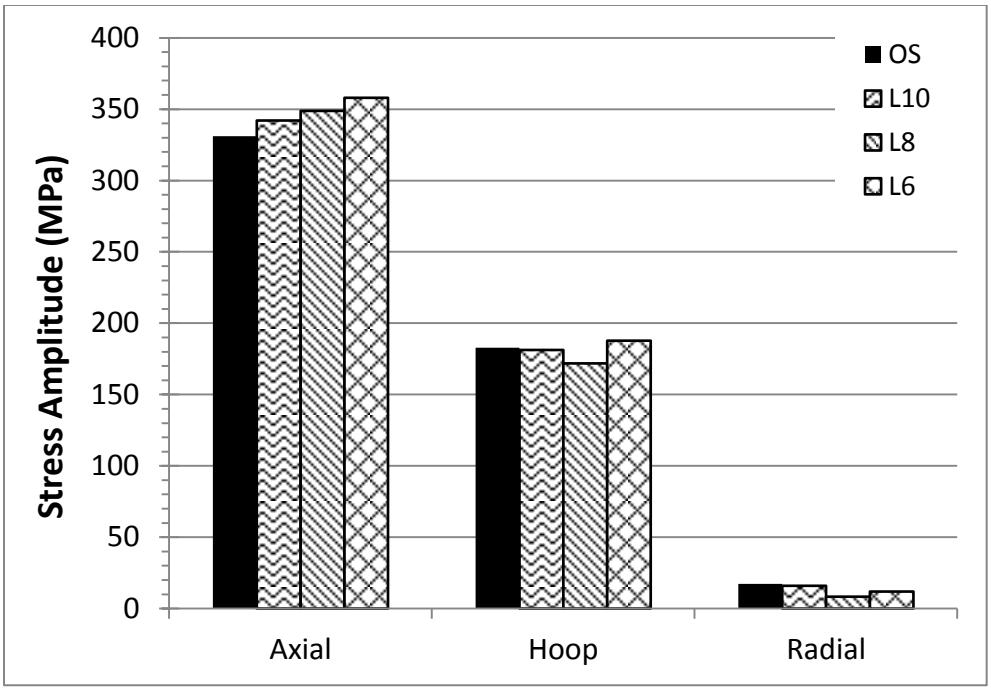

Figure 3-8: Effect of slot length on stress amplitudes at the mid-column location during second cycle

Table 3-9: Mid-column location stress amplitude results and percent change due to slot length during second cycle

Model	Axial Stress Amp.		Hoop Stress Amp.		Radial Stress Amp.	
	Value (MPa)	% Change	Value (MPa)	% Change	Value (MPa)	% Change
OS	331.2	-	182.9	-	17.2	-
L10	342.1	3.3	181.2	-1.0	16.0	-7.2
L8	348.7	5.3	171.7	-6.1	8.3	-52.0
L6	357.9	8.1	187.7	2.6	11.9	-31.0

Table 3-10: Maximum equivalent stress and plastic strain results at mid-column location and percent change due to slot length during second cycle

Model	Max Equivalent Stress		Max Plastic Strain	
	Value (MPa)	% Change	Value (%)	% Change
OS	365.5	-	0.144	-
L10	369.1	1.0	0.150	3.8
L8	369.8	1.2	0.148	2.9
L6	371.1	1.5	0.151	5.0

3.5.3 Effect of Junction-to-Slot Distance *d* on Junction Stress/Strain Response

The second-cycle amplitudes of the main junction stress components are shown graphically in Figure 3-9. The results are summarized in Table 3-11. In the "Model" column, the number after the letter "D" is the distance between the junction and the top of the slot in inches. For example, "D1" means the distance is 1 inch (25.4 mm). The original slot (OS) model has slots placed 3 inches (76.2 mm) away from the junction. It can be seen that decreasing the junction-to-slot distance, thereby placing the top of the slot closer to the junction weld, causes a varied response in the stress amplitudes. In general, the largest stress amplitude (axial) experiences a slight increase when the slot is placed closer to the junction weld. An increase in junction-to-slot distance is found to cause a minor decrease in junction stress amplitudes.

As shown in Table 3-12, a slight increase in maximum equivalent stress is accompanied by a significant increase in maximum plastic strain when the slot is placed closer to the junction weld. The sudden increase in equivalent stress and plastic strain is attributed to the proximity of the top keyhole to the weld surface. It has been concluded in previous sections that a significant amount of stress concentration occurs at the slot ends of the OS design, which can be expected to adversely affect the junction stress and strain response when the slot is placed closer to the junction. Initially as the junction-to-slot distance is increased, the maximum junction equivalent stress does not experience any significant change and the maximum plastic strain decreases slightly when compared to the OS design. As the slot is moved further away, both the maximum junction equivalent stress and plastic strain experience a slight increase when compared to the previous design.

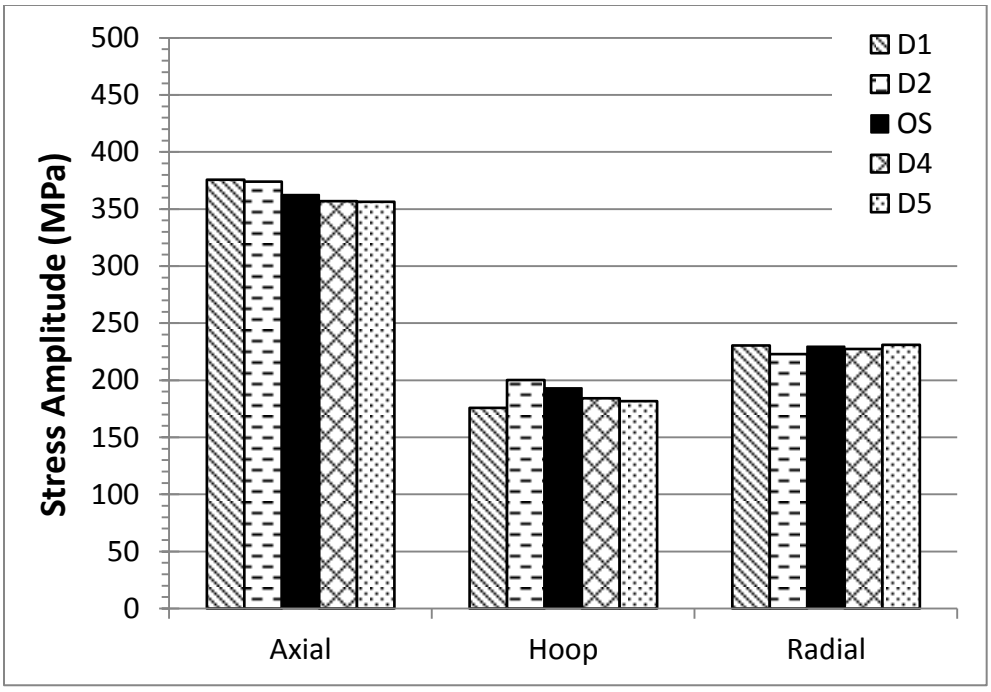

Figure 3-9: Effect of junction-to-slot distance on inner junction stress amplitudes during second cycle

Table 3-11: Inner junction stress amplitude results and percent change due to junction-to-slot distance during second cycle

Model	Axial Stress Amp.		Hoop Stress Amp.		Radial Stress Amp.	
	Value (MPa)	% Change	Value (MPa)	% Change	Value (MPa)	% Change
OS	362.5	-	193.3	-	229.6	-
D1	375.7	3.6	175.9	-9.0	230.5	0.4
D2	374.1	3.2	200.1	3.5	222.9	-2.9
D4	356.8	-1.6	184.3	-4.6	227.5	-0.9
D5	356.3	-1.7	181.8	-5.9	231.0	0.6

Table 3-12: Maximum equivalent stress and plastic strain results at inner junction and percent change due to junction-to-slot distance during second cycle

Model	Max Equivalent Stress		Max Plastic Strain	
	Value (MPa)	% Change	Value (%)	% Change
OS	318.3	-	0.026	-
D1	352.5	10.8	0.083	221.9
D2	329.4	3.5	0.047	83.8
D4	315.4	-0.9	0.019	-26.6
D5	330.2	3.8	0.022	-14.6

Based on the results presented in this section, it can be determined with certainty that a decrease in junction-to-slot distance adversely affects the junction weld. It can also be said that a skirt with identical slots about 25.4 mm (1 inch) further away from the junction may potentially be more effective at protecting the weld area.

3.5.4 Effect of Junction-to-Slot Distance *d* on Slot Area Stress/Strain Response

Top Keyhole Location

Figure 3-10 shows the comparison of second-cycle stress amplitudes at the top keyhole between each of the examined designs. It can be seen that the stress amplitudes at the top keyhole location are directly correlated with the junction-to-slot distance. In other words, the stress amplitudes decrease as the distance decreases and increase as the distance increases as shown in Table 3-13. The maximum equivalent stresses and plastic strains for each design are summarized in Table 3-14. The maximum equivalent stress is found to follow the same trend as the stress amplitudes. As expected, the maximum plastic strain at the top keyhole location decreases significantly as the slot is moved closer to the junction, and increases significantly as the slot is moved further away. The observed behavior can be attributed to the location of the top keyhole in relation to the axial thermal gradient and skirt deformation profile. As determined in Figure 3-3, the thermal gradient is not significantly affected by changes in the junction-to-slot distance. Therefore, altering the distance changes the location of the slot ends relative to the thermal gradient. In this case, the top keyhole location is moved either closer or further away from the equilibrium temperature. Additionally, moving the slot further up places the top keyhole closer to the junction which experiences less deformation relative to the coke drum vessel compared to a point further down the skirt.

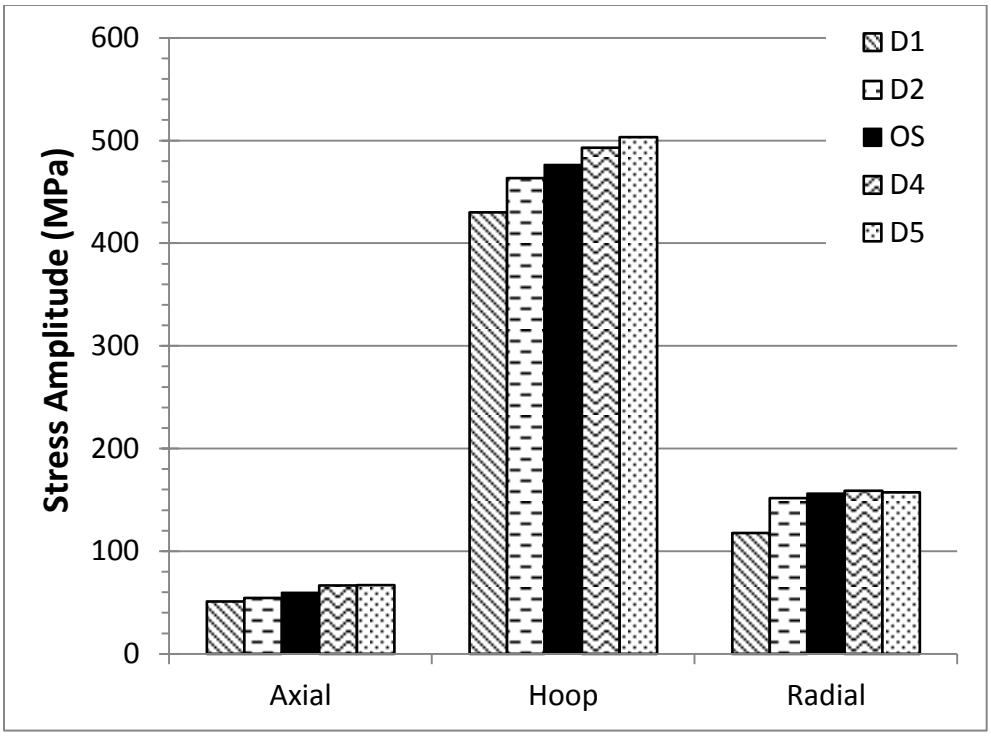

Figure 3-10: Effect of junction-to-slot distance on stress amplitudes at the top keyhole location during second cycle

Table 3-13: Top keyhole location stress amplitude results and percent change due to junction-to-slot distance during second cycle

Model	Axial Stress Amp.		Hoop Stress Amp.		Radial Stress Amp.	
	Value (MPa)	% Change	Value (MPa)	% Change	Value (MPa)	% Change
OS	59.7	-	476.4	-	156.3	-
D1	51.1	-14.5	430.2	-9.7	117.8	-24.6
D2	54.5	-8.7	463.3	-2.7	151.6	-3.0
D4	66.7	11.8	493.0	3.5	159.0	1.7
D5	67.0	12.1	503.2	5.6	157.3	0.7

Table 3-14: Maximum equivalent stress and plastic strain results at top keyhole and percent change due to junction-to-slot distance during second cycle

Model	Max Equivalent Stress		Max Plastic Strain	
	Value (MPa)	% Change	Value (%)	% Change
OS	422.7	-	0.769	-
D1	382.9	-9.4	0.298	-61.3
D2	408.0	-3.5	0.557	-27.5
D4	438.9	3.8	0.907	18.0
D5	442.7	4.7	0.996	29.6

Bottom Keyhole Location

The comparison of second-cycle stress amplitudes at the bottom keyhole location is shown graphically in Figure 3-11. The results are summarized in Table 3-15. It can be seen that the radial stress amplitude reaches a maximum value at the minimum junction-to-slot distance. Both the axial and hoop stress amplitudes slightly increase as the slot is moved closer to the junction, while moving the slot further away causes both stress amplitudes to decrease when compared to the OS design. As shown in Table 3-16, the maximum equivalent stress is found to decrease slightly as the junction-to-slot distance is increased. The maximum plastic strain at the bottom keyhole location is found to increase significantly as the slot is moved closer to the junction and decrease significantly as the slot is moved further away. The observed correlation between maximum plastic strain and junction-to-slot distance can be attributed to the changing position of the bottom keyhole location in relation to the axial thermal gradient near the top of the skirt.

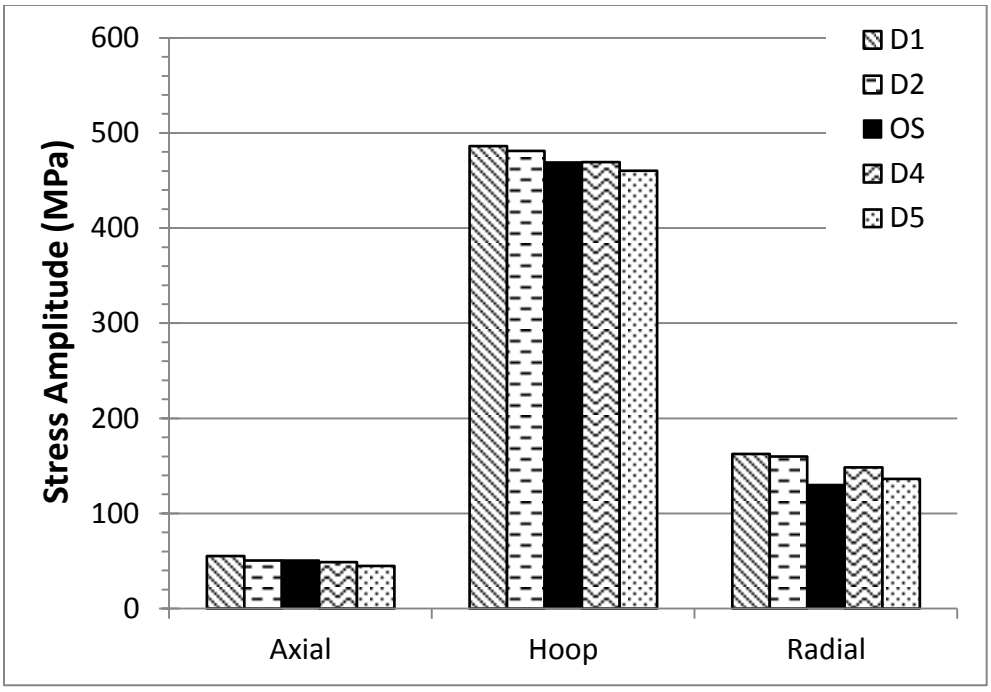

Figure 3-11: Effect of junction-to-slot distance on stress amplitudes at the bottom keyhole location during second cycle

Table 3-15: Bottom keyhole location stress amplitude results and percent change due to junction-to-slot distance during second cycle

Model	Axial Stress Amp.		Hoop Stress Amp.		Radial Stress Amp.	
	Value (MPa)	% Change	Value (MPa)	% Change	Value (MPa)	% Change
OS	50.7	-	469.2	-	130.4	-
D1	55.1	8.6	486.1	3.6	162.4	24.6
D2	50.5	-0.5	481.1	2.5	159.7	22.5
D4	48.9	-3.6	469.4	0.0	148.5	13.9
D5	44.9	-11.5	460.4	-1.9	136.3	4.6

Table 3-16: Maximum equivalent stress and plastic strain results at bottom keyhole and percent change due to junction-to-slot distance during second cycle

Model	Max Equivalent Stress		Max Plastic Strain	
	Value (MPa)	% Change	Value (%)	% Change
OS	405.0	-	0.294	-
D1	407.5	0.6	0.415	41.3
D2	404.3	-0.2	0.360	22.6
D4	401.1	-1.0	0.235	-19.9
D5	398.0	-1.7	0.196	-33.4

Mid-Column Location

Figure 3-12 shows the comparison of second-cycle stress component amplitudes at the mid-column location. The results are summarized in Table 3-17. It can be seen that the mid-column hoop stress amplitude is most affected by the change in junction-to-slot distance. Furthermore, the axial stress amplitude experiences a significant drop as a result of moving the slot further away from the slot. As shown in Table 3-18, the maximum mid-column equivalent stress experiences a minor decrease which is accompanied by a significant decrease in maximum plastic strain when the slot is moved closer to the junction.

Table 3-17: Mid-column location stress amplitude results and percent change due to junction-to-slot distance during second cycle

Model	Axial Stress Amp.		Hoop Stress Amp.		Radial Stress Amp.	
	Value (MPa)	% Change	Value (MPa)	% Change	Value (MPa)	% Change
OS	331.2	-	182.9	-	17.2	-
D1	323.9	-2.2	27.5	-85.0	0.2	-98.9
D2	353.8	6.8	132.8	-27.4	17.4	1.2
D4	297.4	-10.2	251.2	37.3	4.9	-71.8
D5	256.3	-22.6	282.4	54.4	0.3	-98.4

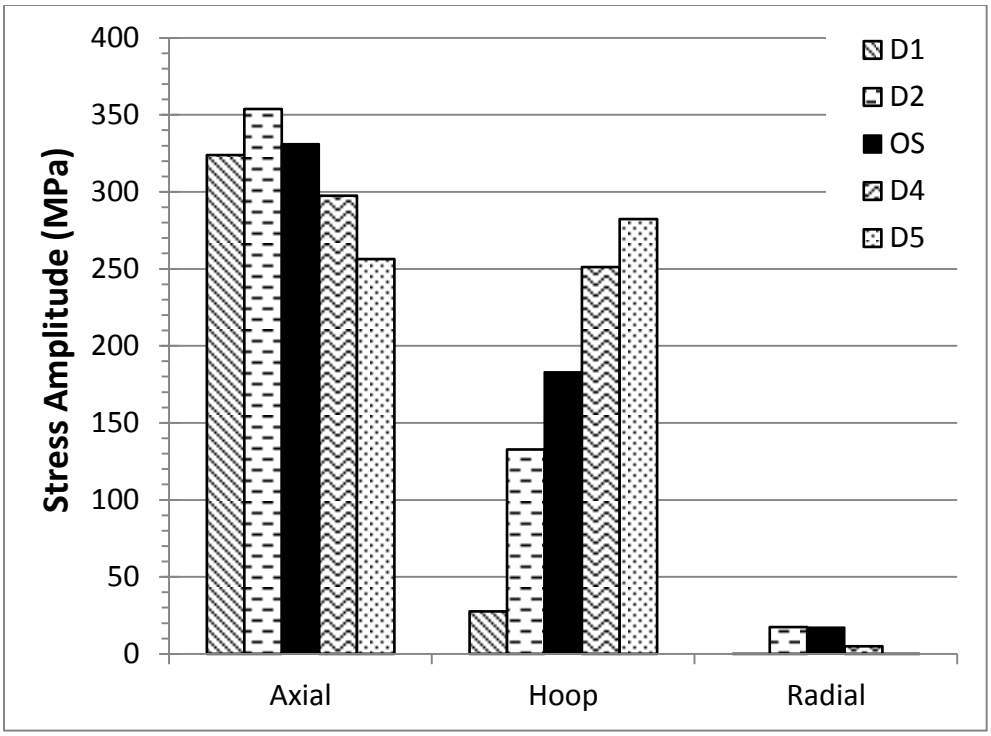

Figure 3-12: Effect of junction-to-slot distance on stress amplitudes at the mid-column location during second cycle

Table 3-18: Maximum equivalent stress and plastic strain results at mid-column and percent change due to junction-to-slot distance during second cycle

Model	Max Equivalent Stress		Max Plastic Strain	
	Value (MPa)	% Change	Value (%)	% Change
OS	365.5	-	0.144	-
D1	324.5	-11.2	0.078	-46.1
D2	361.7	-1.1	0.068	-53.1
D4	366.0	0.1	0.154	6.7
D5	369.0	0.9	0.157	9.2

3.5.5 Effect of Skirt Slot Width *w* on Junction Stress/Strain Response

The comparison of second-cycle stress component amplitudes at the inner junction face of each examined design is shown in Figure 3-13. The results are summarized in Table 3-19. The number after the "W" in each model designation is the width of the slot in inches. For example, the "W1" model has slots which are 1 inch (25.4 mm) wide. For reference, the original slot (OS) model has slots which are 0.125 in (3.175 mm) wide. It can be seen that the each of the stress amplitudes initially experience a slight increase in magnitude at the first tested slot width (W1) before decreasing with each subsequent design. As shown in

Table 3-20, the wider slot designs cause a slight decrease in maximum junction equivalent stress. Additionally, the maximum plastic strain decreases significantly as the slots are made wider, eventually being completely eliminated at the widest tested slot width (W3). The observed behavior can be attributed to a reduction of local stiffness near the junction weld due to the thinner columns of the slotted section. This finding is significant as it shows that widening the skirt slots is an effective way to considerably decrease the magnitude of plastic deformation near the critical junction weld area. Hence, it can be said that increasing the width of the skirt slot achieves the initial goal of improving the protection of the junction weld.

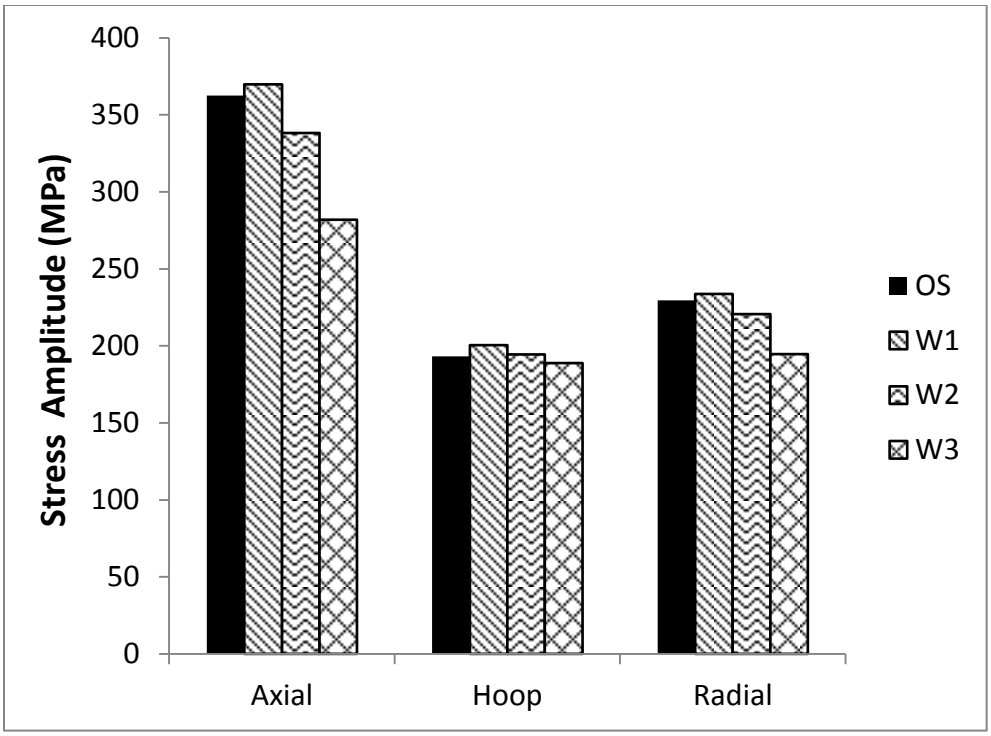

Figure 3-13: Effect of slot width on inner junction stress amplitudes during second cycle

Table 3-19: Inner junction stress amplitude results and percent change due to slot width during second cycle

Model	Axial Stress Amp.		Hoop Stress Amp.		Radial Stress Amp.	
	Value (MPa)	% Change	Value (MPa)	% Change	Value (MPa)	% Change
OS	362.5	-	193.3	-	229.6	-
W1	369.8	2.0	200.4	3.7	233.7	1.8
W2	338.3	-6.7	194.4	0.6	220.7	-3.9
W3	281.9	-22.2	188.9	-2.3	194.7	-15.2

Table 3-20: Maximum equivalent stress and plastic strain results at inner junction and percent change due to slot width during second cycle

Model	Max Equivalent Stress		Max Plastic Strain	
	Value (MPa)	% Change	Value (%)	% Change
OS	318.3	-	0.026	-
W1	317.6	-0.2	0.025	-4.7
W2	292.5	-8.1	0.014	-46.6
W3	299.9	-5.8	0.000	-100.0

3.5.6 Effect of Skirt Slot Width *w* on Slot Area Stress/Strain Response

Top Keyhole Location

Figure 3-14 shows the comparison of second-cycle stress component amplitudes at the top keyhole location between each of the examined slot widths. The results are summarized in Table 3-21. It can be seen that the increase in slot width causes a significant drop in all stress component amplitudes. Furthermore, the maximum equivalent stress and plastic strain values also decrease considerably as shown in Table 3-22. The observed phenomena can be attributed to the larger keyhole radius of the wide slot design as previously shown in Figure 3-1, which mitigates the stress concentration effect at the slot ends.

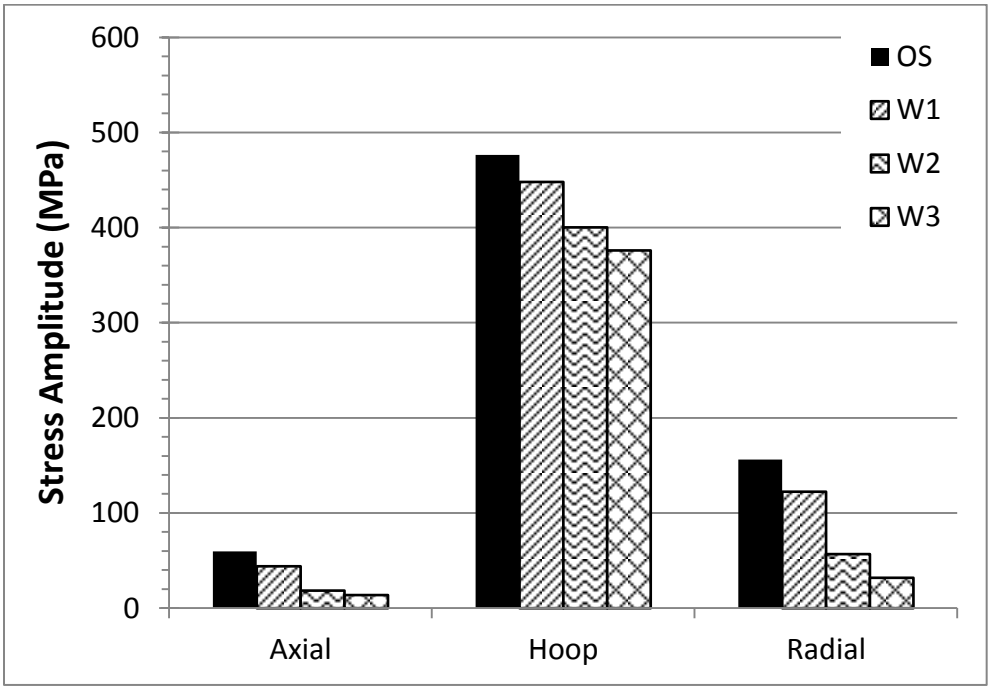

Figure 3-14: Effect of slot width on stress amplitudes at the top keyhole location during second cycle

Table 3-21: Top keyhole location stress amplitude results and percent change due to slot width during second cycle

Model	Axial Stress Amp.		Hoop Stress Amp.		Radial Stress Amp.	
	Value (MPa)	% Change	Value (MPa)	% Change	Value (MPa)	% Change
OS	59.7	-	476.4	-	156.3	-
W1	44.1	-26.1	448.1	-5.9	122.5	-21.6
W2	18.6	-68.8	400.2	-16.0	56.8	-63.6
W3	13.7	-77.1	376.1	-21.0	32.1	-79.5

Table 3-22: Maximum equivalent stress and plastic strain results at top keyhole and percent change due to slot width during second cycle

Model	Max Equivalent Stress		Max Plastic Strain	
	Value (MPa)	% Change	Value (%)	% Change
OS	422.7	-	0.769	-
W1	404.1	-4.4	0.573	-25.4
W2	379.9	-10.1	0.316	-58.9
W3	365.3	-13.6	0.210	-72.7

Bottom Keyhole Location

Figure 3-15 shows the comparison of second-cycle stress component amplitudes at the bottom keyhole location between each of the explored slot widths. The results are summarized in Table 3-23. It can be seen that the stress amplitudes decrease significantly as the slot width increases. The percent changes of each of the stress amplitudes are found to be very similar to those of the top keyhole. This finding acts as further evidence that the larger keyhole radius lessens the stress concentration at the slot ends. The maximum equivalent stress and plastic strain results are summarized in Table 3-24. At the widest examined slot, a slight increase of maximum equivalent stress is accompanied by a significant rise in maximum plastic strain. It should be noted that each increment of slot width is accompanied by a decrease in slot length in order to protect the slotted area from buckling failure, as previously mentioned in Section 3.2. As shown

in previous sections, the mean temperature of the material immediately surrounding the keyhole is directly affected by its axial position on the skirt. Hence, the elevated temperature at the bottom keyhole at the widest tested slot width (W3) causes the surrounding material to undergo more plastic deformation compared to the other designs.

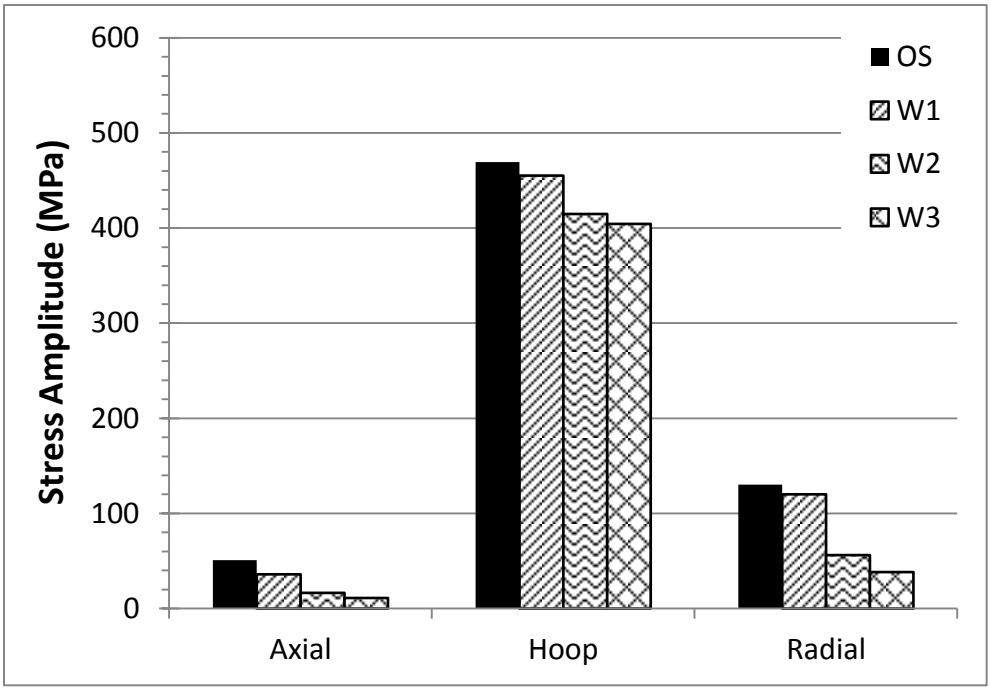

Figure 3-15: Effect of slot width on stress amplitudes at the bottom keyhole location during second cycle

Table 3-23: Bottom keyhole location stress amplitude results and percent change due to slot width during second cycle

Model	Axial Stress Amp.		Hoop Stress Amp.		Radial Stress Amp.	
	Value (MPa)	% Change	Value (MPa)	% Change	Value (MPa)	% Change
OS	50.7	-	469.2	-	130.4	-
W1	35.9	-29.2	455.3	-3.0	120.1	-7.9
W2	16.6	-67.2	414.8	-11.6	56.3	-56.8
W3	11.3	-77.8	404.6	-13.8	38.3	-70.6

Table 3-24: Maximum equivalent stress and plastic strain results at bottom keyhole and percent change due to slot width during second cycle

Model	Max Equivalent Stress		Max Plastic Strain	
	Value (MPa)	% Change	Value (%)	% Change
OS	405.0	-	0.294	-
W1	404.4	-0.1	0.281	-4.4
W2	403.9	-0.3	0.266	-9.4
W3	422.0	4.2	0.401	36.6

Mid-Column Location

The comparison of second-cycle stress component amplitudes at the mid-column location between each of the examined skirt slot designs is shown in Figure 3-16. The results are summarized in Table 3-25. The increase in stress amplitude in the axial direction as the slots are made wider can be attributed to the increasing bending stress experienced by the columns as they become thinner. The significant decrease in stress amplitude in the hoop direction can be attributed to the reduction of stress concentration effect at the slot ends as previously mentioned. It can be seen from Table 3-26 that the maximum equivalent stress and plastic strain initially decrease at the first tested slot width (W1) due to the aforementioned reduction in hoop stress amplitude. The maximum plastic strain then increases significantly as the slot is further widened due to increasing levels of axial stress amplitude. It should be noted that the results suggest that there is a critical point between the W1 and W2 designs. The observed effect can be attributed to a switch from slot end stress concentration to column bending stress as the main contributor of stress.

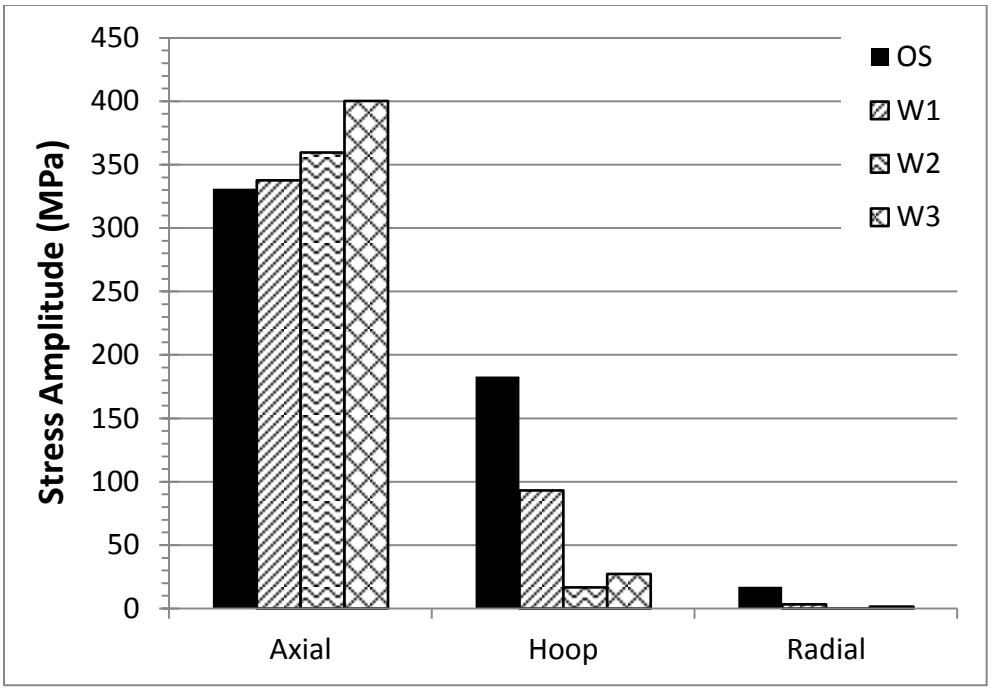

Figure 3-16: Effect of slot width on stress amplitudes at the mid-column location during second cycle

Table 3-25: Mid-column location stress amplitude results and percent change due to slot width during second cycle

Model	Axial Stress Amp.		Hoop Stress Amp.		Radial Stress Amp.	
	Value (MPa)	% Change	Value (MPa)	% Change	Value (MPa)	% Change
OS	331.2	-	182.9	-	17.2	-
W1	337.6	1.9	93.1	-49.1	3.3	-81.0
W2	359.6	8.6	16.8	-90.8	0.3	-98.3
W3	400.2	20.9	27.2	-85.1	1.6	-90.5

Table 3-26: Maximum equivalent stress and plastic strain results at mid-column and percent change due to slot width during second cycle

Model	Max Equivalent Stress		Max Plastic Strain	
	Value (MPa)	% Change	Value (%)	% Change
OS	365.5	-	0.150	-
W1	323.4	-11.5	0.094	-37.6
W2	357.9	-2.1	0.208	39.0
W3	406.2	11.1	0.524	249.5

3.6 Summary and Conclusions

The goal of this study was to optimize the slot dimensions to increase protection of the junction weld area and decrease the possibility of failure near the slot ends. This was accomplished by individually altering slot dimensions while considering the feasibility of each design. The individual stress component amplitude, maximum equivalent stress, and maximum plastic strain values from critical points of interest were used to compare the effect of each change in dimension. The optimization study conducted in this chapter has found that:

- Slot length and junction-to-slot distance has no significant effect on the axial thermal gradient of the skirt during the quench stage
- An increase in slot width causes the axial thermal gradient during the quench stage to become more severe due to higher conductive heat transfer rate through relatively thinner columns
- A decrease in slot length:
    - adversely affects junction area and bottom keyhole location
    - causes maximum equivalent stress and plastic strain to decrease at top keyhole location
    - does not significantly affect the mid-column location
- A decrease in junction-to-slot distance:
    - Adversely affects junction area and bottom keyhole location
    - causes maximum equivalent stress and plastic strain to decrease at top keyhole and mid-column locations
- An increase in junction-to-slot distance:
    - Adversely affects top keyhole location

- Causes maximum equivalent stress and plastic strain to decrease slightly at junction area and bottom keyhole location
- Does not significantly affect the mid-column location

- An increase in slot width accompanied by a decrease in slot length:
  - Adversely affects bottom keyhole location
  - Causes significant reduction in maximum equivalent stress and plastic strain in junction area and top keyhole area
  - Initially favorably affects the mid-column location (W1), then adversely affects with further widening of slot (W2, W3)

Thus, it can be concluded that the effects caused by increasing slot width are far more beneficial to the overall skirt design than the effects caused by altering any of the other slot dimensions. However, it should be noted that increasing slot width past 50.8 mm (2 in.) will subject the columns between the slots to severe levels of plastic deformation. The final optimal dimensions are shown in Table 3-27. The stress component amplitudes, maximum equivalent stress, and maximum plastic strain results from the optimal design are compared to the original slot design in Table 3-28.

Table 3-27: Dimensions for optimal slot design

Dimension	Original Design Value		New Design Value	
	(mm)	(in)	(mm)	(in)
d	76.2	3	76.2	3
L	304.8	12	203.2	8
w	3.175	0.125	50.8	2
r_k	9.525	0.375	25.4	1
s	101.6	4	101.6	4

Table 3-28: Changes in stress amplitudes, equivalent stress and plastic strain due to optimal slot

Parameter	Percent Difference Compared to OS (%)			
	Inner Junction	Top Keyhole	Bottom Keyhole	Mid-Column
Axial Stress Amp.	-6.7	-68.8	-67.2	8.6
Hoop Stress Amp.	0.6	-16.0	-11.6	-90.8
Radial Stress Amp.	-3.9	-63.6	-56.8	-98.3
Max. Equiv. Stress	-8.1	-10.1	-0.3	-2.1
Max. Plastic Strain	-46.6	-58.9	-9.4	25.9

CHAPTER 4 ANALYSIS OF ORIGINAL AND OPTIMAL SKIRT SLOT DESIGNS USING ACCURATE QUENCH MODEL

4.1 Introduction

The objective of the current chapter is to expand upon the work completed thus far to conduct a more thorough analysis on the original and optimal skirt slot designs. In the previous chapter, finite element models of an existing coke drum with various skirt slot designs were created. The designs were generated by independently altering the junction-to-slot distance, slot width, and slot length. The skirt slots were compared to the original slot design using nodal stress and strain results in the skirt-to-shell junction and slot area. Results from the optimization study suggested that slot width has a significant effect on the junction stress response, with a wider slot causing decreases of stress component ranges, maximum equivalent stress and maximum plastic strain in all critical locations. In this chapter, a more rigorous approach will be employed to compare the most effective slot designs:

- Fillets are added around the slot edges of each model.
- Mesh dependency analyses are conducted on the areas on interest to ensure accuracy of results.
- Each analysis consists of three full operation cycles using transient thermal boundary conditions.
- The effect of quench water being introduced with a finite rise speed is considered.

Additionally, the more accurate results due to the approach outlined above allows for a more elaborate method to be used to compare the designs. The method of comparison is adapted

from the procedure detailed in the ASME Sec. VIII, Div. 2, Part 5 for the evaluation of fatigue life of any component [23].

4.2 Model Set-Up

Finite element models of the same coke drum vessel considered in the previous chapters are created using the original and optimized skirt slot designs. A total of two skirt designs are considered: Original Slot (OS) and Optimal Slot (PS). The 2 mm thick layer of clad material is given the appropriate material properties of SA240-TP410S stainless steel, as shown previously in

Table 2-3. As with the base metal, the bilinear kinematic hardening model is used to simulate plasticity. Two solid models are created for each skirt design: a global model identical in dimensions to the models considered in the previous chapters, and a local sub-model of the skirt slot area. Figure 4-1 shows the global and local models of the Original Slot (OS) model. Fillets around the edges of the slot are absent from the global model but are included in the local model. In the global models, the mesh is refined near the skirt-to-shell weld while the slot area is kept coarse. The mesh around the slots is refined in the local sub-model. Body temperature data and cut boundary nodal displacement results are imported from the global model to the slot sub-model. Validation of the local model and mesh dependency studies will be shown in the sections below.

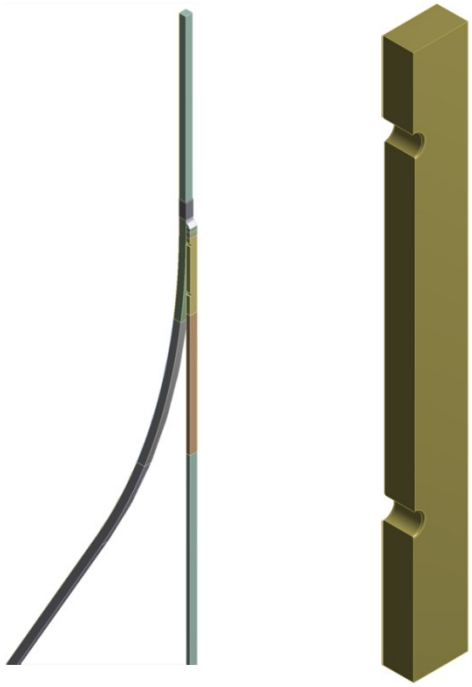

Figure 4-1: Global (Left) and Local (Right) models of the Original Slot (OS) model

To simulate each stage of the operation cycle, transient convection and pressure boundary conditions, summarized in Table 2-4, are applied to the inner surface. During the preheating and filling stages, the appropriate parameters are step-applied to the entire inner surface at once. In other words, it is assumed that the prescribed convective boundary condition is independent of the fill rate of hot oil. In reality, the hot oil fills the coke drum at a finite rise speed. However, results obtained by Xia et al. [8] show that the measured temperatures at all points along the drum reach the hot feed temperature almost immediately as the oil filling stage begins. This effect is attributed to complex radiative and convective heat transfer phenomena occurring inside the coke drum as soon the oil is introduced. For the quenching stage, the convective load of rising water is applied starting from the bottom node of the inner surface and advances upwards with a rise speed V_w = 3 mm/s by overriding the previous convective load from the oil filling stage. Time step sizes between 90-1000 s were used for the coupled thermal-structural analysis, with the step size set to automatically change based on solution convergence. To ensure

convergence of results during the quench phase, the time step was set to the minimum 90 s. Three complete process cycles are solved to ensure the stability of the stress and strain response.

The remaining thermal and structural boundary conditions summarized below can be found in detail in Section 2.3.2:

- Adiabatic boundary conditions specified on insulated surfaces and all cut surfaces.
- Fixed support boundary condition is applied to the skirt base.
- Circumferential displacement is set to zero at all cyclic symmetry cut boundaries.
- Pressure loads equivalent to the forces applied by the weight of the drum, as well as internal and hydrostatic pressures are applied to the top and bottom cut surfaces
- 'Plane-remains-plane' condition is applied to the cut surfaces to simulate the discarded sections of the vessel.

4.2.1 Validation of the Local Sub-Model

To verify that the imported body temperatures and cut boundary displacements lead to a valid solution of the slot area sub-model, the results from the top keyhole location of the Original Slot (OS) global model are compared to same location in the local model. The element size constraint between the two models is kept constant at 5 mm and an all-quad mesh is enforced to ensure similarity between meshes. Figure 4-2 and Figure 4-3 show the comparison of equivalent stress and strain results from final cycle of each of the global and local models.

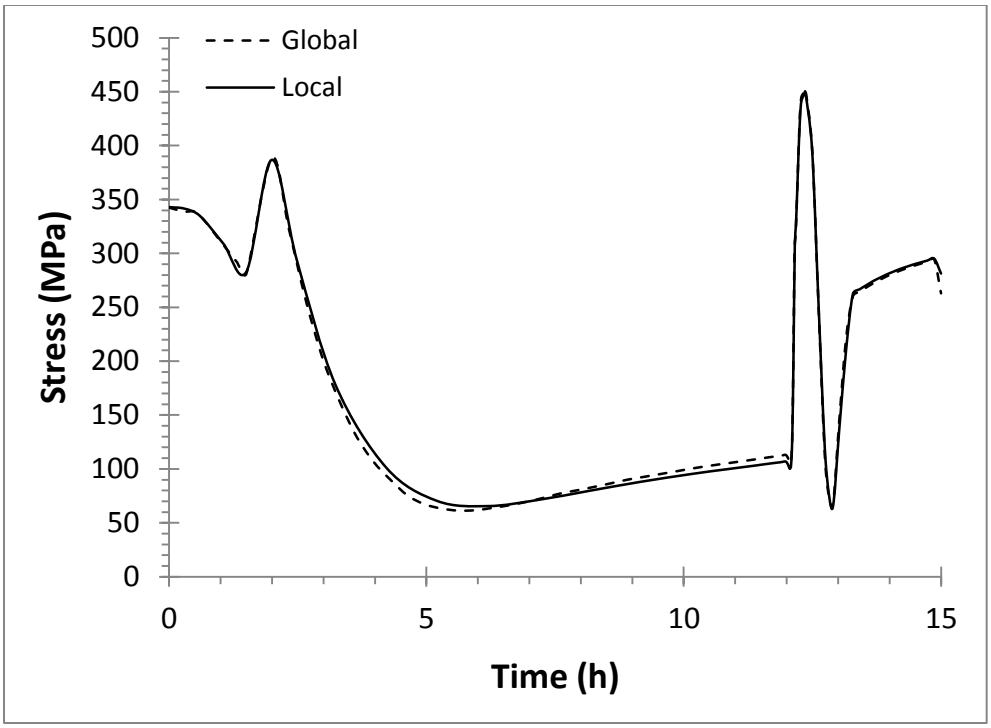

Figure 4-2: Comparison of equivalent stress results from top keyhole location of OS design Global and Local models

It can be seen that the stress and strain responses from the local model are in good agreement with the global model. The percent differences between the global and local models in the maximum stress and strain (which occurs during the quench stage of the cycle) are 0.6% and 2.2%, respectively. Hence, it is determined that the results from the local model are adequately accurate.

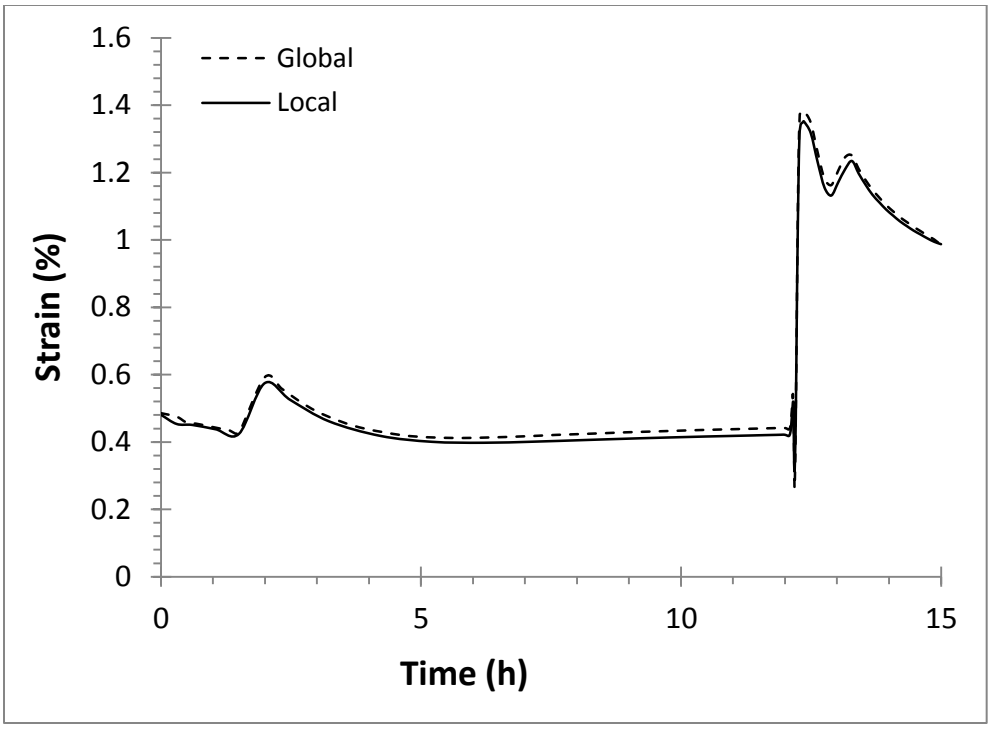

Figure 4-3: Comparison of equivalent total strain results from top keyhole location of OS design Global and Local models

4.2.2 Mesh Dependency of Junction Face (Global Model) and Slot Area (Local Model)

Due to the presence of plasticity at each of the critical locations, both equivalent plastic strain and equivalent stress results are used to determine the dependency of the results on mesh density. The maximum values occurring in the two critical areas of interest (Junction Face and Slot Area) are compared across varying mesh densities. Only results from the final cycle of each solution are considered.

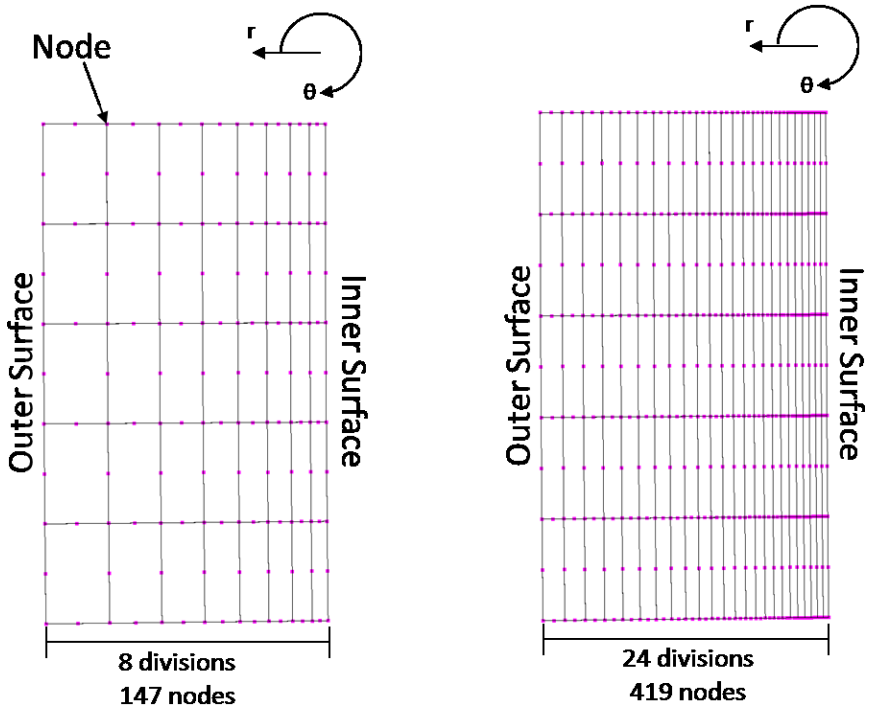

Figure 4-4: Junction face mesh refinement (Left: Coarse, Right: Fine)

In the junction face area, the critical element dimensions are the axial and radial lengths, since the stress and strain responses are not expected to differ significantly in the circumferential direction. For simplicity, the axial length of the mesh is held constant at about 2 mm. Furthermore, it has been previously shown that the inner edge of the junction face (surface in contact with the vessel) experiences the highest stress levels. Therefore, the radial length of the elements is set to decrease towards the inner edge as shown in Figure 4-4. A total of 5 mesh densities are tested for the junction face. Each level of mesh density is characterized using the elements with the shortest radial length found near the inner junction surface.

Table 4-1: Maximum equivalent stress and plastic strain results from the global model inner junction surface at different mesh densities

Element Size at Inner JF (mm)	Maximum During Final Cycle		Approximate Solution Time (h)
	Equivalent Stress (MPa)	Equivalent Plastic Strain (%)	
1.5	363.1	0.04	3.5
1.28	368.7	0.07	4.5
1.05	375.1	0.125	6
0.83	384.1	0.159	7.5
0.6	385.5	0.164	9

Table 4-1 shows the maximum junction equivalent stress and plastic strain for the Original Slot (OS) model during the final cycle at each of the tested mesh densities. Also shown are the approximate solution times for each of the models. Each of the maximums occurred at the inner junction surface. It can be seen that the maximum equivalent stress does not clearly show signs of mesh dependency, as expected. However when considering the maximum plastic strain values, it is found inner junction face results are highly sensitive to the subsequent mesh refinement at the original mesh density (1.5 mm) which indicates a need for higher localized mesh density. The percent differences of maximum equivalent plastic strain between the first and last mesh refinements are 75% and 3.1%, respectively. Thus, an inner junction face element size of 0.6 mm is found to produce the results which are the least mesh dependent while maintaining a reasonable solution time (one ‘full’ night of rest, or, less than 10 hours).

The mesh dependency of results in the slot area is examined using results from the local sub-model. Since it has previously been proven that the peak stress and strain occurs at the slot ends, special consideration is taken to increase the mesh density around the keyholes. Furthermore, the fillets around the keyholes also require an increased density of elements to

mesh properly. As shown in Figure 4-5, mesh inflation is used to control the element size near these critical areas. Hence, the minimum element size limit set by this method is used as the characteristic dimension for each of the mesh densities.

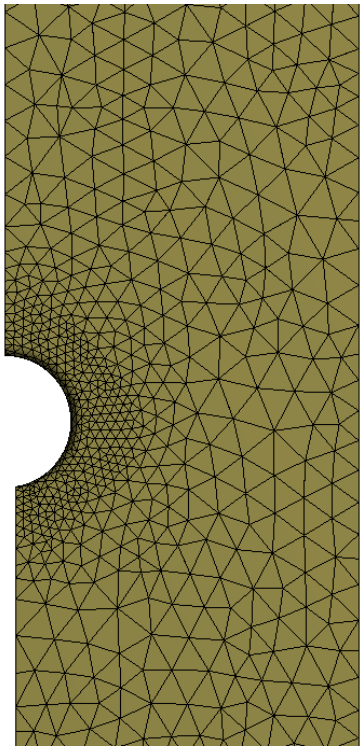

Figure 4-5: Mesh inflation around keyhole (local model)

Table 4-2: Maximum equivalent stress and plastic strain results from the local model top keyhole location at different mesh densities

Minimum Element Size (mm)	Maximum During Final Cycle		Approximate Solution Time (h)
	Equivalent Stress (MPa)	Equivalent Plastic Strain (%)	
5	453.7	1.13	3.5
3.5	460.1	1.19	4.5
2	462.3	1.22	9

The effect of mesh density on the maximum equivalent stress and plastic strain in the slot area of the OS local model is summarized in Table 4-2. The maximum values occur in the top keyhole. It can be seen that the percent differences in plastic strain results between the coarse and fine meshes is 8%. Additionally, the approximate solution time of the finer mesh is double that of the coarse mesh. It is known that a small difference in strain results may be significant in the estimation of fatigue life. Thus, the finest mesh (minimum size limit = 2 mm) is chosen since the results are found to be least mesh dependent.

4.3 Thermal Analysis of Coke Drum Skirt

In the analyses conducted in previous chapters, the quenching stage of each cycle was simulated by applying the convective boundary condition to all nodes on the inner surface of the vessel model at once. This was done to save computational expense since a larger time step could be used. In this chapter, the finite rise speed of quench water is taken into consideration, which is a more accurate representation of the quenching stage but results in longer solution times. Figure 4-6 shows the comparison of the temperature response between the simplified (BC1) and realistic (BC2) convective boundary conditions during the quench stage. The results are scoped from the inner surface of the skirt at the point of attachment of each model.

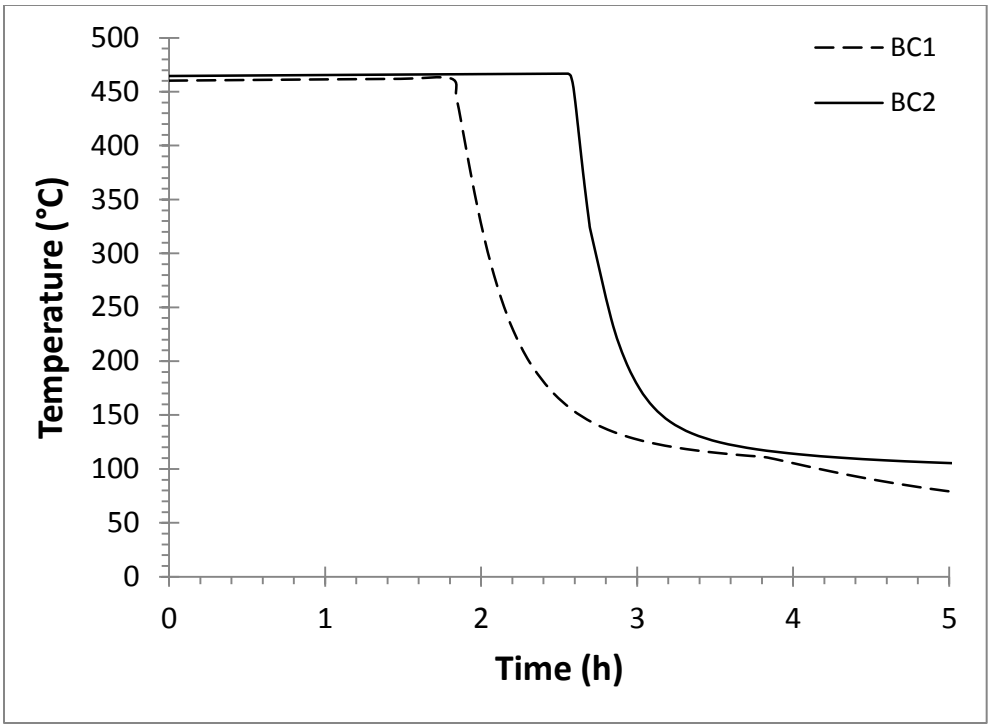

Figure 4-6: Difference in temperature response between simplified (BC1) and realistic (BC2) convective boundary conditions during the quench stage

As can be seen in Figure 4-6, the quench stage starts at about the 2 hour mark as shown clearly by the rapid fall in temperature. It can be seen that the temperature decreases immediately when using the simplified convective boundary condition. The temperature response of the realistic convective boundary condition is delayed by about 0.6 hours, as this is the amount of time required for the quench water level to reach the point of attachment. Despite this delayed response, the rate of temperature change is similar between the two boundary conditions.

Figure 4-7 shows the axial thermal gradients starting from the weld toe (point of attachment) and moving down along the inner side of each skirt design. The temperature distributions shown are taken from a point in time approximately 1 hour after the quenching stage begins. It can be seen that the Original Slot (OS) design has a slightly more severe thermal

gradient compared to the Optimal Slot (PS) design. The maximum thermal gradient of the OS and PS designs are 204°C and 171°C, respectively.

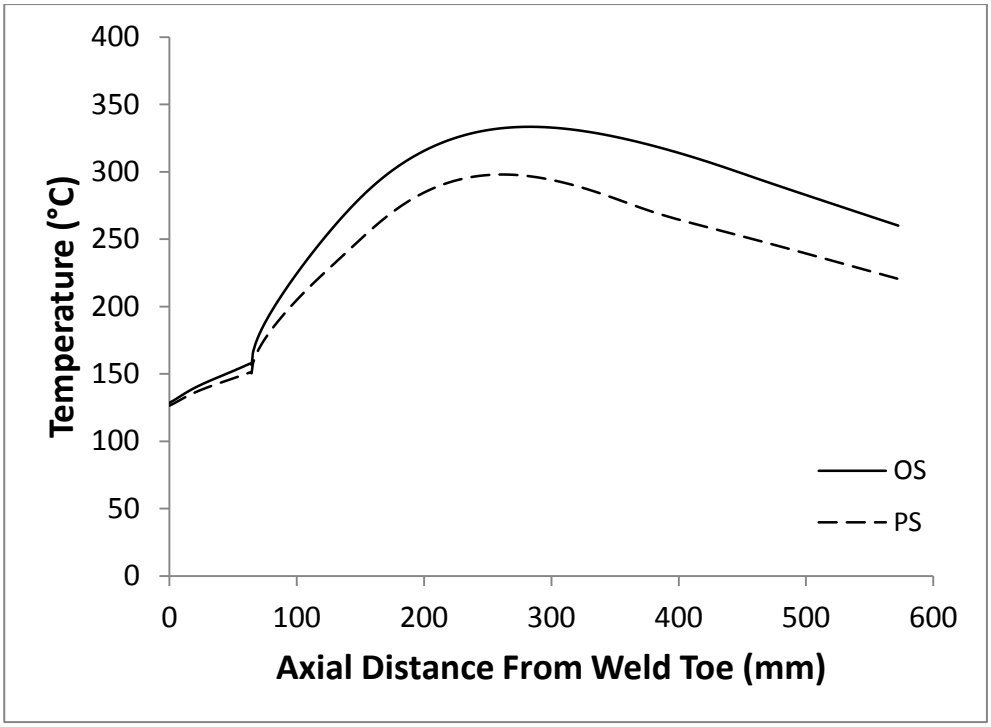

Figure 4-7: Comparison of axial inner skirt thermal gradients

4.4 Stress Analysis of Coke Drum Skirt

4.4.1 Deformation of Coke Drum Vessel and Skirt

Figure 4-8 shows the deformation profile of the coke drum vessel and skirt during quenching stage just as the water level reaches the point of attachment. The deformation is scaled up by 20 times in the figure to show the deformed shape more clearly. It can be seen that the rising water level causes a bending effect in the vessel wall which travels upward as the quench stage progresses. This effect is referred to as "vasing" due to the resultant shape of the vessel

caused by the contraction of the rapidly cooling material below the water level while the relatively hot material above remains in its expanded state.

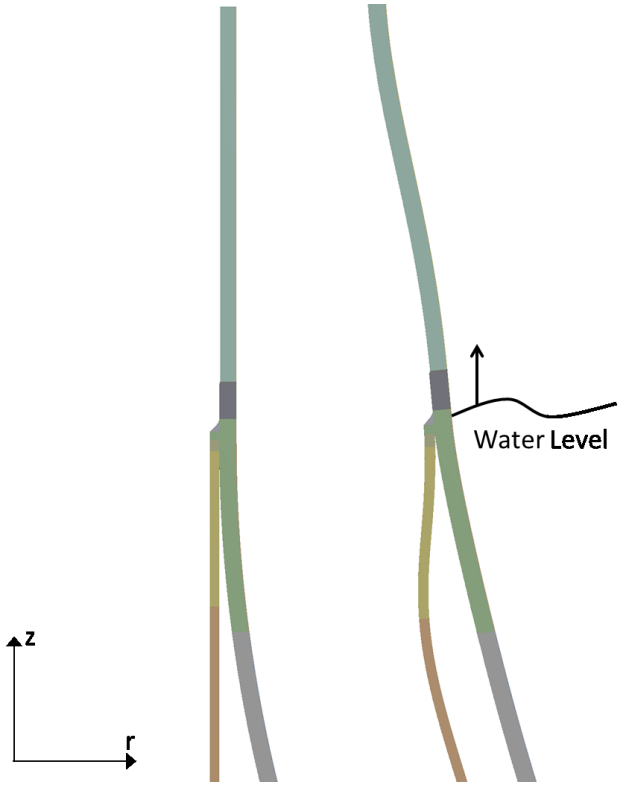

Figure 4-8: Skirt deformation profile during water quench stage (Left: Un-deformed, Right: Water level reaches junction area)

Figure 4-9 shows the differences of inner junction axial (z-direction) strain responses during the quench stage when using simplified (BC1) and realistic (BC2) convective boundary conditions. When compared to the simplified model, the maximum axial strain magnitude increases by 71% when using the realistic quench model. It is obvious that as the water level passes through the junction area, significant bending is caused by the "vasing" effect in the skirt attachment weld area. The "vasing" effect is found to also affect the results in the slot area as can be seen in Figure 4-10. The maximum hoop (θ-direction) strain magnitude in the top keyhole is found to increase by 35% due to the realistic quench model.

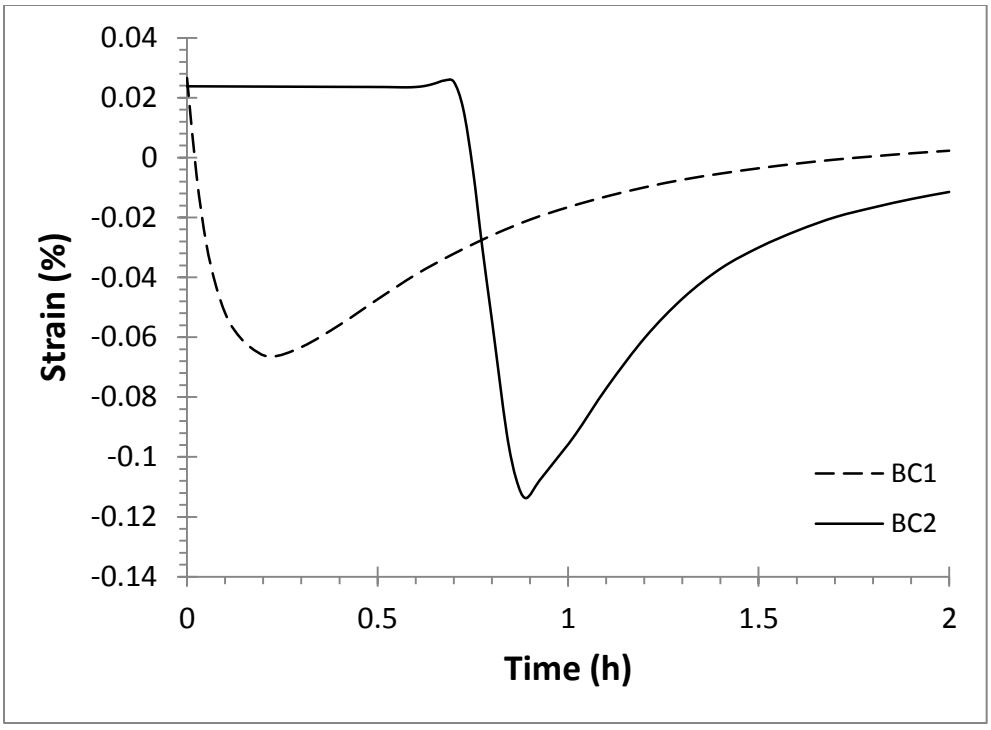

Figure 4-9: Effect of realistic quench convective boundary condition (BC2) on inner junction axial strain response

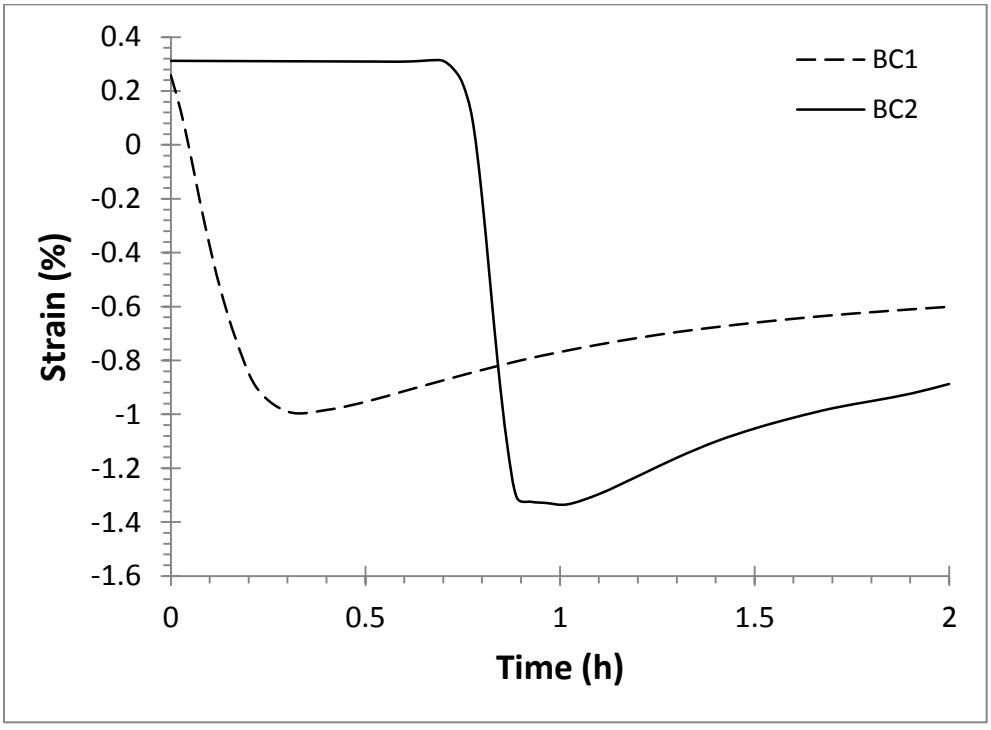

Figure 4-10: Effect of realistic quench convective boundary condition (BC2) on hoop strain response at top keyhole location

4.4.2 Junction Face Stress Response

The final cycle equivalent stress and plastic strain responses at the inner junction surface of each skirt slot design are shown in Figure 4-11 and Figure 4-12. The maximum and range values are summarized in Table 4-3.

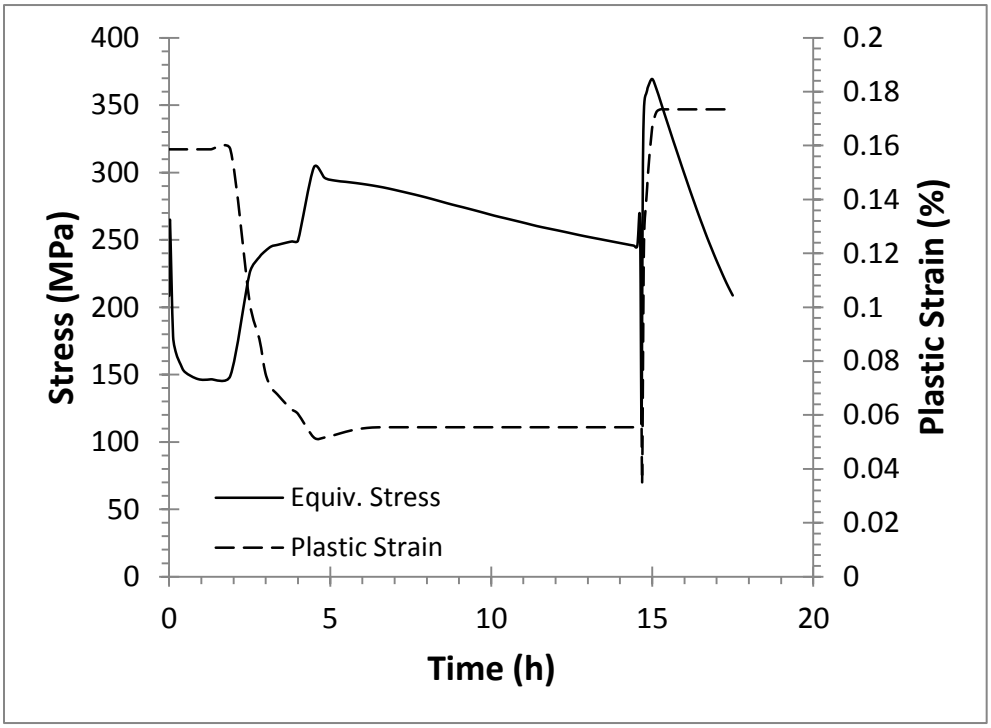

Figure 4-11: Inner junction equivalent stress and plastic strain response over the final cycle of the OS model

It is found that the peak junction stress and strain values in each of the models are much greater than previously determined in the previous chapter. The difference in results can be attributed to the increase in mesh density and the increased cyclic bending in the junction caused by the "vasing" effect. The maximum junction equivalent stress in the PS model is found to rise by 1.2% while the plastic strain decreases by 6.8% when compared to the OS model. It should also be noted that the plastic strain range is found to decrease by 28% in the PS model.

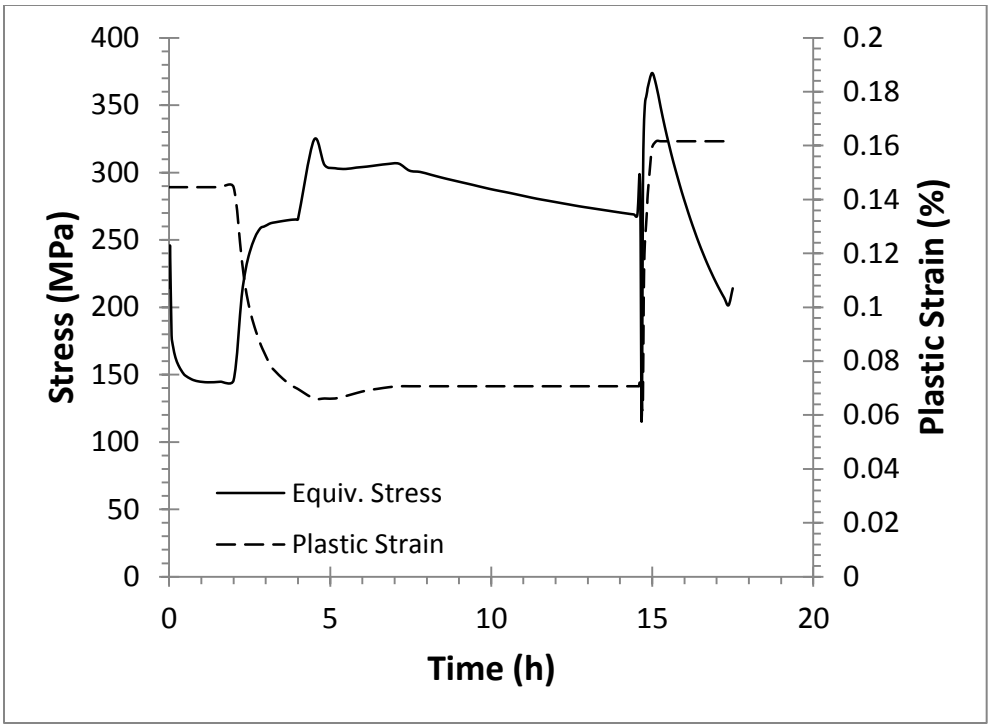

Figure 4-12: Inner junction equivalent stress and plastic strain response over the final cycle of the PS model

Table 4-3: Summary of inner junction equivalent stress and plastic strain maximums and ranges of each considered design

Model	Equivalent Stress (MPa)		Equivalent Plastic Strain (%)	
	Maximum	Range	Maximum	Range
OS	369.5	256.3	0.173	0.139
PS	373.9	258.8	0.162	0.100

4.4.3 Slot Area Stress Response

Figure 4-13 and Figure 4-14 show the final cycle equivalent stress and plastic strain responses at the top keyhole location of each skirt slot design. The maximum and range values are summarized in Table 4-4.

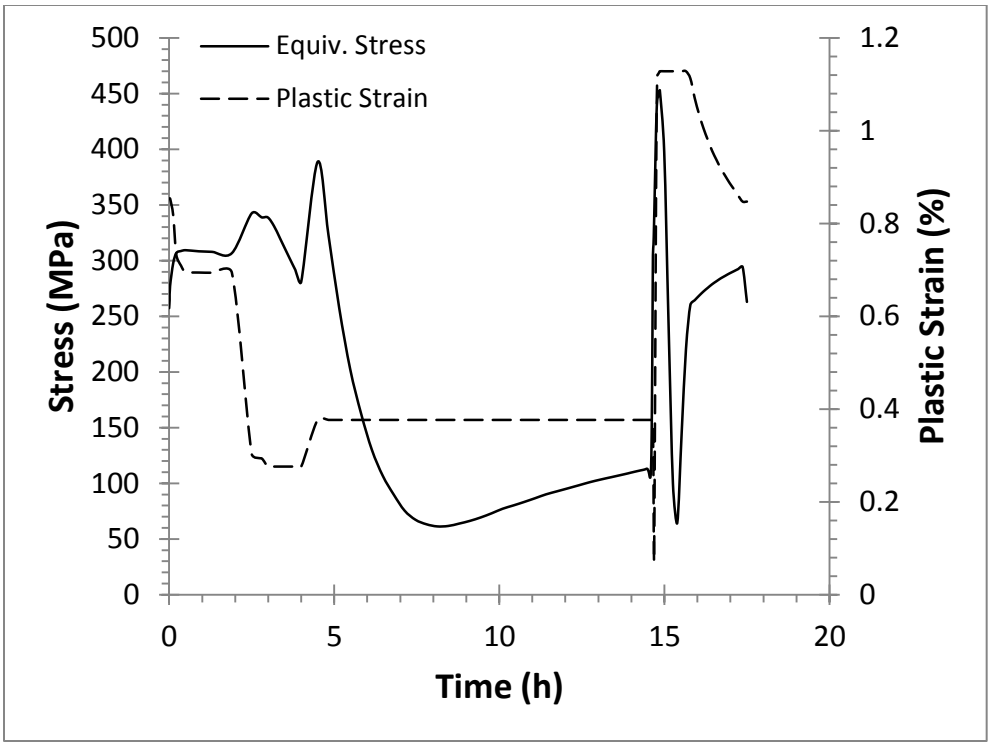

Figure 4-13: Top keyhole location equivalent stress and plastic strain response over the final cycle of the OS model

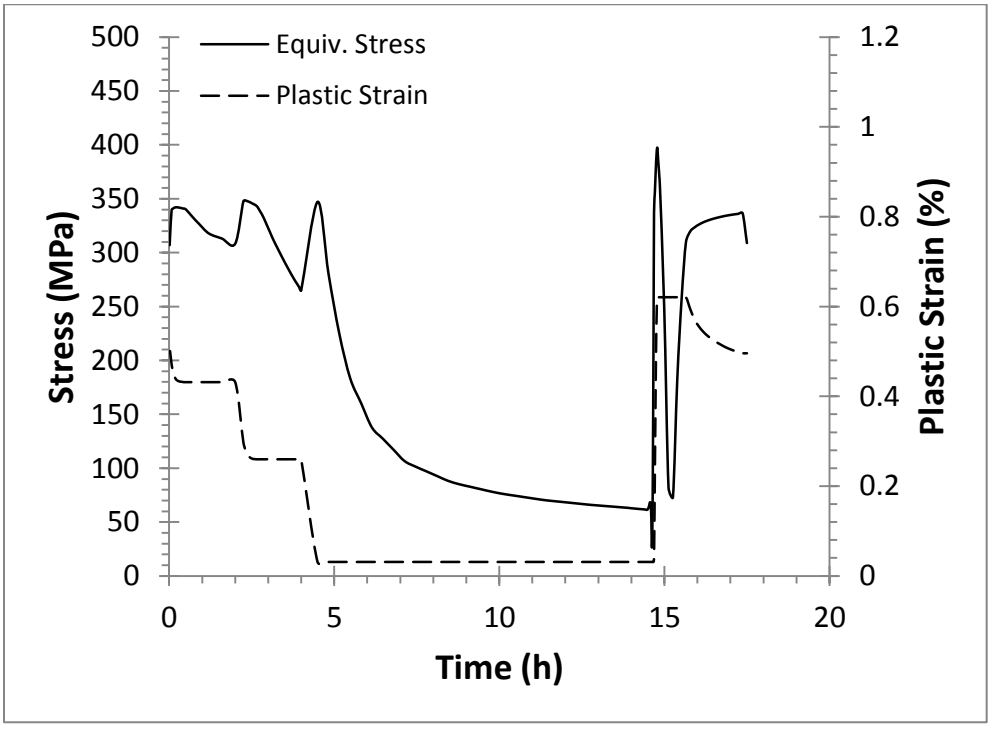

Figure 4-14: Top keyhole location equivalent stress and plastic strain response over the final cycle of the PS model

Table 4-4: Summary of top keyhole equivalent stress and plastic strain maximums and ranges of each considered design

Model	Equivalent Stress (MPa)		Equivalent Plastic Strain (%)	
	Maximum	Range	Maximum	Range
OS	453.1	391.7	1.13	1.06
PS	397.5	371.2	0.621	0.590

Similar to the junction area, the equivalent stress and plastic strain response at the top keyhole location is also found to be significantly larger than in the analyses conducted in the previous chapter. Again, the rise in stress and strain is caused by the increased mesh density and "vasing" effect. The maximum stress and equivalent plastic strain are found to decrease by 12% and 45%, respectively. The equivalent stress and plastic strain ranges drop by 5% and 44%, respectively. Therefore, it can be concluded that the critical slot end of the PS design experiences less severe stress concentration and plastic strain compared to the OS design.

4.5 Estimation of Fatigue Life

The method used in this study to estimate the fatigue life is based on procedures and fatigue design curves from ASME Sec. VIII Div. 2, Part 5 [23]. The assessment relies on the calculation of an effective strain range $\Delta\varepsilon_{eff}$ to evaluate fatigue damage given below.

$$\Delta\varepsilon_{\mathrm{eff},k} = \frac{\Delta s_{\mathrm{p},k}}{E_{\mathrm{ya},k}} + \Delta\varepsilon_{\mathrm{peq},k} \quad (1)$$

Where k is the cycle number, $E_{\mathrm{ya},k}$ is the Young's Modulus of the material at the average temperature of the operational cycle; and the calculated von Mises equivalent stress range $\Delta s_{\mathrm{p}.k}$

and maximum equivalent plastic strain range $\Delta\varepsilon_{\mathrm{peq},k}$ can be directly obtained from a finite element stress analysis.

The effective strain range is then used to determine the effective alternating equivalent stress $S_{\mathrm{alt},k}$ calculated as

$$S_{\mathrm{alt},k} = \frac{E_{\mathrm{ya},k} \cdot \Delta\varepsilon_{\mathrm{eff},k}}{2} \tag{2}$$

Finally, the permissible number of cycles N_k can be determined for the alternating equivalent stress from the fatigue curves also provided in the ASME Sec. VIII, Div. 2, Annex 3-F [23]. The fatigue curve for series 3XX high alloy steels is shown in Figure 4-15.

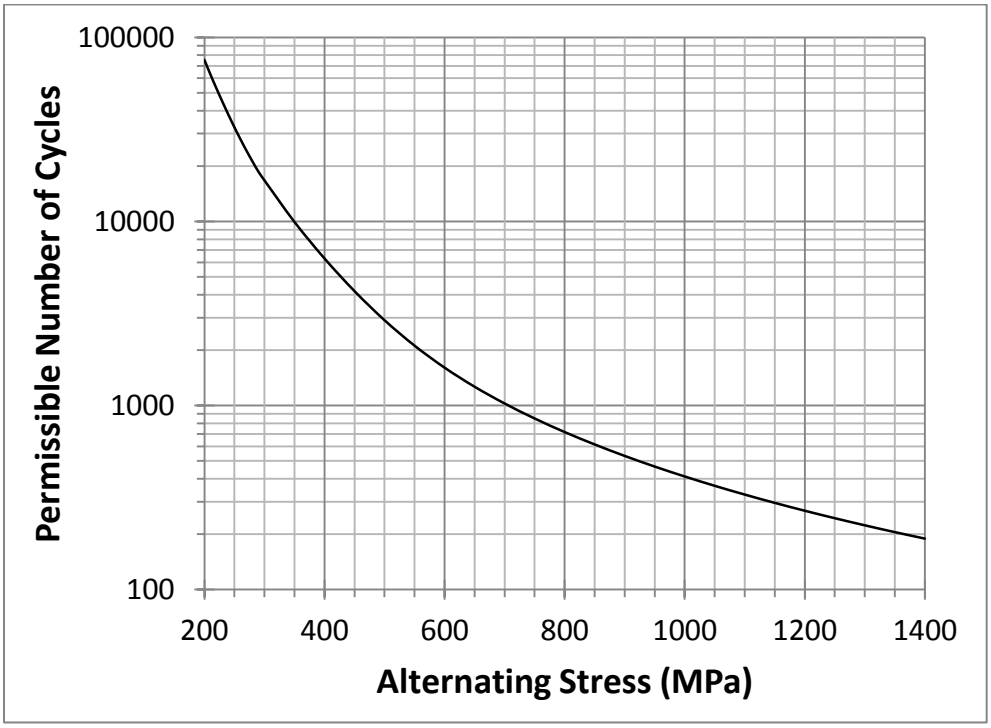

Figure 4-15: ASME fatigue curve for series 3XX high alloy steels

Normally, this method of evaluation for fatigue life invokes the cumulative damage rule known as Miner's rule where the fatigue damage $D_{f,k}$ is calculated for each (k^{th}) cycle as

$$D_{\mathrm{f},k} = \frac{n_k}{N_k} \tag{3}$$

where n_k is the actual number of repetitions of the k^{th} cycle.

The part being examined is considered to still be acceptable for continued operation as long as the following inequality is satisfied.

$$\sum_{k=1}^{M} D_{\mathrm{f},k} \leq 1.0 \tag{4}$$

Where M is the number of stress ranges determined by a cycle-counting method.

This approach is especially useful for pressure vessels in cyclic service which have large fluctuations in stress/strain between cycles, or different loading events between cycles. However, for the purposes of this study it is assumed that the damage caused by each subsequent cycle is identical to the final cycle. Thus, it can be shown that $M = 1$ and if $k = 1$ is used to represent the final cycle, Eqn. 4 can be simplified as

$$\frac{n}{N} \leq 1.0 \tag{5}$$

Essentially, the stress/strain ranges from the final cycle are used in Eqn. 1 to calculate the alternative equivalent stress and determine the admissible number of cycles for each critical location.

It should be noted that the fatigue life results obtained in this study are rough approximations. The methods used in this study are not to be used to accurately predict fatigue life since there are many variables in practice which affect material performance such as corrosion, random temperature fluctuations, and weld quality. Furthermore, Sasaki and Niimoto [17] have shown that the ASME fatigue curve does not perfectly match experimentally

determined fatigue curves for materials similar to those used in the current study. Therefore, the actual fatigue lives in reality are expected to be much lower than the values reported in this section. However, the methods are deemed acceptable as a means to quantify and compare the difference in stress and strain response at the critical locations of each slot design.

The estimated fatigue lives at the critical junction and slot areas of each slot design are summarized in Table 4-5 and Table 4-6.

Table 4-5: Estimated fatigue life of junction weld area

Design	$\Delta\varepsilon_{eff}$ (%)	S_{alt} (MPa)	N
OS	0.278	256.7	**29332**
PS	0.240	221.9	**51138**

Table 4-6: Estimated fatigue life of top keyhole location

Design	$\Delta\varepsilon_{eff}$ (%)	S_{alt} (MPa)	N
OS	1.27	1174.0	**282**
PS	0.790	730.9	**911**

As predicted, the PS design substantially improves junction weld fatigue life while also providing a slight improvement on the critical slot area fatigue life compared to the OS design. It can be seen that the estimated junction fatigue life is more sensitive to changes in alternating stress compared to the estimated slot area fatigue life. As shown by the fatigue curve in Figure 4-15, the magnitudes of junction area alternating stress present in each model are on the left-most section of the curve whereas the slot area alternating stresses occur towards the middle and right

side of the curve. Hence, the sensitivity can be attributed to the difference in the magnitude of alternating stress experienced by each area.

4.6 Summary

In this chapter, more detailed analyses are conducted on the skirt slot designs which were found to be most effective from the optimization study conducted in the previous chapter. A total of two slot designs were examined: Original Slot (OS) and Optimal Slot (PS). Features previously omitted to reduce computational cost such as clad layer, fillets around the slot edges, and finite quench water rise speed are included in the analyses. Mesh dependency analyses are conducted to ensure adequate mesh density in the critical areas. Finally, equivalent stress and plastic strain ranges are used to calculate the estimated fatigue life of the critical areas by using a method adapted from the ASME Boiler and Pressure Vessel Code.

It is found that the more realistic convective boundary condition which models the rising water during the quench stage has a significant effect on the results in both critical areas. Compared to the simplified model, the maximum axial strain magnitude at the inner junction face is found to increase by 71% when using the realistic quench model. Furthermore, the maximum hoop strain magnitude at the top keyhole location is found to increase by 35%.

In the junction area, the final cycle plastic strain range is found to decrease by 28% in the PS model. Moreover, the equivalent stress and plastic strain ranges in the slot area drop by 5% and 44%, respectively. The reduction in stress and strain ranges due to the PS design is found to increase the estimated fatigue lives of the junction and slot areas by 21806 and 629 cycles, respectively, when compared to the OS design. Hence, the results from this study confirm that

wider skirt slots with larger keyholes are better suited than the current accepted design to protect the shell-to-skirt attachment weld.

CHAPTER 5 ANALYSIS OF SLIDING AND PINNED-SLIDING SKIRT SUPPORT STRUCTURES

5.1 Introduction

In previous chapters, it has been shown that an effective method to reduce stress in the skirt-to-shell attachment weld is to add vertical slots to the upper portion of a cylindrical skirt support structure. However, it was also found that the inclusion of slots causes the critical stress location to migrate from the attachment weld to the slot ends due to stress concentration effect. Furthermore, the magnitude of plastic strain in the slot ends was found to be 5-10 times greater than in the junction weld. Hence, further research into alternative skirt designs can be conducted to improve the overall reliability of the support structure. The primary objective of this chapter is to determine the theoretical advantages of the alternative design concepts. To accomplish this, alternative skirt designs are analyzed for their effectiveness to reduce the critical stress and plastic deformation at the point of attachment and its surroundings.

Several alternative skirt designs have been discussed previously in Section 1.2.2. The sandwiched sliding plate design [16], shown in Figure 1-3, is chosen for the current study since the added circumferential degree of freedom theoretically allows the drum to expand and contract with less resistance than the conventional skirt design. However, the bending effect in the vessel wall caused by the rising quench water level (referred to as “vasing”) has previously been shown to significantly affect the stress response at the point of attachment. Therefore, the addition of a degree of rotational freedom about the circumferential axis at each point of attachment is also analyzed. Thus, a separate design which incorporates a pinned connection with the original sliding plate design is also presented.

Similar to the analyses conducted in previous chapters, 3-D cyclicly symmetric models are created and solved using identical coke drum vessel dimensions, materials, and boundary conditions. The resulting thermal gradients, deformation profiles, and peak stress/strain values are analyzed and used to compare the alternate designs to the conventional slotted skirt design. The results from the Optimal Slot (PS) design from Chapter 4 are used as a baseline for comparison. It is found that the sliding plate design reduces stress at the point of attachment. However, critical stresses resulting in severe plastic deformation are found to occur at the corner formed by the support rib and slide plate. It will be shown that the addition of pinned connections to the sliding plate results in a promising design from a reliability standpoint.

It should be noted that the skirt support structure designs examined in this chapter are simple examples and do not explicitly meet the standards set out by the ASME Boiler and Pressure Vessel Code. In practice, many different designs could be conceived which follow the same basic principles as the designs presented in this chapter. Hence, the solid models in this chapter are simplistic in nature and serve only to examine the general characteristics of sliding and pinned-sliding skirt support structures.

5.2 Model Set-Up

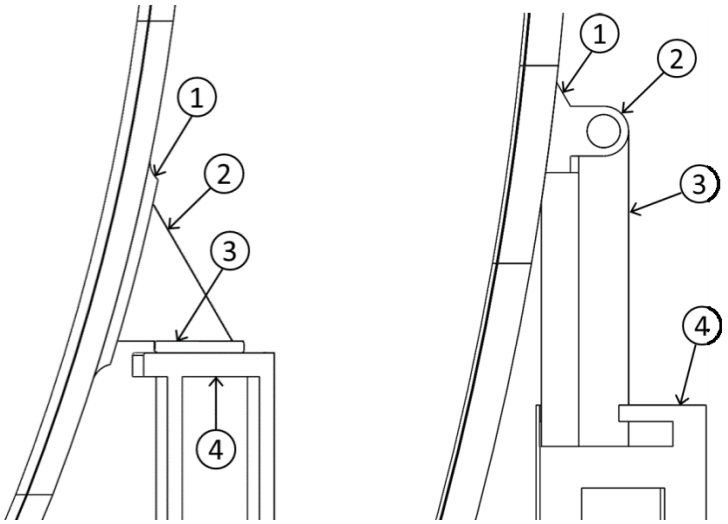

Figure 5-1: Main components of the sliding plate (left) and pinned-sliding plate (right) designs

The dimensions of the vessel used for this study are identical to those used in previous chapters and shown in Figure 2-1. The materials used (SA387-12-2 base, TP410S clad) also remain unchanged. The material properties are summarized in Table 2-2 and Table 2-3.

The sliding plate design, shown on the left in Figure 5-1, is comprised of four main components: (1) welded attachment plate; (2) support ribs; (3) horizontal sliding plate; and (4) lower support structure. The weight of the vessel is transferred through welded attachment plates and support ribs to circumferential horizontal plates which are free to slide in the radial direction relative to the vessel. The horizontal slide plates are sandwiched between a lower supporting plate and upper retaining plates which prevent the coke drum from tipping or falling over. The lower support structure is anchored to a concrete support similarly to the conventional skirt design. It can be seen that several sharp corner are inherent to the original sliding plate design

which are created by the junction between the support ribs and attachment plates. It will be shown in a later section that critical stresses occur in these corners.

The pinned sliding plate design is comprised of four main components as shown on the right in Figure 5-1: (1) Circumferential support ring; (2) Pinned connection; (3) Sliding plate; and (4) Lower support structure. The support ring is either attached to the vessel with a continuous circumferential weld or integrated into the shell course, while the supports for each pinned connection are welded to the support ring. The weight of the vessel is transferred by the support ring to the sliding plate through a flat surface which extends outwards in the radial direction. In this way, the shear forces due to vessel weight are minimized in the pinned connection. Finally, the vessel weight is transferred to the lower support structure through the sliding plates. To allow space for the thermal expansion and contraction of the vessel, the sliding plates extend downward from the point of attachment to the point of contact with the lower support structure.

Detailed schematics of the original and pinned sliding plate designs are shown in Figure 5-2 and Figure 5-3. In both designs, the points of attachment are chosen such that the skirt reaction is in line with the mean diameter of the skirt. Hence, the bending moment caused by the vessel weight at the point of attachment is minimized. The material properties of the base material (SA387-12-2) are assigned to each of the skirt component models.

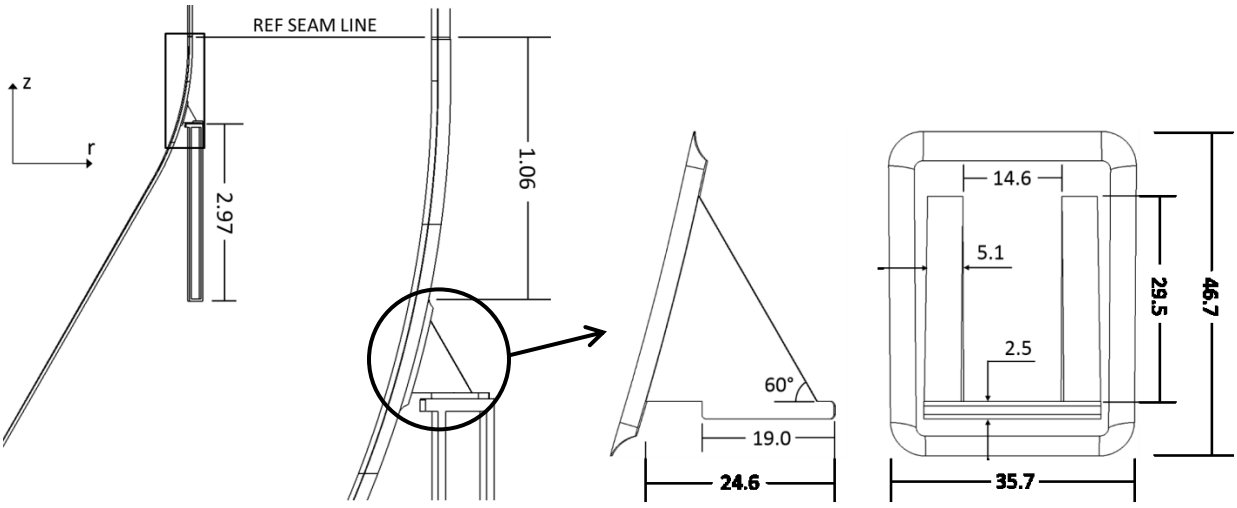

Figure 5-2: Important dimensions of the sliding plate design

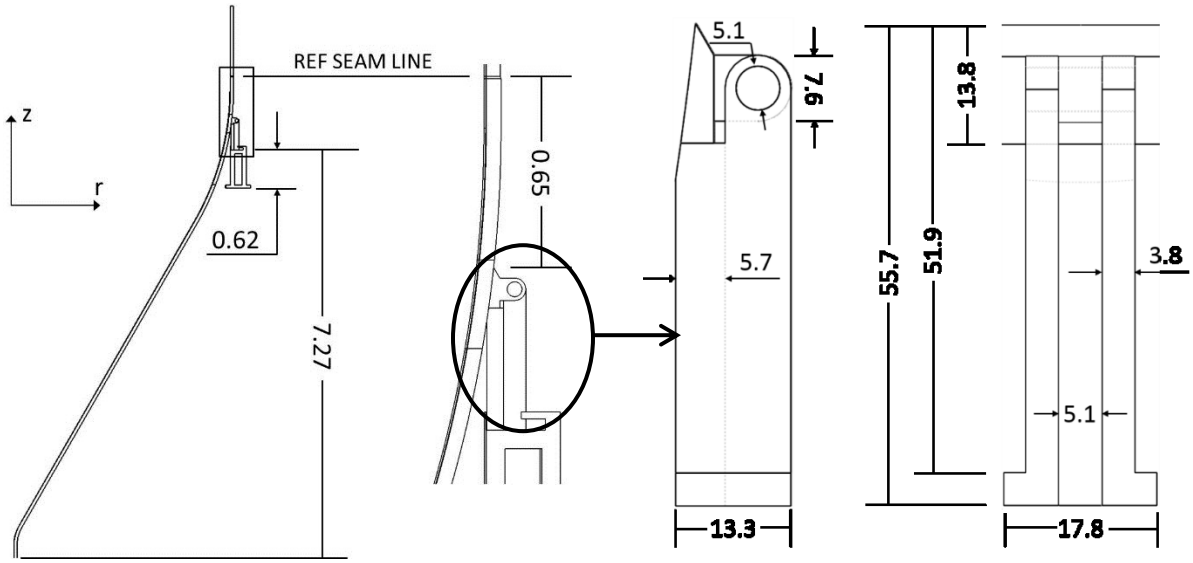

Figure 5-3: Important dimensions of the pinned-sliding plate design

Methods similar to those used in previous chapters are used to model and mesh the geometry. Mesh controls are used to make the mesh relatively coarse away from the areas of interest to save on computational expense, while the mesh close to the areas of interest is made very fine to guarantee convergence. The element size of the support ribs/ring is set to 8 mm for both models. Due to the even spacing and symmetry of support/sliding plates, a cyclic symmetric slice from the midpoint of a sliding plate to the midpoint of an adjacent gap is modelled. Where

required, frictionless contact elements are specified. The contact elements associated with sliding surfaces are restricted from separating in order to simulate the presence of retaining plates which serve the same purpose in practice. The bilinear kinematic hardening plasticity model is used for the elastic-plastic analysis.

The loading and constraints of both models are as follows:

- The bottom surface of each lower support structure is fixed
- Circumferential displacement is set to zero at all cyclic symmetry cut boundaries
- Pressure loads equivalent to the forces applied by the weight of the drum, as well as internal and hydrostatic pressures are applied to the top and bottom cut surfaces
- 'Plane-remains-plane' condition (all nodes coupled in z-direction) prescribed to top and bottom cut boundaries
- Adiabatic condition specified on all external surfaces and all cut boundaries
- Convective and pressure loads applied to the inner surfaces of the vessel. The loading parameters are summarized in Table 2-4.

As with the analyses conducted in the previous chapter, the convective and pressure loads are step-applied during the preheating and oil filling stages. Also, the effects of rising water during the quench stage are simulated by applying the convective load from the bottom inner surface node to the top sequentially with a finite rise speed of V_w = 3 mm/s. A time step size of 90 s is used to ensure convergence during the quench stage. Two complete process cycles are solved to ensure the stability of the stress response and to check for accumulation of plastic deformation.

5.3 Analysis of Sliding Plate Design

5.3.1 Transient Thermal Analysis of Sliding Plate Design

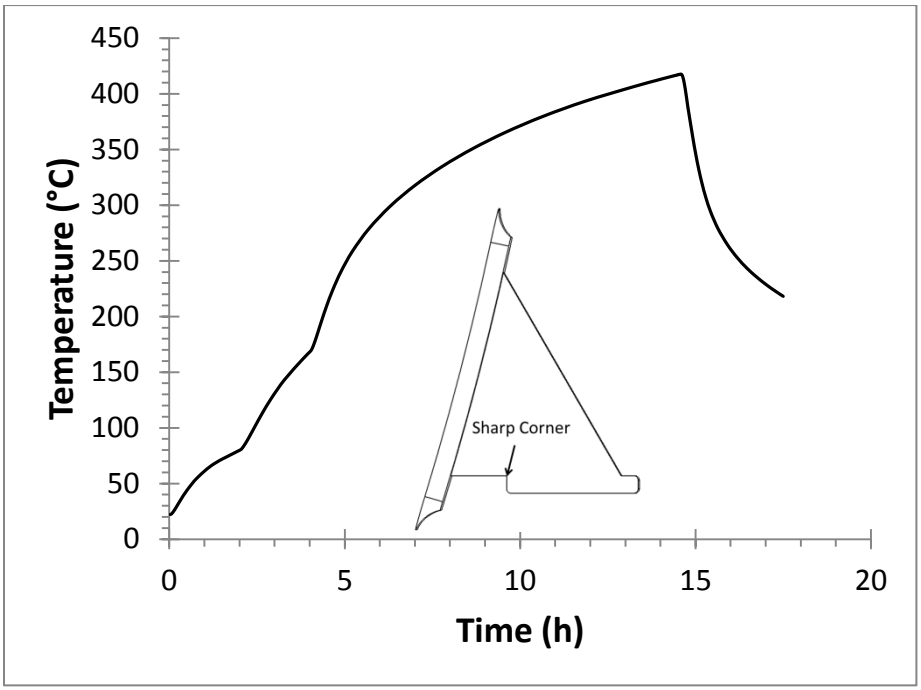

Figure 5-4: Temperature response at rib-plate corner over one complete cycle

As mentioned previously, it can be seen that several sharp corners are inherent to the sliding plate design. It will be shown in the next section that the sharp corners created by the junction between the support ribs and sliding plate are areas of critical stress. The temperature results over a complete cycle at the rib-plate corner are shown in Figure 5-4. It can be seen that the corner is located in an area that experiences elevated temperatures, which indicates that the area is susceptible to excessive plastic deformation when combined with high stress.

Due to the height of the welded attachment plates, it is expected for the rising water during the quench stage to have a considerable effect on the thermal gradient between the top and bottom ends. As can be seen in Figure 5-5, the maximum temperature difference between points at the top and bottom of the welded attachment plate is about 90°C during the quench

stage. This finding suggests that the "vasing" effect will have a large impact on the stress response of the support structure.

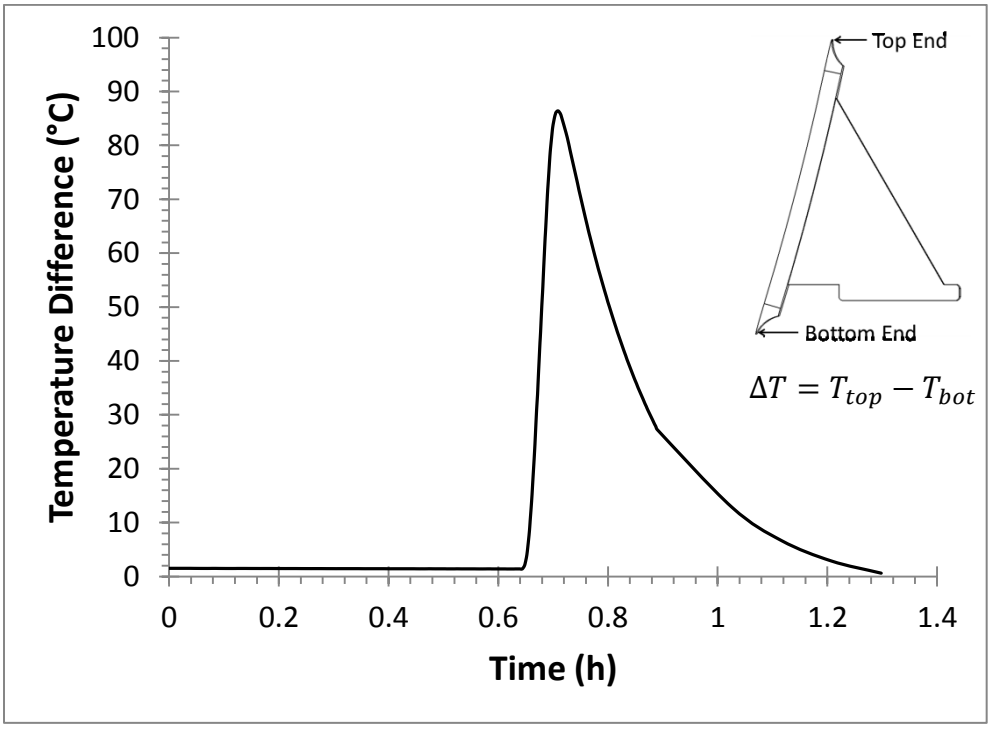

Figure 5-5: Temperature difference between top and bottom end of attachment plate during quench stage

5.3.2 Stress Analysis of Sliding Plate Design

The radial displacements at the point of attachment for the sliding plate and conventional slotted skirt design are compared in Figure 5-6. The maximum displacement of the sliding plate design is greater by about 0.4 mm despite being free to move in the radial direction. This finding suggests that the conventional cylindrical skirt does not limit the magnitude of expansion and contraction experienced by the vessel.

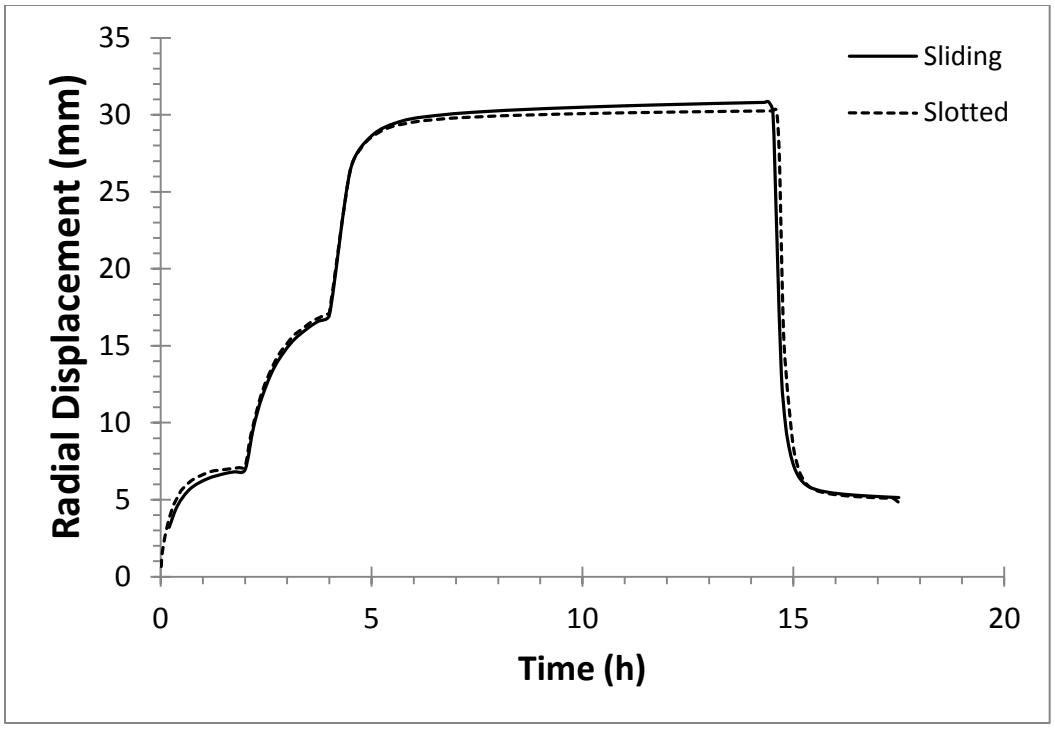

Figure 5-6: Comparison of radial displacement between sliding plate and slotted skirt designs at point of attachment

Figure 5-7 shows the comparison of second-cycle equivalent stress profiles near the point of attachment between the sliding plate and slotted skirt designs. The equivalent stress results and their differences are summarized in Table 5-1. The location of the scoped equivalent stress for the sliding plate design relative to the attachment plate is shown in the upper corner of Figure 5-7. The stress profile shown for the slotted skirt design is taken from the inner surface of the junction weld. It can be seen that the peak stress during the quench stage is reduced significantly. Additionally, the magnitude of stress during the expansion phase (pre-heating and oil filling stages) is effectively reduced in the sliding plate design. As the results in Table 5-2 show, the reduction in stress prevents any further accumulation of plastic strain in the coke drum shell during the second cycle. The presented findings suggest that the added radial degree of freedom due to the sliding action effectively reduces damage to the coke drum shell at the point of attachment when compared to the slotted skirt design.

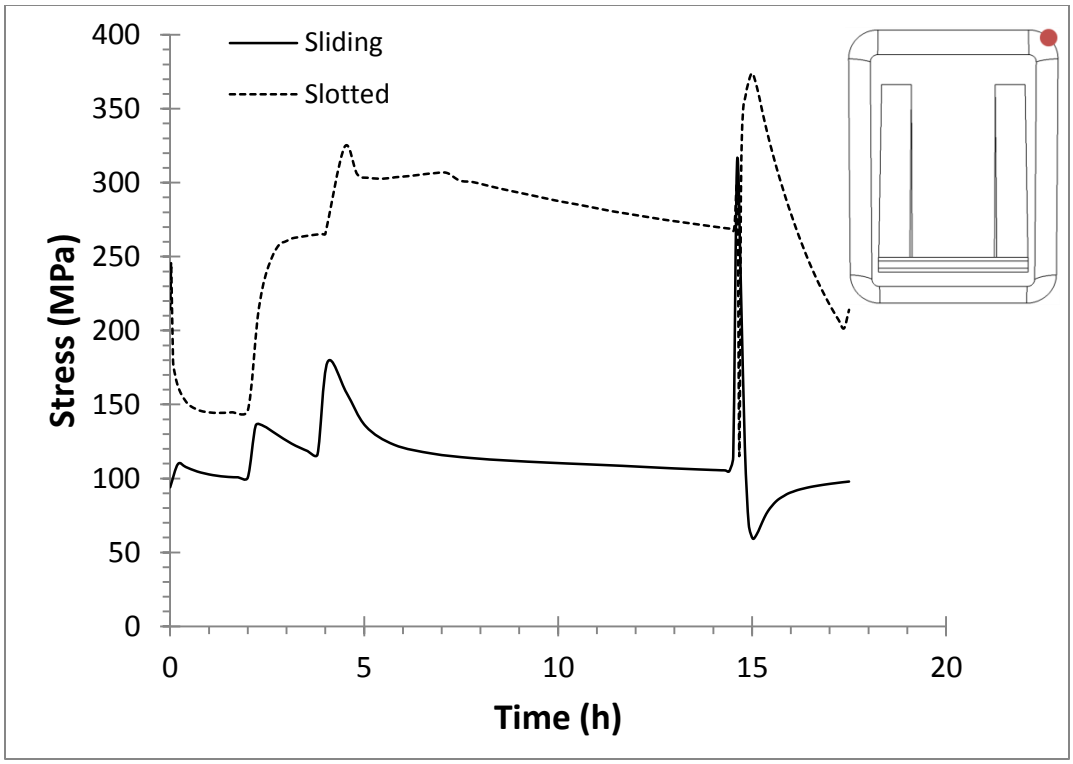

Figure 5-7: Comparison of second-cycle equivalent stress profiles between sliding plate and slotted skirt designs at point of attachment

Table 5-1: Summary of sliding plate and slotted skirt second-cycle equivalent stress results at point of attachment

Model	Equivalent Stress (MPa)		
	Vapor Heating End	Oil Filling End	Quench Peak
Slotted	324.1	268.7	373.9
Sliding	178.6	104.9	314.1
ΔS_{eqv}	-145.5	-163.8	-59.8
% Difference	-45	-61	-16

Table 5-2: Summary of sliding plate and slotted skirt equivalent plastic strain results at point of attachment

Model	Equivalent Plastic Strain (%)			
	Cycle 1		Cycle 2	
	Min	Max	Min	Max
Slotted	0	0.079	0.022	0.131
Sliding	0	0.047	0.047	0.047

The effect of the rising water level during the quench cycle on the sliding attachment plate is shown in Figure 5-8. It should be noted that the deformation is scaled up by a factor of 20 for ease of viewing. As expected, the plate experiences severe bending about the support ribs due to the "vasing" effect and the maximum stress occurs in the corner between the slide plate and support rib. The corner is the location of maximum equivalent stress in the entire skirt support structure. The second-cycle equivalent stress responses at the critical stress locations of the sliding plate (rib-plate corner) and cylindrical slotted (top keyhole location) models are shown in Figure 5-9. The equivalent stress results from the critical stress locations are summarized in Table 5-3.

It can be seen from the plastic strain results summarized in Table 5-4 that severe plastic deformation occurs at the rib-plate corner in the sliding plate design. The maximum plastic strain is about 3.8 times greater in the rib-plate corner of the sliding plate design than at the top keyhole location of the slotted skirt design. The severe plastic deformation can be attributed to a combination of geometry, bending of the coke drum vessel, and elevated temperature at the rib-plate corner.

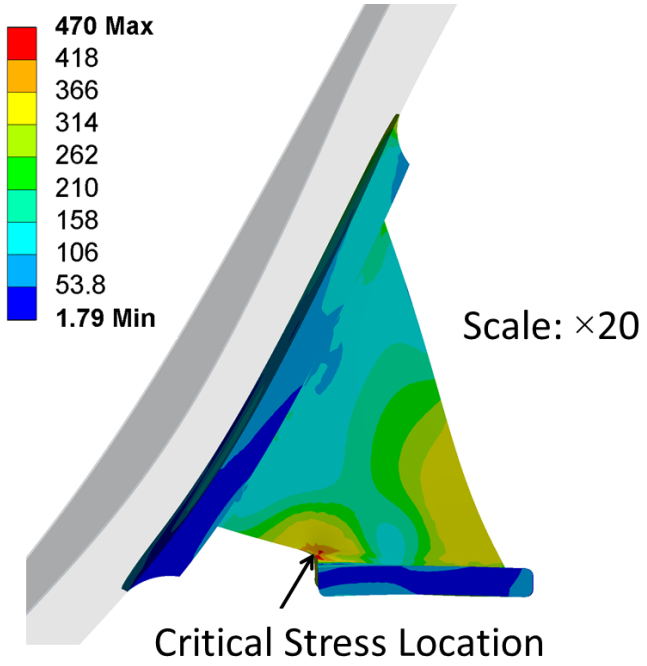

Figure 5-8: Bending of support rib and location of critical stress

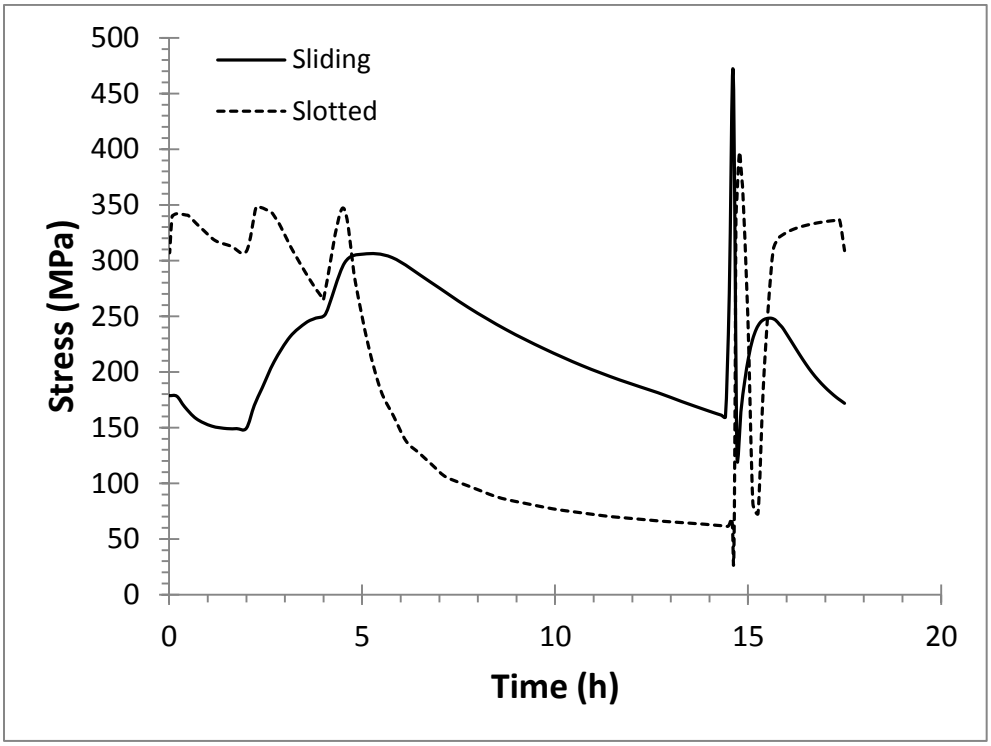

Figure 5-9: Comparison of second-cycle equivalent stress profiles between sliding plate and slotted skirt designs at critical stress location

Table 5-3: Summary of sliding plate and slotted skirt second-cycle equivalent stress results at critical stress location

Model	Equivalent Stress (MPa)		
	Vapor Heating End	Oil Filling End	Quench Peak
Slotted	347.1	61.4	397.5
Sliding	305.8	159.6	470.1
ΔS_{eqv}	-41.3	98.1	72.6
% Difference	-12	160	18

Table 5-4: Summary of sliding plate and slotted skirt plastic strain results at critical stress location

Model	Equivalent Plastic Strain (%)			
	Cycle 1		Cycle 2	
	Min	Max	Min	Max
Slotted	0	0.616	0.023	0.618
Sliding	0	2.041	0.707	2.329

5.4 Analysis of Pinned Sliding Plate Design

5.4.1 Transient Thermal Analysis of Pinned Sliding Plate Design

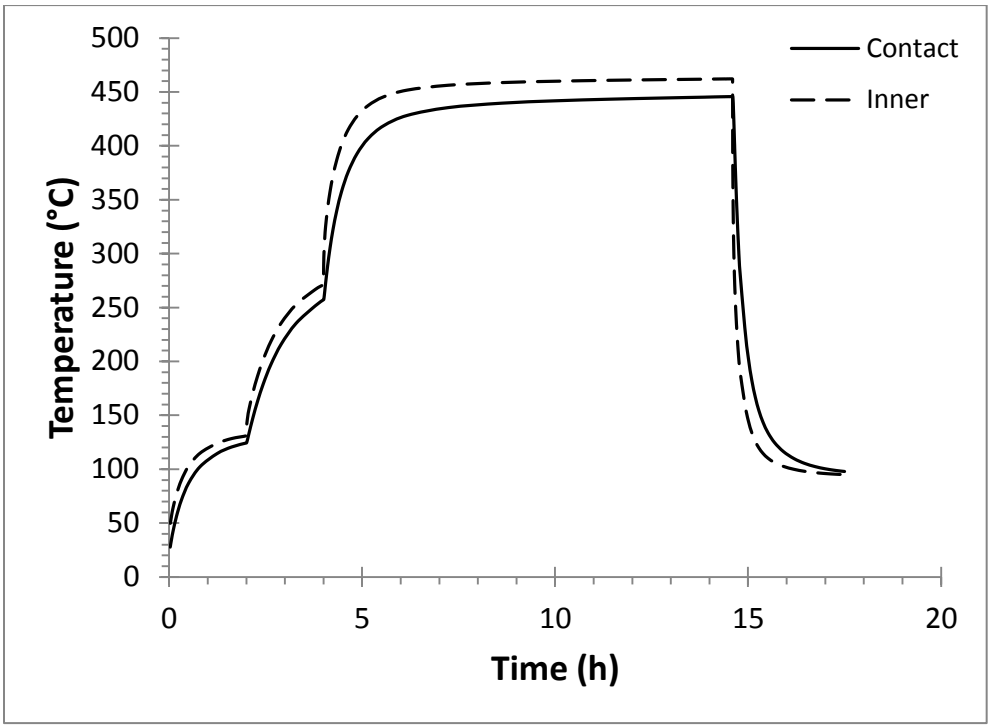

Figure 5-10: Temperature response at contact interface between support ring and sliding plate

The temperature over a complete cycle at the contact interface between the support ring and sliding plate is shown in Figure 5-10. The temperature response follows the temperature of the inner surface of the drum at the same height very closely, despite the vessel wall effectively being thicker due to the presence of the support ring at the scoped point. The temperature difference between the top and bottom ends of the support ring during the quench stage is shown in Figure 5-11. The initial positive temperature difference found at the beginning of the quench stage is due to heat transfer with the relatively cool slide plate. Once the water reaches the point of attachment, the top becomes cooler than the bottom of the support ring primarily due to the high retention of heat energy in the area of increased thickness. It can be seen that the maximum thermal gradient experienced by the support ring is about 45°C.

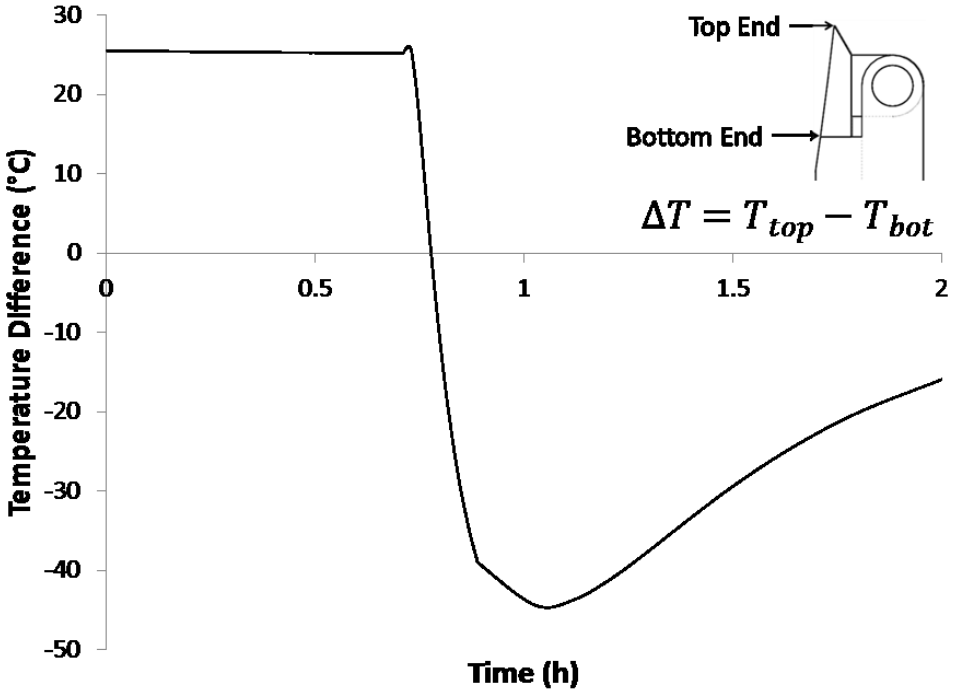

Figure 5-11: Temperature difference between top and bottom end of cylindrical support ring during quench stage

5.4.2 Stress Analysis of Pinned Sliding Plate Design

The radial displacement at the point of attachment of the pinned sliding plate design does not differ significantly from the slotted skirt and original sliding plate designs, as shown in Figure 5-12. The maximum difference in radial displacement between the pin-slide and slotted skirt design is 0.35 mm.

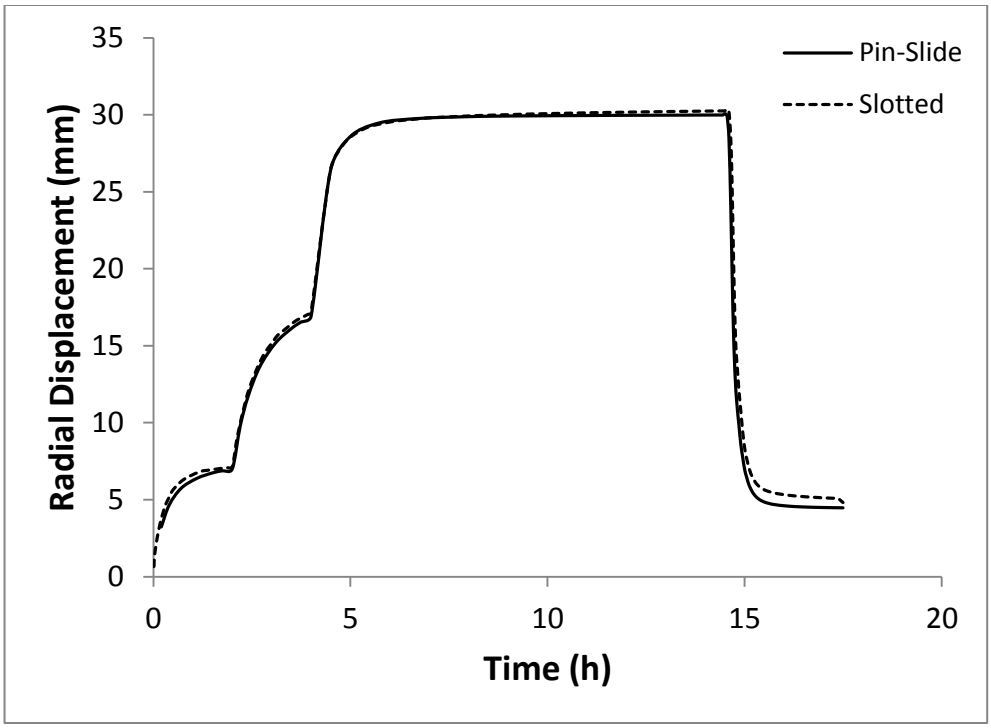

Figure 5-12: Comparison of radial displacement between pinned-sliding plate and slotted skirt designs at point of attachment

The second-cycle equivalent stress profiles at the points of attachment of the pinned-sliding plate and slotted skirt designs are compared in Figure 5-13 and summarized in Table 5-5. The location of scoped equivalent stress in the pinned-sliding plate design is along the "top end" of the support ring as previously shown in Figure 5-12. It can be seen that the stress response is largely reduced over the entire cycle when compared to the stress response at the inner junction face of the slotted skirt model. More importantly, the stress level does not exceed the yield strength of the material at any moment of the cycle. Hence, plastic deformation does not occur at any point on the outer surface of the shell near the point of attachment.

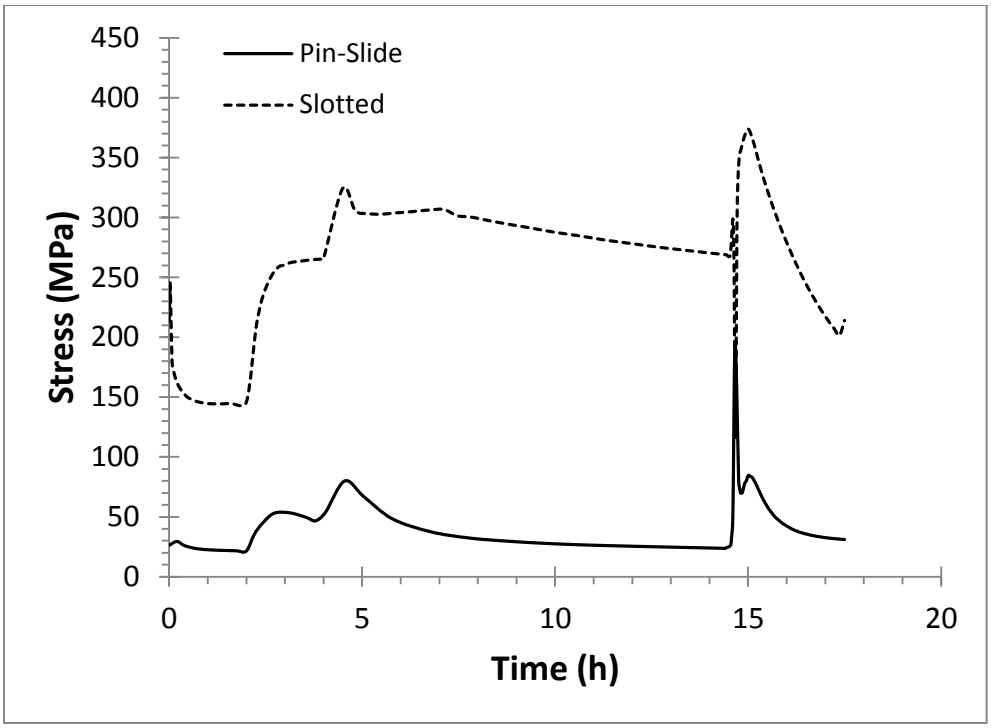

Figure 5-13: Comparison of second-cycle equivalent stress profiles between pinned-sliding plate and slotted skirt designs at point of attachment

Table 5-5: Summary of pinned-sliding plate and slotted skirt second-cycle equivalent stress results at point of attachment

Model	Equivalent Stress (MPa)		
	Vapor Heating End	Oil Filling End	Quench Peak
Slotted	324.1	268.7	373.9
Pin-Slide	79.9	27.0	191.3
ΔS_{eqv}	-244.1	-241.7	-182.6
% Difference	-75	-90	-49

The pinned connection is shown at its state of maximum rotation in Figure 5-14. As mentioned previously, the cause of the rotation of the pinned connection is the bending of the vessel shell due to the rising water level in the vessel during the quench stage. It should be noted

that the deformation is scaled up 10 times to show the rotation more clearly. The maximum gap between the bottom surface of the support ring and the top surface of the slide plate is found to be 0.9 mm. The findings provide substantial evidence that the pinned-sliding connection effectively reduces stress by allowing the vessel to bend freely about the point of attachment as the level of quench water passes through.

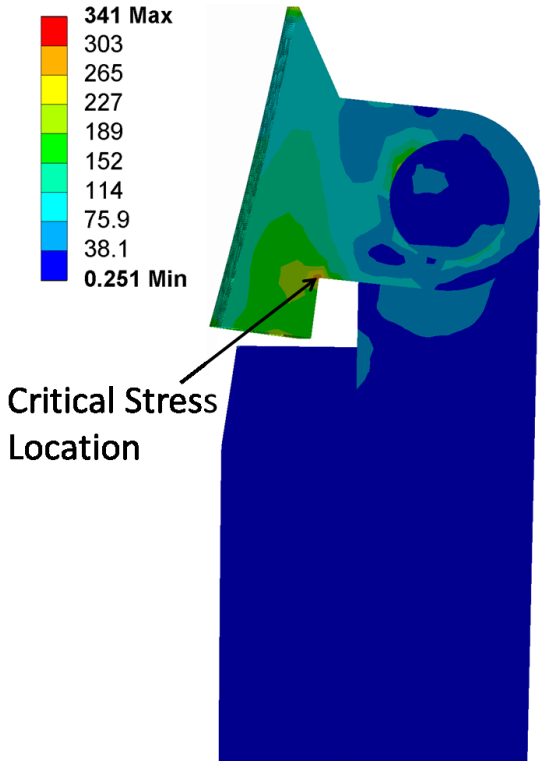

Figure 5-14: Maximum rotation of pinned connection and location of critical stress

Also shown in Figure 5-14 is the location of the critical stress in the overall skirt structure. The second-cycle equivalent stress profile at the critical location of the pinned-sliding plate design is compared with the top keyhole location of the slotted skirt design in Figure 5-15. The equivalent stress results at key moments during the cycle are summarized in Table 5-6. It can be seen that the critical stress is significantly lower during the entire cycle in the pinned-sliding plate design. However, the peak stress during the quench stage is significantly higher in

magnitude (about 3 times) than the next highest stress peak. Furthermore, the peak stress exceeds the yield strength of the material due to elevated temperatures. As a result, a small amount of plastic deformation occurs near the critical stress location. As shown in Table 5-7, the amount of plastic deformation at the critical stress location in the pinned-sliding design is about 91 times smaller in magnitude than in the slotted skirt. It is recommended for future iterations of the design that fillets are added in the corner where the critical stress exists in order to reduce the stress concentration effect of the sharp corner and potentially eliminate plastic deformation from the entire skirt structure.

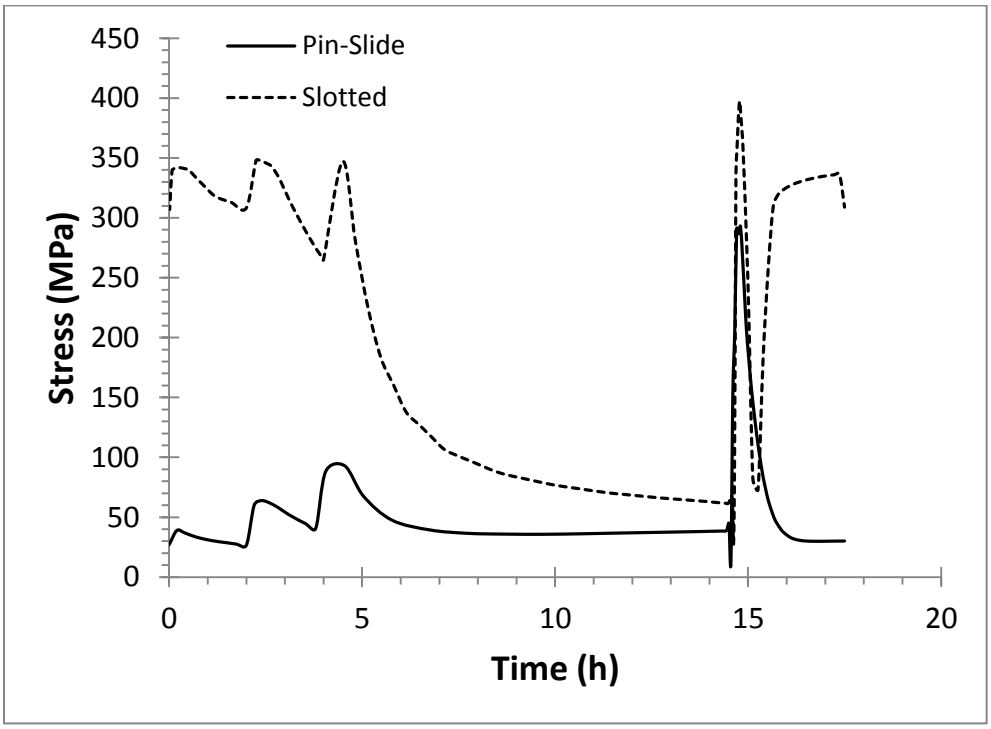

Figure 5-15: Comparison of second-cycle equivalent stress profiles between pinned-sliding plate and slotted skirt designs at critical stress location

Table 5-6: Summary of pinned-sliding plate and slotted skirt second-cycle equivalent stress results at critical stress location

Model	Equivalent Stress (MPa)		
	Vapor Heating End	Oil Filling End	Quench Peak
Slotted	347.1	61.4	397.5
Pin-Slide	93.0	39.6	291.1
ΔS_{eqv}	-254.2	-21.8	-106.4
% Difference	-73	-35	-27

Table 5-7: Summary of sliding plate and slotted skirt plastic strain results at critical stress location

Model	Equivalent Plastic Strain (%)			
	Cycle 1		Cycle 2	
	Min	Max	Min	Max
Slotted	0	0.616	0.023	0.618
Pin-Slide	0	0.007	0.007	0.007

5.5 Summary

In this chapter, alternative skirt support designs which add translational and rotational degrees of freedom to the points of attachment were analyzed and compared to the conventional slotted skirt design. The results from the sliding plate design have shown that the added translational degree of freedom improves the stress and plastic strain response at the point of attachment to the vessel shell when compared to the slotted skirt design. However, bending of the vessel due to the rising quench water level was found to cause very high stress in the corners between the support ribs and slide plate. As a result, the level of plastic deformation that occurs in the rib-plate corner was found to be about 3.8 times greater than in the top keyhole of the slotted skirt design.

The results from the pinned-sliding plate design have shown that adding both translational and rotational degrees of freedom significantly improves the stress response, thereby eliminating plastic deformation at the points of attachment. Furthermore, the critical stress in the pinned-sliding design was found to be about 27% lower compared to the slotted skirt design resulting in a significant reduction of peak plastic strain. Hence, the pinned-sliding plate design was found to be a promising candidate to improve the overall reliability of the skirt support structure.

CHAPTER 6 CONCLUSIONS

6.1 Summary

In this study, thermal-mechanical elastoplastic 3-D finite element models of coke drums were created to analyze the effect of different skirt designs on the stress/strain field near the shell-to-skirt junction weld, as well as any other critical stress locations in the overall skirt design. Using these models, the work presented in this thesis has completed the following objectives:

- The effect of conventional slots on the stress and strain response in the junction weld and slotted section has been determined by comparing identical coke drum models with un-slotted and slotted skirts.
- An optimal skirt slot design has been presented after analyzing the effect of incrementally changing each slot dimension individually.
- The sandwiched sliding plate alternate skirt design has been analyzed for any potential advantages because of its added radial degree of freedom
- A novel design which adds a pinned connection to the sliding-plate design has been presented based on observations from the slotted and sliding-plate model results.

Conventional vertical slots, which are defined as being thin relative to their circumferential spacing and placed close to the top of the skirt, have been found to significantly improve the stress and strain response in the junction weld area when compared to the un-slotted skirt model. Thus, it has been concluded that the skirt slots provide effective protection against damage to the junction weld. However, it has also been found that the stress concentration effect causes severe stress and strain to occur at the slot ends. Thus, it can be said that the inclusion of

skirt slot causes the critical stress location to migrate from the shell-to-skirt junction weld to the slot area.

Through the process of individually changing slot dimensions one at a time and analyzing each resultant slot design, it has been found that an increase in slot width significantly improves the stress and strain response in both the junction weld and slot ends. Hence, the presented optimal slot design is substantially wider than the conventional slot design (3.175 to 50.8 mm). The improvements in stress and strain response are also found to significantly improve estimated fatigue life in the junction weld and slot ends.

The sliding plate design is found to improve the stress and strain response at the welded attachment point. However, the combination of the bending vessel wall due to rising water level and sharp corners inherent to the design caused severe plastic deformation to occur near the support ribs. The pinned-sliding plate design is found to completely eliminate plastic deformation at the welded attachment point and significantly decrease the critical stress compared to the original sliding plate design. Thus, it can be said that the pinned-sliding plate design is a promising candidate due to the absence of plastic deformation at the critical junction weld location.

6.2 Recommendations for Future Work

Since 3-D analyses were required, one very apparent limitation on the work done in this thesis was computational expense. With more powerful computing, more analyses could be conducted to achieve a more thorough understanding of the effects of different slot dimensions, especially at increased slot width. Ideally, enough data points can be obtained to find a

correlation between dimension and stress/strain. Furthermore, the following experimental work is also recommended:

- Determine and verify material properties of the weld material and heat-affected zones. In future studies, these material properties assigned to the appropriate areas for a more accurate solutions.
- Install strain and temperature gauges near the critical locations of slotted coke drum skirts to gather data for the verification of simulation results.
- Develop a pinned-sliding plate design which complies with ASME Code for any given coke drum vessel and expand understanding of its advantages and limitations in a practical setting.

BIBLIOGRAPHY

[1] American Petroleum Institute, "1996 API Coke Drum Survey Final Report." November 2003.

[2] D.R. Moss. "Design of Vessel Supports." *Pressure Vessel Design Manual: Illustrated Procedures for Solving Major Pressure Vessel Design Problems.* Amsterdam: Gulf Professional Pub., 2004. pp. 185-296.

[3] A. Ramos, C. C. Rios, J. Vargas, T. Tahara, and T. Hasegawa. "Mechanical Integrity Evaluation of Delayed Coke Drums," Fitness for Adverse Environments in Petroleum and Power Equipment, *ASME 1997 Pressure Vessels and Piping Conference*, vol. 359, pp. 291-298, July 1997.

[4] A. Ramos, C.C. Rios, E. Johnsen, M. Gonzalez, and J. Vargas. "Delayed Coke Drum Assessment Using Field Measurements & FEA," Analysis and Design of Composite, Process, and Power Piping and Vessels, *ASME/JSME 1998 Joint Pressure Vessels and Piping Conference*, vol. 368, pp. 231-237, July 1998.

[5] M. Oka, H. Ambarita, M. Daimaruya, and H. Fujiki. "Initiation of Bulges in a Coke Drum Subjected to Cyclic Heating and Cooling, also Cyclic Mechanical Loads", *Journal of Thermal Stresses*, vol. 33, no. 10, pp. 964-976, Jan 2010.

[6] Z. Yan, Y. Zhang, J. Chen, and Z. Xia. "Statistical method for the fatigue life estimation of coke drums," *Engineering Failure Analysis*, vol. 48, pp. 259-271, February 2015.

[7] J. A. Penso, Y. M. Lattarulo, A. J. Seijas, J. Torres, D. Howden, and C. L. Tsai. "Understanding Failure Mechanisms to Improve Reliability of Coke Drum," Operations, Applications, and Components, *ASME 1999 Pressure Vessels and Piping Conference*, vol. 395, pp. 243–253, August 1999.

[8] Z. Xia, F. Ju, and P. DuPlessis. "Heat transfer and stress analysis of coke drum for a complete operating cycle," *ASME Journal of Pressure Vessel Technology,* vol. 132, no. 5, pp. 051205-051205-9, October 2010.

[9] M. Nikic. "Optimal Selection of Delayed Coke Drum Materials Based on ASME Section II Material Property Data," Master's Thesis, University of Alberta (Canada), 2013.

[10] J. Chen. "Experimental Study of Elastoplastic Mechanical Properties of Coke Drum Materials," Master's Thesis, University of Alberta (Canada), 2010.

[11] H. Rahman. "Characterization of Thermal-Mechanical Properties and Optimal Selection of Coke Drum Materials," Master's Thesis, University of Alberta (Canada), 2015. Accessed from: https://doi.org/10.7939/R3542JH3B

[12] M. Oka, H. Ambarita, K. Kawashima, and M. Daimaruya. "Effect of hot feed injection time on thermal fatigue life of shell-to-skirt junction area of coke drums," *ASME 2010 Pressure Vessels and Piping Conference*, vol. 7, pp. 37-43, July 2010.

[13] N. A. Weil, and J. J. Murphy. "Design and Analysis of Welded Pressure-Vessel Skirt Supports," *ASME Journal of Engineering for Industry,* vol. 82, no.1, pp. 1-13*,* February 1960.

[14] Cheng, D. H., and N. A. Weil. "The Junction Problem of Solid-Slotted Cylindrical Shells," *ASME Journal of Applied Mechanics,* vol. 27, no. 2, pp. 343-349, June 1960.

[15] Stewart, Coby W, et al. "Coke Drum Design." *Petroleum Technology Quarterly*, 5 May 2006, www.cbi.com/getattachment/1c85539c-2424-4b76-ba93-74445b8d6fb6/Coke-Drum-Design-Reliability-Through-Innovation.aspx. Accessed 6 Apr. 2017.

[16] R. Lah, "Coke drum skirt", US Patent #7871500, 2011.

[17] Y. Sasaki, and S. Niimoto. "Study on skirt-to-shell attachment of coke drum by evaluation of fatigue strength of weld metal," *ASME 2011 Pressure Vessel and Piping Conference*, vol. 3, pp. 305-310, July 2011.

[18] Y. Sasaki and S. Niimoto, "Support structure of a coke drum", US Patent #8317981, 2012.

[19] M. Oka, H. Ambarita, M. Daimaruya, and H. Fujiki. "Study on the Effects of Switching Temperature on the Thermal Fatigue Life of the Shell-to-Skirt Junction of Coke Drum," *ASME Journal of Pressure Vessel Technology*, vol. 133, pp. 061210-1-11, December 2011.

[20] ANSYS® Workbench, Release 15.0

[21] ASME, ASME Boiler and Pressure Vessel Code, Section II, Part D Properties, 2007.

[22] ANSYS® Academic Research, Release 15.0, Help System, Contact Guide, ANSYS, Inc.

[23] ASME, ASME Boiler and Pressure Vessel Code, Section VIII, Division 2, Rules for Construction of Pressure Vessels, 2015.